A Novel Sensor Concept for Selective and Self-Powered Gas Detection

Martin W. G. Hoffmann

Doctoral Thesis

Presented for partial fulfillment of the requirements for the

Degree of Doctor by the Univeristat de Barcelona

A Novel Sensor Concept for Selective and Self-Powered Gas Detection

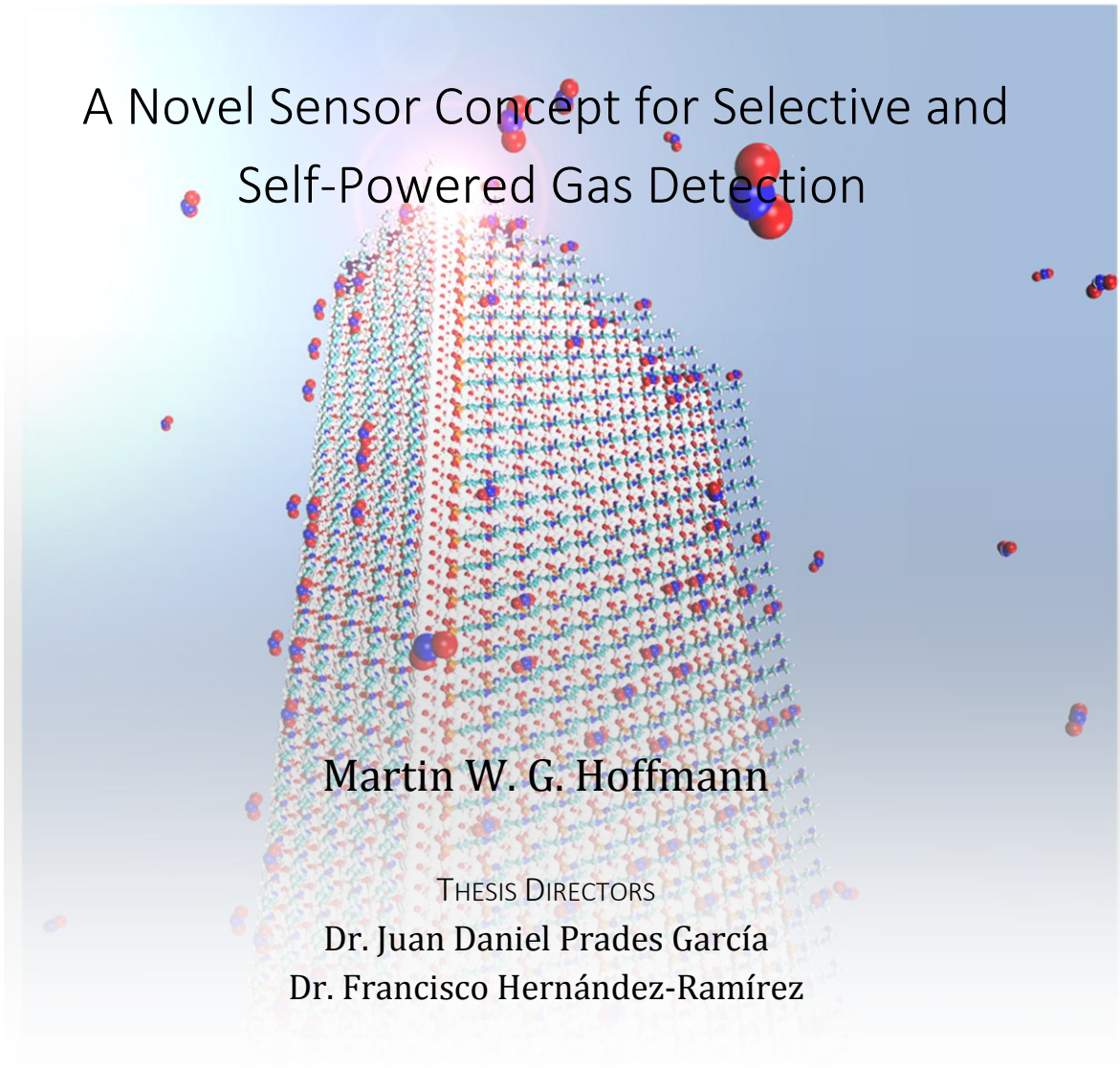

Martin W. G. Hoffmann

Thesis Directors

Dr. Juan Daniel Prades García

Dr. Francisco Hernández-Ramírez

Tutor

Prof. Albert Cornet i Calveras

Universitat de Barcelona

Faculty of Physics

Department of Electronics

MIND Group, IN^{2}UB

Barcelona, September 2014

PROGRAMA DE DOCTORAT EN
ENGINYERIA I TECNOLOGIES AVANÇADES

A Novel Sensor Concept for Selective and Self-Powered Gas Detection

Tesi que presenta
Martin W. G. Hoffmann

per optar al títol de Doctor per la Universitat de Barcelona

DIRECTORS DE TESI
Dr. Juan Daniel Prades García
Dr. Francisco Hernández-Ramírez

TUTOR
Prof. Albert Cornet i Calveras

FACULTAT DE FÍSICA
DEPARTAMENT D´ELECTRÒNICA
GRUP DE MICRO-NANOSCÒPIES PER DISPOSTIUS ELECTRÒNICS I FOTÒNICS (MIND)
INSTITUT DE NANOCIÈNCIA I NANOTECNOLOGIA (IN^{2}UB)

FÜR BRITTA

Resum

Les tecnologies de sensors de gas basades en semiconductors presenten limitacions importants de selectivitat i consum d'energia. Per tant, esdevé necessari l'assaig de nous conceptes de dispositius capaços de satisfer aquests dos requeriments per aplicar-los en plataformes mòbils. En aquesta tesi es presenta una tecnologia de sensors altament selectiva i autònoms des d'un punt energètic, incloent la seva avaluació experimental i l'anàlisi dels mecanismes físico-químics de detecció subjacents. S´han fabricat materials nano-híbrids, basats en nanofils inorgànics (NWs), funcionalitzats amb monocapes "auto-acoblades" (SAMs). A la dissertació es mostren les extraordinàries característiques en termes de selectivitat i sensibilitat de gas que exhibeixen aquests materials; els estudis teòrics són consistents amb les observacions experimentals disponibles i permeten identificar l'estructura electrònica dels orbitals moleculars de frontera SAM, que és el paràmetre crucial per a garantir una interacció eficaç entre el sensor i els gasos. A més a més, es presenta un nou concepte de sensor autònom sobre la base d'una heteroestructura p-Si/n-ZnONW que respon exclusivament a la llum solar sense necessitar d'altres fonts d'energia externes. Els canvis de la tensió de circuit obert (ΔV_{oc}), que s'utilitzen per controlar la presència d'espècies de gasos, mostren una correlació directa amb la densitat de portadors de càrrega (N_d) al nanofil de n-ZnO. Finalment, es presenta l'aplicació de tècniques de microfabricació en el disseny d'un dispositiu que integra els conceptes de selectivitat i autonomia energètica, capaç per tant de detectar concentracions de NO_2 rellevants per a aplicacions de seguretat (nivell de ppb) sense la necessitat de fonts d'energia externes. La mida compacta, la baixa demanda d'energia i la robustesa de la tecnologia fan que el concepte de sensor que aquí es presenta sigui molt prometedor per a la seva integració futura en plataformes electròniques mòbils.

Abstract

Contemporary semiconductor based gas sensor technologies could already prove their high sensitive characteristics but exhibit crucial debilities in terms of target selectivity and power consumption. As both criteria have to be fulfilled for the application in mobile sensor platforms, new device concepts are needed. Within the here presented thesis the development of a highly selective and self-powered as well as experimental evaluations and analysis of the underlying sensing mechanisms are presented. First, hybrid nano materials are fabricated, based on inorganic nanowires (NWs) functionalized with self-assembled monolayers (SAMs), and show extraordinary characteristics in terms of gas selectivity and sensitivity. Theoretical mechanistic studies are consistent with the experimental observations and identify the electronic structure of the SAM frontier molecular orbitals as crucial parameter for efficient sensor-gas interactions. Furthermore, a novel self-powered sensor concept is presented based on a p-Si/n-ZnO NW heterostructure that is solely driven by solar light and without the need of external energy sources. Changes of the open cirquit voltage (ΔV_{oc}) that are used to monitor the presence of gas species are shown to correlate with the charge carrier density (N_d) within the n-ZnO NW upon gas-sensor interactions. Finally, microfabrication techniques are applied to unify the selective and self-powered concepts within a single sensor device that is capable to selectively and quantitatively detect NO_2-gas concentrations within security relevant concentrations (ppb level) and without the need of external energy sources. The compact size, low energy demand and validity of signal information make the here presented sensor concept very promising for the integration into mobile electronic platforms.

Acknowledgement

The realization of the here presented thesis goes along with the handling of various scientific and technical disciplines that could never be solved alone by myself in their entirely. Therefore, this acknowledgement is dedicated to all persons that helped and supported me within the years in Cologne, Barcelona and Braunschweig.

At first, I want to give very special thanks to my thesis supervisors Daniel Prades and Francisco Hernandez-Ramirez, as well as Hao Shen for their extraordinary support and inspiration during all my thesis work in scientific fields and far beyond. Thank you for showing me the joy and confidence to work on new and exciting projects that allowed me to learn a lot about their physical background. It was a pleasure to work with you during this thesis! Thank you very much Dani for your great hosting during all my visits and for showing me a part of the real Barceolona.

Also, I want to give a special thank to Andreas Waag for giving me the chance and trust to take part in the development of exciting strategic projects. This fruitful and inspiring collaborations always had a high value for my personal development.

Alaaeldin, thank you very much for being my friend and for sharing all ups and downs during this time. I really appreciate to work with you and to develop our -sometimes crazy- ideas. Here, I also want to thank Lorenzo, Dennis and Hao for being my friends here in the far north, and especially Lorenzo for giving me the chance to lose various kicker-table bets. I am really thankful to share thoughts with all of you inside-, and especially outside the lab.

This thesis would not have the same scientific value without the excellent theoretical models developed by Leonhard Mayrhofer from the Fraunhofer IWM in Freiburg. Thank you very much for this inspiring cooperation that enabled us to get an idea about the complex mechanism of selective gas detection. I also want to thank Tommi Järvi and Michael Moseler for the support of these works.

As mentioned above, this thesis could not be done without the support of my colleagues.
I want to thank all IHT´ler for their helping hands in many aspects. A special thank to Angelika S. and Juliane for their excellent technical support to realize self-powered sensor devices. Sincere thanks to Angelika J. for the great organization of various urgent needs and Klaudia for the support in the LENA project. Thanks to Andrej, Alex, Frederik, Sönke and Ito for world class football matches, Jana and Xue for providing high quality GaN strucutures, as well as all the colleagues in Braunschweig: Andrey, Doris, Erwin, Feng, Hergo, Jandong, Johannes, Mahmud and Xiaodan.

I want to thank the fantastic colleagues from the MIND group: Olga for giving me a deeper insight into semiconductor physics and the quality of red wine, Jordi for showing me the easy handling of E-beam lithography facilities, as well as Oriol and Giovanni for many helping hands in the lab. Thanks for feeling home in Barcelona.

Alexandra, Daniela, Jan, Kai, Micha, Rainer, Robin, Stefan and Thomas; thanks a lot for the long journey and your friendship. You are great!

Am Ende möchte ich den für mich wichtigsten Menschen danken: Britta für die einzigartige Freude, Motivation, Unterstützung und Geduld während der gesamten Arbeit sowie Mama, Jan, Simon Rike, Justin und Bärbel. Ich hoffe, dass ich Euch in dieser Zeit trotz aller Gedanken um diese Arbeit Eure Bedeutung für mich zeigen konnte.

Content

1

Introduction

The past decades were determined by a fast growing earth population and an ambitious industrial growth of emerging economies in Asia and Latin America. A consequent transformation from agriculturally dominated structures to urban societies let metropolises grow to megacities as Mumbai, Shanghai, Istanbul or São Paulo.[1] So far, a fast economic growth was rated with higher priority than the caused environmental impact. A more and more serious pollution of air, water and agricultural areas in urban regions with consequences on human health and even social unrest led to a change of thinking and a political intent for vigorous efforts to target environmental problems within the next decades. As Industrial production sites are mainly concentrated in urban regions, the close proximity to the living environment creates a complex challenge to ensure sustained economic growth in uprising metropolitan areas.[2]

The development of new gas monitoring systems will play an essential role in programs to realize a higher life quality. A sufficient control of densely populated areas requires close meshed sensor networks with high detection accuracy in terms of location and gas selectivity to identify threads and to take efficient actions. Moreover, people will be interested to identify harmful threads also in their personal environment without the need of a public infrastructure. Mobile devices like smart phones could serve as platforms to integrate the needed sensor technologies and ensure an on-demand accessibility. A low impact on the battery lifetime of such devices and an easy interpretation of the detection results, even for non-specialist users, is essential for a successful commercial application. Therefore, to facilitate wide spread and personal analyses of the air quality, **gas sensors have to accomplish two major requirements:**

- **high target selectivity**
- **low power consumption**

Both qualifications cannot be sufficiently fulfilled by current sensor technologies.[3] Electrochemical or optical analysis systems can offer a high specificity, but their bulky

dimensions, as well as high power consumption and costs do not allow them to be applied for mobile or wireless applications.[4,5] Resistive gas sensors, based on semiconducting metal oxide materials, with their relative small size, simple setup, high sensitivity, robustness and low costs have shown a high potential on the way to be implemented into common silicon based platforms. For metal oxide materials, the gas interaction process proceeds via a gas adsorption at lattice oxygen sites (O_{lat}) or terminal hydroxyl groups (-OH) on the semiconductor surface.[6,7] These sites can be described as target receptors.[8] Depending on the oxidative or reductive character of the gas species, the charge carrier density (electrons or holes in case of n- or p-type materials respectively) within the material surface area is modulated via a chemical interaction with intrinsic oxygen vacancies ($V_O^{\bullet\bullet}$) as described for oxygen by equation (1):

$$\tfrac{1}{2}\,O_2 + V_O^{\bullet\bullet} + 2e^- \rightleftharpoons O_{lat}^{2-} \qquad (1)$$

Nano structuring of sensing materials led to significant improvements in terms of sensitivity due to high surface to volume ratios and defined conduction channels.[9,10] However, the unspecific adsorption and redox interaction of the native oxygen receptors cannot discriminate specific gases. Additionally, high activation energies, delivered by external heaters or UV light sources, are needed to facilitate the gas-surface interactions and create a measurable signal to monitor the surface processes (e.g. voltage or conductance).

So far there are no specific concepts to overcome these limitations. Therefore, this thesis is devoted (a) to develop a new pathway for gas selective semiconductor based gas sensors beyond current technologies and (b) to realize a sensor concept that is capable to operate without the need of external energy sources. Finally, both principles should be implemented in one device to accomplish both criteria of selectivity and low power consumption in one material system.

1.1 Selective Sensing

Previous works towards the development of gas-specific “electric noses” were concentrating on inorganic modifications of metal oxides with noble metals,[8,11] chemically reversible hetero materials, as CuO [12] or Ag_2O [8] or statistical analyses of sensor arrays.[13–15] Nevertheless, these devices go along with restricted diversity of targeted gas species or a high system complexity. In contrast to those systems, the human olfactory system is based

on organic structures and can discriminate up to one trillion distinct odors, even at concentrations in the range of parts per billion (ppb).[16]

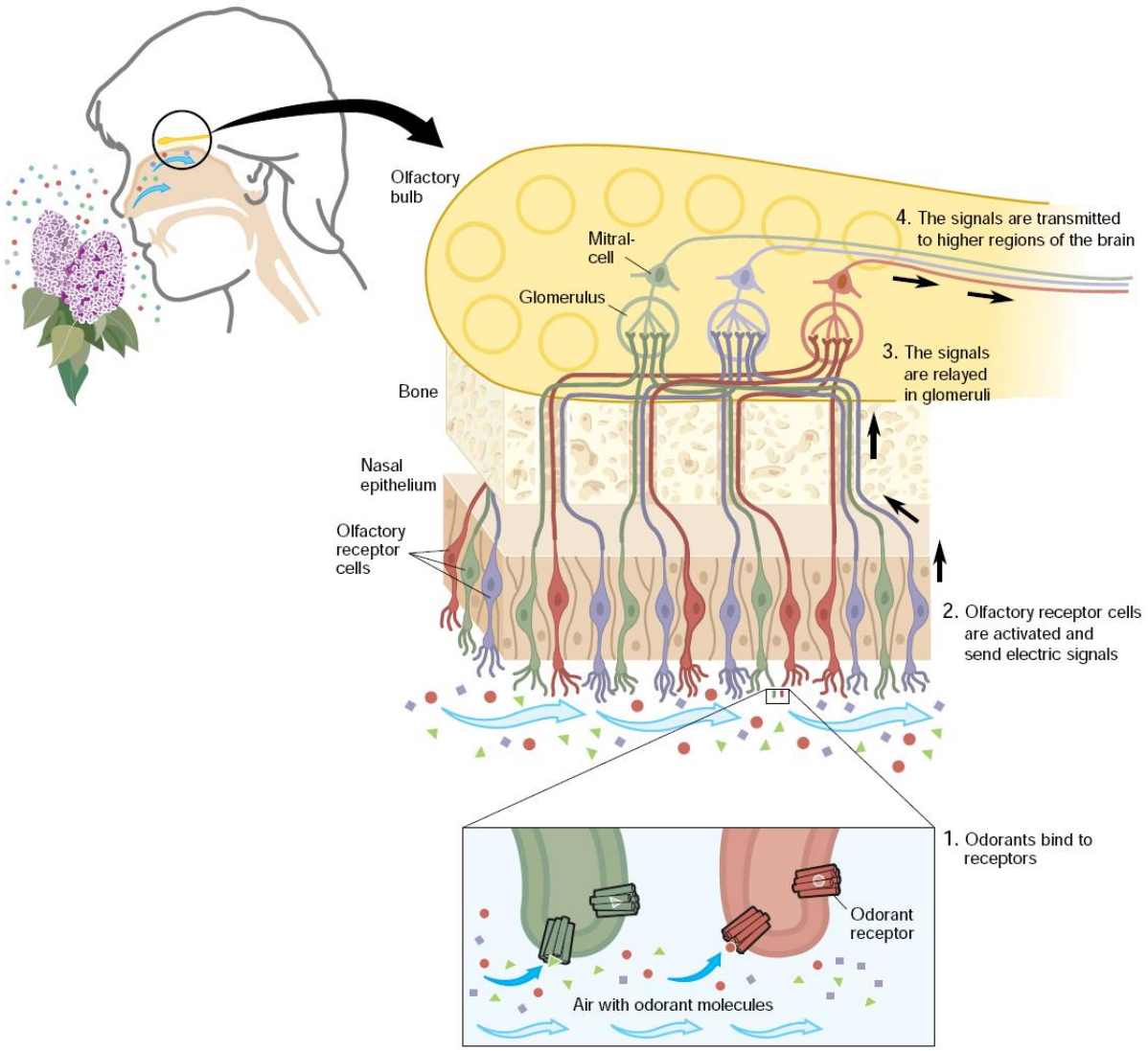

Fig. 1.2: The organization of the human olfactory system with schematic illustration of odorant receptor proteins as molecular binding sites (reprinted from *The Nobel Assembly at Karolinska Institutet*).[17]

The recognition of certain molecular specie begins with a binding interaction of a receptor protein and a consequent signal transduction trough the receptor cells to the brain. A mimicking concept with receptor proteins or antibodies and inorganic nanowires (NWs) as signal transduction paths has been successfully applied for the detection of biological targets in the liquid phase.[18–20] Even selective orthogonal on/off response characteristics could be achieved. Recent works indicate that organic surface modifications could also play an important role as specific and flexible receptors for selective target discrimination in the gaseous phase.[21–24] In contrast to these works introduced until today, the obtained studies of

the here presented thesis indicate that not only the selective binding interaction between the organic receptor and a gas species, but more importantly the mechanism of the charge transfer process between the organic surface molecules and the inorganic semiconductor material are critical for a selective sensing. Therefore, a brief insight into these organic-inorganic interface charge transfers will be given prior to a discussion of the relatively new field of hybrid gas sensor systems.

Electrical modulation of semiconductors by organic surface molecules

An obvious method for the deposition of organic components on inorganic materials is the plain physical vapour deposition (PVD) under vacuum conditions.[25,26] The control of the layer thickness and conformal deposition, however, is not easy to control and requires high analytical efforts and optimization. Alternatively, self-assembled monolayers (SAMs) represent a very convenient way to modify the surface of semiconducting materials with organic functionalities. SAMs are formed by the adsorption of molecular constituents from the gas phase or solution. These molecules possess a terminal chemical functionality with high affinity to bind with the material surface (head group) and a tail with desired chemical composition (see figure 1.3).[26,27] Binding to material surfaces can occur e.g. via condensation reactions (as in case of reactions of silanes with metal oxides), hydrogen substitution (Thioles with gold) or π-π interactions (terminal aromatic groups with carbon nanotubes). The saturation of the material surface after adsorption of the first organic monolayer prevents the biding of further monomers, as no more free sites of the semiconductor surface are accessible.

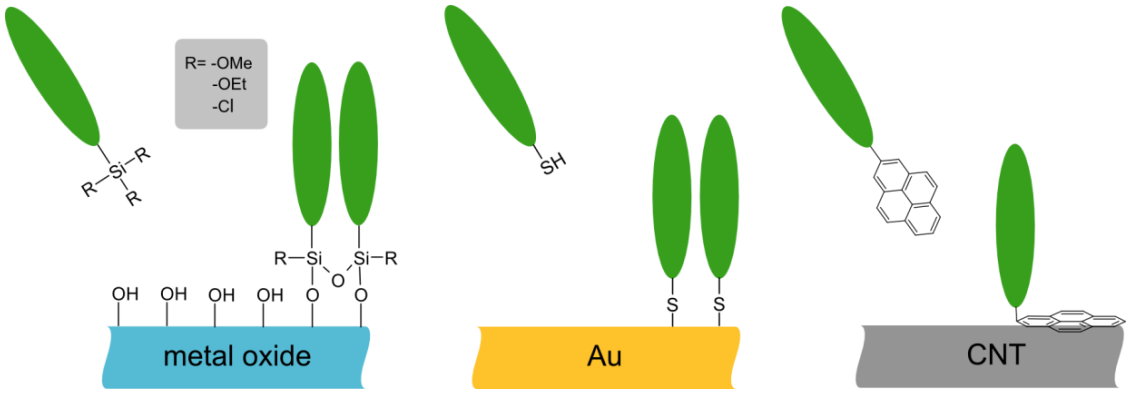

Fig. 1.3: Schematic description of SAM formation on semiconductor surfaces and exemplary redpresentation of surface affine head groups for immobilizations on metal oxides, gold,[26] and CNTs.[28]

When organic molecules get in contact with a surface of inorganic materials, the electrical properties of the semiconducting material can be considerably changed. The use of nanomaterials, (e.g. quasi 1D NWs) is beneficial for this interplay, as the reduced radius of

these structures causes a higher fraction of the surface area (*S*) in comparison to the volume of the bulk material (*V*):

$$\frac{S}{V} = \frac{2\pi r l}{\pi r^2 l} = \frac{2}{r} \qquad (2)$$

Here, *r* is the radius and *l* the length of the NW. It is evident from equation 2 that the surface to volume ratio (*S/V*) is increased with decreasing NW radius. Consequently, the SAM modified surface has a stronger influence on the overall material properties for nano sized materials compared to their macroscopic counterparts.

Beside the size effect of the NW, the donor/acceptor properties of the organic counterpart, as well as the bulk work function are responsible for the materials electrical modulation.[29] Kong *et al.* already reported in 2001 that the adsorption of amine containing organic SAM, formed by the surface immobilization of 3′-(aminopropyl)tri-ethoxysilane (APTES), had a considerable influence on the electrical conductance of semiconducting p-type carbon nanotubes (CNT).[30] It was proposed that these changes were induced by electron donation from APTES to p-CNTs and a consequent reduction of the p-type charge carriers. This effect was described as *chemical gating*. Although a lack in theoretical understanding of the underlying charge transfer mechanism was mentioned in this study, this term is still used to describe the electrical response of organic surface modified biosensors after target binding.[19,31]

Qi *et al.* could develop a model to describe the electronic states and charge transfer interactions of strong organic electron acceptor groups and intrinsically undoped bulk materials before and after a direct contact or binding interactions.[25,32] The consequent phenomenon of induced bulk conductivity is known as *surface transfer doping*. In this study, intrinsically non-conductive hydrogenated diamond (diamond:H) and the strong organic electron acceptor tetrafluoro-tetracyanoquinodimethane (F_4-TCNQ, el. affinity: χ = 5.24 eV) were used. As F_4-TCQN has no affine head group, the molecules were deposited by simple evaporation. Photoemission spectroscopy (PES) experiments of core levels (CL) and valence regions (VR) before and during the organic deposition clearly demonstrated shifts of the intrinsic energy levels that were interpreted as upward bend bending at the diamond:H surface and the formation of an interface dipole with negative charge on the electron accepting organic group. In other words, these findings described a charge transfer from diamond to the electron affine F_4-TCNQ, resulting in a p-doping close to the interface, as an access of holes was created in the diamond valence band (VB) (see figure 1.4).

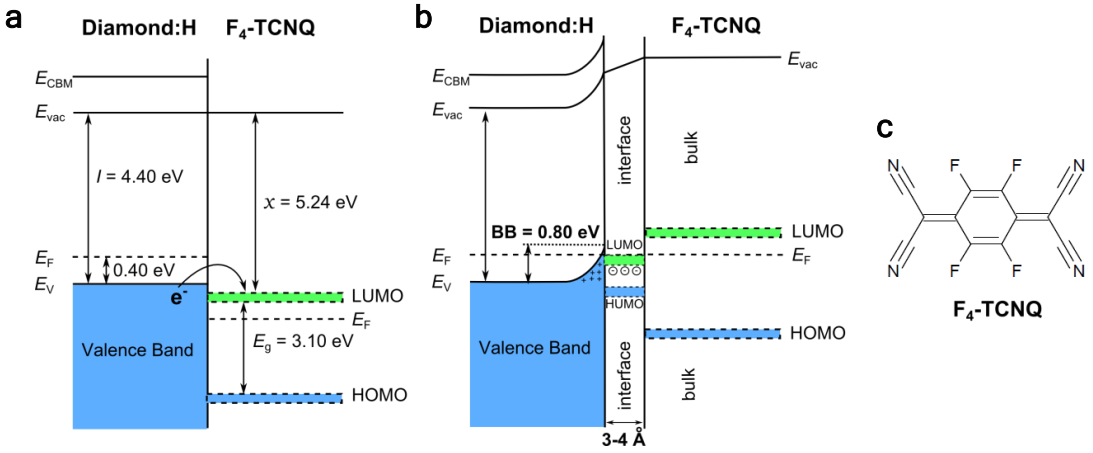

Fig. 1.4: Schematic energy diagram of bulk material (hydrogenated diamond) and an organic electron acceptor (F4-TCNQ) (a) before and (b) after surface transfer doping.[32] (c) Chemical structure of F_4-TCNQ.

A critical requirement for an efficient charge transfer from bulk to the electron acceptor is a lower energetic position of the lowest unoccupied molecular orbital (LUMO) of the organic acceptor with respect to the bulk Fermi energy (E_F). The electron transfer proceeds until the LUMO energy position aligns with the bulk E_F. Notably, no further charge transfer was observed with ongoing acceptor deposition after the first organic monolayer.

The same effect of surface doping by an organic surface functionalization was observed for bulk organic semiconductors, as single crystalline rubrene, when fluorinated SAMs as (tridecafluoro-1,1,2,2-tetrahydrooctyl)trichlorosilane (FTS) were attached to their surface.[33] A conductivity increase as big as five orders of magnitude could be observed in such a system with respect to the unmodified material.

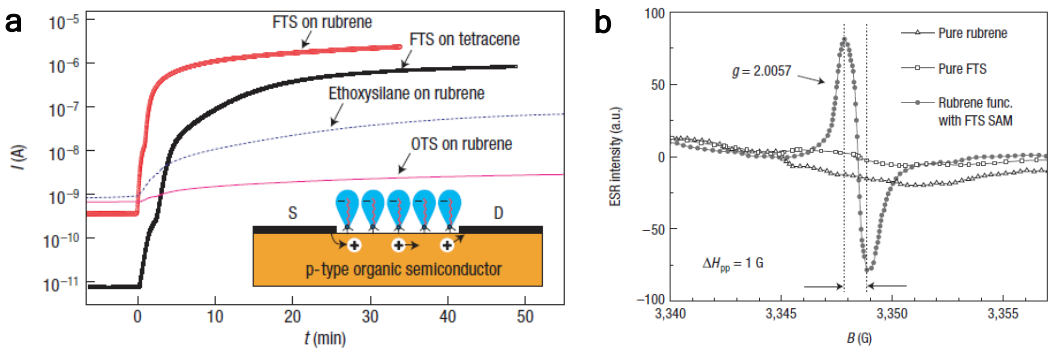

Fig. 1.5: a) *In situ* semi-log plot of the source-drain current for organic semiconductors (rubrene, tetracene) during SAM deposition. Fluorinated (FTS) and non fluorinated SAMs (Ethoxysilane, OTS) were deposited at $t = 0$. b) Electron spin resonance (ESR) spectra of pure and combined components (semiconductor, SAM). The pronounced resonance indicates unpaired electrons as well as delocalized holes for the rubrene/FTS-SAM system. (Reprinted by permission from Macmillan Publishers Ltd: Nat. Mater [33], copyright 2008.)

As in the case of diamond:H, the strong electron withdrawing ability of the SAMs lead to an efficient charge transfer, leaving unpaired electrons (transferred to the SAM), as well as delocalized holes (charge carriers in the semiconductor) in the semiconductor (see figure 1.5).

From the above mentioned studies it can be concluded that organic monolayers can strongly influence the electrical properties of semiconducting materials by modulating their charge carrier concentrations close to the bulk-organic interface. For this reason, the use of nano structured semiconductors with high surface to volume ratio is beneficial to achieve a strong deviation of the initial electronic properties. The electron affinity (χ) of the organic monolayer, which is defined by the LUMO position with respect to the vacuum level (E_{vac}), is the most critical parameter for an efficient charge transfer. It is shown in the here presented thesis that binding interactions of gas molecules to SAMs modulate the LUMO energy of the organic surface molecules. A mechanism how these modulations can lead to a selective response of a SAM-NW sensor system is described in the papers 1 and 4.

Recent developments in the field of SAM-NW hybrid bio/gas sensors

Organic surface modifications were used first to gain selectivity for NW based biosensors in liquid phase. Antibodies,[19] peptides,[34] as well as single stranded DNA[35] were used as receptor groups. However, the detailed charge transfer mechanism between the organic surface component and the semiconductor antenna was not taken into account systematically, but the selectivity was meant to be exclusively induced by selective target-receptor binding and consequent changes of the NW surface potential (Ψ_0). The relationship between Ψ_0 and the charge (σ_0) of the sensor conduction channel (here the NW) is usually described by the *Graham equation*:[3]

$$\sigma_o = \sqrt{8\varepsilon_W \varepsilon_0 kTC_o}\,\sinh\left(\frac{e\Psi_o}{2kT}\right) \qquad (3)$$

Where k is the Bolzmann constant, T is the temperature, e the elementary charge, ε_0 the permittivity of free space ε_w the dielectric constant of water, and C_0 is the ionic strength of the buffer solution. In the case of bio sensing, a wide know how about these key-lock interactions from well understood fields of biotechnology could be transferred to new nanotechnology applications. Antibodies can be designed as counterpart for defined antigens, as cancer marker proteins or viruses, by methods as recombinant *in vitro* antibody production techniques.[36] As the chemical and sterical structure of a targeted antigen possesses a number of specific binding sites and characteristic structural properties, which are reflected in the structure of the adequate antibody, a very specific binding interaction can be achieved.[37–39] The first NW biosensor based on this concept was described by Lieber

et al. in 2001 for the biotin/m-antibiotin target/receptor couple and silicon NWs as electric channel material.[40] Furthermore, the same group could develop this system to realize antibody functionalized NW sensors that showed an extraordinary selectivity towards respective parostate cancer markers in concentrations as low as 0.9 pg/mL. The fact that these measurements were performed using undiluted serum samples indicated the high potential for diagnosis applications.[19] The principle of key-lock interactions is also used for the detection of single stranded DNA (ssDNA) by immobilizing DNA strands with a respective amino acid sequence to achieve specific DNA hybridization.[41,42]

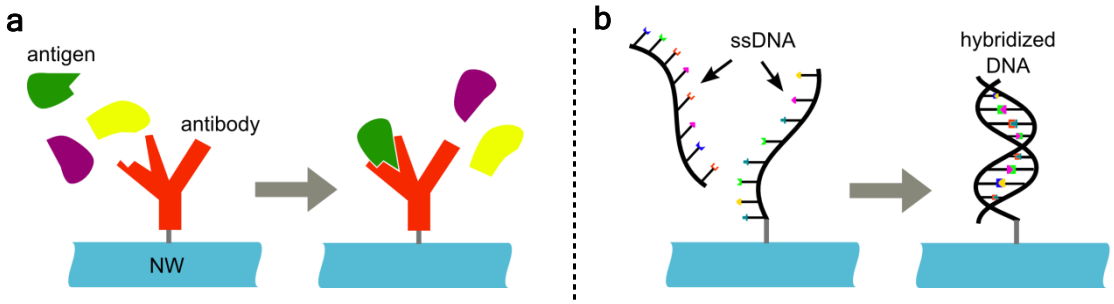

Fig. 1.5: Schematic illustration of biosensor concepts based on specific a) antibody-antigen binding and b) hybridization of immobilized receptor- and target DNA strands.

These hybridization interactions can be monitored with a very high accuracy and low noise level. Therefore, it was possible to perform even single molecule measurements with high time resolutions in the micro second range,, using a point defect CNT based FET system. Beside specific on/off detection signals, even characteristics of the molecular interaction kinetics, as temperature dependent dwell-time of target ssDNA, could be studied.[35,43]

The use of organic receptor molecules for biosensors is evident, as these immobilized species possess similar sizes, functionalities and atomic structures compared to the targeted antigens. On the same time, organic structures can be realized in an infinite number of variations of primary or secondary structures to accomplish the desired functionality. Learning from natural olfactory systems, the use of defined organic receptors, also for small molecules in the gas phase, seems to be a very promising route to solve current selectivity issues of pure inorganic semiconductor sensors. Up to date, just a few works have been presented to study the potential of well defined organic/inorganic hybrid materials for gas sensing applications. In 2008, McAlpine *et al.* used silicon nanowires decorated with known recognition peptides for the detection of acetic acid and ammonia vapours in dry nitrogen.[44] For relatively high concentration of 100 ppm, a remarkable discrimination could be observed in presence of interfering gases, as CO_2 and acetone. As the peptide-target interaction causes a protonation or deprotonation of the peptide in case of acidic acid or ammonia, respectively, the sensor signal was found to be not reversible. Additionally, the

absence of stabilizing buffer solution, as in case of biosensing experiments, led to insufficient peptide stability in presence of even very low humidity values. Possibly, the loss of the protein secondary structure after water adsorption caused the loss of the specific binding ability with the respective target molecule.

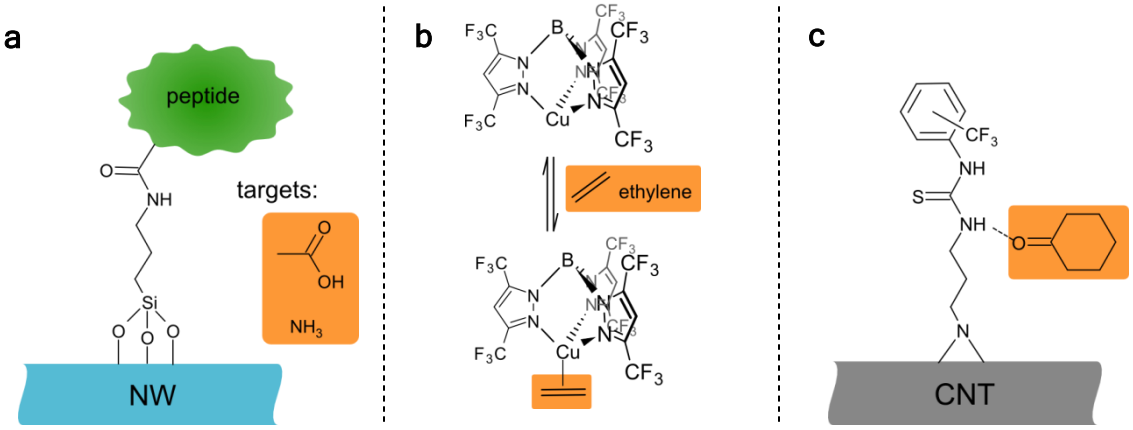

Fig. 1.6: Different approaches for the realization of gas sensors with organic receptor units: a) Covalent immobilization of tailored ammonia or acetic acid binding peptides;[44] b) metal-organic Cu(I) complexes as receptors for none polar ethylene molecules[23] and c) pure organic thiourea SAMs for the detection of cyclophenon vapours.[45]

A direct transfer of hybrid biosensor concepts to gas sensors by using tailored protein modifications seems to have stability limitations, as the target-receptor interactions take place in none physiological conditions. On the other hand, the small dimension and lower structural complexity of gas molecules, compared to biological antigens, lowers the influence of shape controlled key-lock interactions with receptors. Very recently, pure chemical interactions with receptors in sizes comparable to gaseous targets and secondary structures were found to be very powerful receptors and more stable in gaseous environments. Esser *et al.* used single walled CNTs (SWCNT) modified with organo-metallic Cu(I) complexes for the detection of small and none polar ethylene molecules in the sub-ppm range and with a noticeable selectivity.[23] Other than SAM systems, the metal-organic complex molecules were not covalently bond to the CNT surface, but just mixed in solution and the mixture was drop-casted on an interdigitated electrode. Possibly, the loose interaction between CNT and Cu(II) species led to relatively low sensitivities (sensitivity ~1% for 50 ppm). This system mimics the natural ETR1 ethylene binding receptor, but concentrates only on the essential Cu(I) binding site of the complex protein structure. Such strategies are well known and established in the development of metal-organic and pure organic catalysts,[46–50] as further reduction of the receptor construction leads to purely organic functionalities. Such systems have been demonstrated for the detection of volatile

organic compounds[15,51,52] and explosives.[45,53] Nevertheless, although remarkably higher system sensitivities compared to unmodified materials could be achieved, these systems could not deliver satisfying selectivity towards singular gas species, unless complex pattern recognition algorithms were applied. Up to date, all surface modified hybrid gas sensors systems have been studied empirically. Especially for pure organic SAMs, the chemical and electrical interactions of the NW-SAM-gas systems are not well understood. Schorr *et al.* very recently tried to understand the binding interaction between thiourea functionalized CNTs with cyclohexanone targets by nuclear magnetic resonance (NMR) studies (see figure 1.7c).[45] A direct correlation with interactions in the gas phase is not evident, as these experiments were performed in liquid phase and solvent effects can influence the interaction of both components.[54] The systematic development of tailored hybrid gas sensors -selective towards specific gas species- will need systematic studies not only on binding interactions, but also on the electronic structure that can result in efficient charge transfer and resulting changes in the monitored NW resistivity. The here presented thesis, therefore, is aiming to develop highly selective hybrid sensor systems on one hand, and understand the underlying sensing mechanisms (see papers 1 and 4). The reduction of complexity, in terms of the organic SAMs structure, enables the use of theoretical density functional theory (DFT) methods, and gives insights into molecular and electronic interaction mechanisms that are far beyond the resolution of current experimental analytics. This understanding of the NW-SAM-gas charge transfer and gas-SAM chemical interactions, combined with experimental sensing results will be further used to develop conditions for optimized device operation.

1.2 Self-Powered Gas Sensing

The last two decades of technical development where mainly dictated by groundbreaking innovations in the field of information technologies. Today, there is a wide availability of powerful and compact mobile devices for communication, identification, positioning, tracking or management.[55] Especially within the last few years, the integration of such units in the “internet of things” enabled the correlation of multiple parameters from large areas to gain complex information and a new level of informative value.[56,57] As mentioned earlier, the integration of selective gas sensors in such platforms and their connection in wide spread networks would open the possibility to monitor the atmospheric quality for areas of interest with high local resolution and not only at discrete spots. However, the used sensors must be operated self-sustained and maintenance free conditions to ensure an affordable and

continuous application. The major requirement is a minimal power consumption of the active device to ensure applicable battery lifetimes and costs per piece. Within the past five years, first concepts have been developed to remarkably reduce the energy demand of sensor elements[58] or to integrate separate energy harvesting components with sensors to accomplish self-powered operation of the combined system.[5,59–61] Prades *et al.* made use of the small dimension of a single SnO_2 NW to induce *self-heating* at higher applied currents (>10 nA) and thus, achieved a thermal activation of the semiconductor surface without the need of an external heater (see figure 1.8).[58] This effect could be attained due to the low NW diameter (<100 nm) and a reverse biased SnO_2-Pt Shottky contact (deposited by focused ion beam (FIB) lithography) that posses both a high resistivity (MΩ range). The tiny energy demand (W range) of the nano sized single NW sensor element further enabled the use of a conventional thermoelectric microgenerator (external energy harvester) to realize a self-powered sensor system.[5]

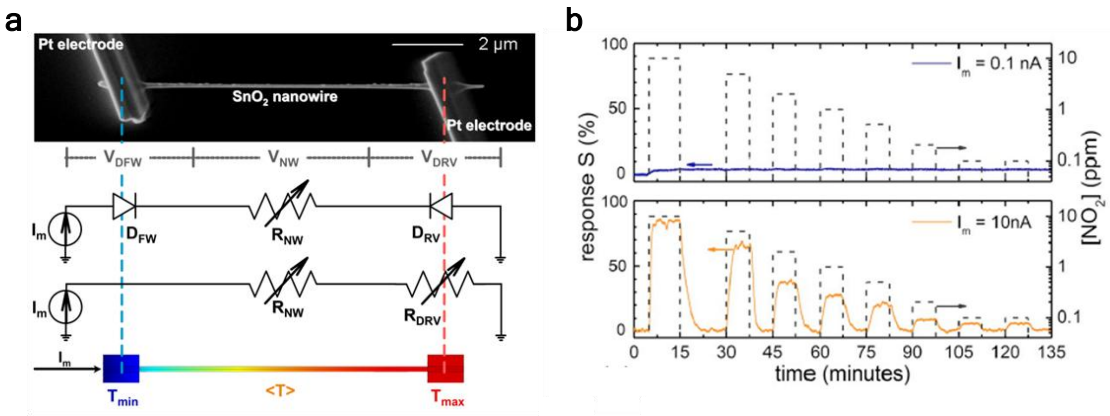

Fig. 1.8: (a) SEM image of a single SnO_2 NW contacted by FIB lithography and schematic illustration of the device resistance, as well as heat induced by the *Joule effect* upon currents ≥10 nA. (b) Sensor responses revealing a thermal SnO_2 surface activation at applied currents ≥10 nA.[58] (Reprinted with permission from [58]. Copyright 2008, AIP Publishing LLC)

The same concept of combining an energy harvesting component and a sensor element in a combined system was used by Wang *et al.*. Most of these works were concentrating on ZnO nanogenerators as energy harvesting unit.[55,60,62,63] These nanogenerators use the piezoelectric effect, induced by changing the compressive stress applied on ZnO NWs, to harvest mechanical energy from the environment (output power up to $P \approx 31.2$ mW/cm^3).[64–66] Mechanical energies are originated from sonic waves, friction or vibrations and thus are a steady energy source to drive sensors in a sustained operation.

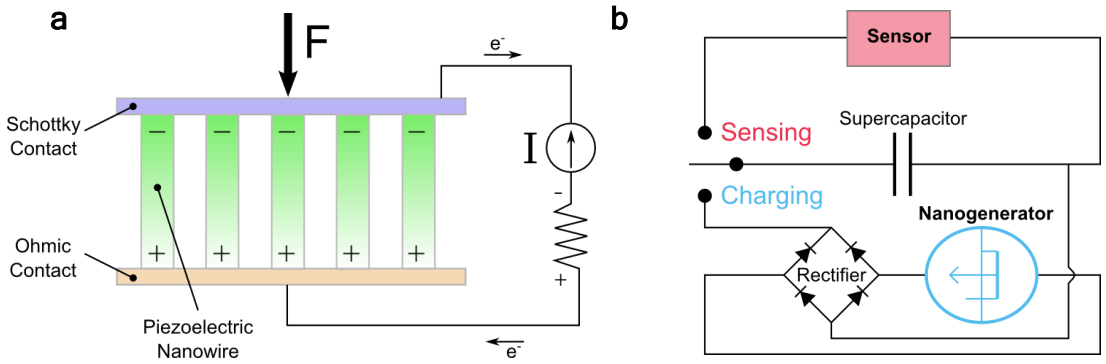

Fig. 1.9: Schemes of a) the working principle of a piezoelectric nanogenerator and b) the integration of sensing and charging units to realize self-powered sensing operations.

By integrating energy storage units, (e.g. Li-ion batteries or super capacitors) as a third component into the sensor system, further stability of the operation could be achieved. These devices can change between a charging and sensing mode. During charging mode, the energy harvesting unit is charging the energy storage unit. For the sensing mode, the storage unit is supplying energy to the sensing unit for detection of the appropriate target.[55] As the self-powered sensor systems are assemblies of individual components, the nature of energy harvesting and sensor units are flexible and can by chosen by the appropriate application. Alternatively to energy harvesting nanogenerators, microbial fuel cells (MFC, $P = 30\ \mu W/cm^2$)[67] or combined hybrid cells could be used. The latter are combined systems of nanogenerators and solar cells or MFS ($P_{max} = 100\ mW/cm^2$).[61,68,69] These combinations could deliver higher energies to the sensor system, due to simultaneous energy harvesting of different environmental energies. Additionally, the sustained power supply, even in absence of one kind of energy, is ensured and allows for a continuous device operation. Although sensors for the detection of pH-values, UV-light or metal ions could be used for such combined systems, the high energy demand of conventional and low cost gas sensors, that is usually in the order of a few hundreds of mW,[70] was disabling an applications in combined harvester/sensor systems.

To overcome the limitations of self-powered sensors for gas sensing applications, a new concept is presented in this thesis. Different from existing approaches, the developed gas sensor device unifies energy harvesting and sensing unit in a singular multifunctional heterostructure. Thus, there is no need of combining two individual components, with consequent decrease of system costs and complexity. Solar light was used as exclusive energy source to (a) facilitate the gas-sensor interaction and (b) generate the monitored sensor signal. The relevant results are presented in the papers 2 and 3.

1.3 Dissertation Outline

The guideline of the here presented PhD thesis was defined by **objectives** that are summarized in the following chapter (*Chapter 2: Objectives*)

The **results** of the PhD work and their detailed **discussion** are presented in three sections (*Chapter 3: Results and Discussion)*, namely: 1-*Selective Sensing*, 2-*Self-Powered Sensing,* and 3-*Combination of Selective and Self-Powered Sensing*. Each section is introduced by a short description of the presented content, followed by the main results obtained (as they were published in scientific peer-review journals), and finally the most significant results are summarized with special focus on the classification in the state of the art research.

The consequent chapter (*Chapter 4: Conclusion*) gives a **conclusion** of the most significant results obtained during the PhD thesis work

Finally, this thesis will present an **outlook** on following activities within the topics of selective and self-powered gas sensors. These upcoming research work will be based on the results of the here presented work and should extend the principles to develop selective sensors towards different target gases and realize highly integrated low power sensing platforms.

Only the publications contained in this list shall be considered for the evaluation of this Ph.D Dissertation. A copy of all these publications can be found in the page indicated.

Section 1:

1. Hoffmann, M. W. G.; Prades, J. D; Mayrhofer, L.; Hernandez-Ramirez, F.: Moseler, M.; Waag, A. and Shen, H. "Highly selective SAM-nanowire hybrid NO_2 sensor: insight into charge transfer dynamics and alignment of frontier molecular orbitals", *Adv. Funct. Mater.* 24, 595–602 (2014). (impact factor: 10.4; inside cover 5/2014) **Page 23**
2. Shao, F.; Hoffmann, M. W. G; Prades, J. D; Zamani, R; Arbiol, J.; Morante, J. R.; Varechkina, E.; Rumantseva, M.; Gaskov, A.; Giebelhaus, I.; Fischer, T.; Mathur, S.; Hernandez-Ramirez, F., "Heterostructured p-CuO (Nanoparticle)/n-SnO_2 (Nanowire) Devices for Selective H_2S Detection", *Sens. Actuat. B* 181, 130-135 (2013). (impact factor: 3.8) **Page 51**

Section 2:

3. Hoffmann, M. W. G.; Gad, A.; Prades, J. D.; Hernandez-Ramirez, F.; Fiz, R.; Shen, H.; Mathur, S., "Solar diode sensor: Sensing mechanism and applications", *Nano Energy* 2, 514–522 (2013). (impact factor: 10.2) **Page 61**
4. Gad, A. E.; Hoffmann, M. W. G.; Hernandez-Ramirez, F.; Prades, J. D.; Shen, H.; Mathur, S., "Coaxial p-Si/n-ZnO nanowire heterostructures for energy and sensing applications", *Mater. Chem. Phys.* 135, 618–622 (2012). (impact factor: 2.1) **Page 79**

Section 3:

5. Hoffmann, M. W. G.; Mayrhofer, L.; Casals, O.; Caccamo, L.; Hernandez-Ramirez, F.; Moseler, M.; Waag, A.; Shen, H.; Prades, J. D., "Highly selective and self-powered gas sensor enabled via organic surface functionalization", *Adv. Mater.*(2014) doi: 10.1002/adma.201403073. (impact factor: 15.4) **Page 87**

2

Objectives

The objectives of the here presented PhD thesis can be summarized in the following thematic line-up:

1. To develop a gas sensor system that possesses high target **selectivity** beyond the state of current technologies. This includes the understanding of the underlying mechanism to be able to extend the sensing concept for other target species.

2. To develop a gas sensor concept that can operate in a fully **self-powered** mode. The system should be designed in a way that it unifies sensing and powering unit in a singular unit.

3. To **combine** the previous results on concepts for **selective and self-powered** gas sensors in one system, to realize a device that fulfils these two major criteria on gas sensors.

3

Results and Discussion

In this chapter, the most relevant results of the PhD work and their discussions will be presented in form of papers published in peer reviewed scientific journals. In succession to the above described objectives of the here presented PhD thesis, the papers are organized in three sections:

- *Section 1*: Selective Sensing
- *Section 2*: Self-Powered Sensing
- *Section 3*: Combination of Selective and Self-Powered Sensing

In the first section, a hybrid organic-inorganic sensor system for highly specific NO_2 detection is presented. The gas sensing performances achieved by this system, in terms of selectivity and sensitivity, were far beyond the capabilities of NW based systems reported up to date. Further discussion of theoretical DFT simulations of the entire hybrid-gas system enabled the identification of crucial mechanistic parameters to achieve selectivity towards single gas species.

The second section is devoted to the development, mechanistic understanding and application of p-Si/n-ZnO heterostructures. During this PhD work, self-powered gas sensors could be realized using these materials, benefiting from its feasibility to generate a sensing signal and interact with the surrounding atmosphere just by harvesting solar light energy.

In the last section of this chapter, the principles of the two previous sections were combined to realize a highly selective and self-powered gas sensing device. Further mechanistic insights for both -selective gas detection by hybrid systems, as well as p-n heterostructures for efficient harvesting- are given in this section. Additionally, a new gas sensor platform was designed and fabricated by micro structuring techniques to ensure high signal intensities and flexibility in terms of inorganic and organic components.

3.1 Selective Sensing

Included paper 1:

Hoffmann, M. W. G.; Prades, J. D; Mayrhofer, L.; Hernandez-Ramirez, F.: Moseler, M.; Waag, A. and Shen, H. "Highly selective SAM-nanowire hybrid NO_2 sensor: insight into charge transfer dynamics and alignment of frontier molecular orbitals", *Adv. Funct. Mater.* 24, 595–602 (2014). (impact factor: 10.4; inside cover 5/2014)

Semiconductor based gas sensors are hampering from low selectivities toward specific gas molecules. The reason for this limitation is the underlying sensing mechanism based on the chemical redox reaction between inorganic surface oxygen groups (in case of metal oxide materials) and the surrounding gas atmosphere. In the here presented paper, organic surface functionalities were anchored as SAMs on a SnO_2 NW surface to gain highly specific gas interactions, caused by the organic surface receptors, that can be monitored by the NW resistance. Nitrogen oxide (NO_2) was chosen as targeted species, as it presents one of the major threads for human health, already in low concentrations (ppb level), and is a common pollutant in urban areas.[71] Different amine terminated methoxysilanes were evaluated as SAM receptors towards NO_2, as amines (nitrogen oxidation state: –II) were expected to act as electron donor when electron deficient nitrogen species –as in case of NO_2 (nitrogen oxidation state: +IV)– are present. Gas sensing experiments showed an extraordinary selectivity towards low concentrations of NO_2 (ppb level) in comparison to various gas species, i.e. usually interfering fossil combustion products (SO_2, CO, NO, CO_2), that were applied in notably higher concentrations (2 to 50,000 ppm). Among the tested amine species, N-[3-(trimethoxysilyl)-propyl]ethylenediamine (en-APTAS) unified the best performances in both, selectivity and sensitivity towards NO_2. It could be shown that fast response/recovery characteristics, as well as quantitative sensing results can be achieved by illuminating the active sensor surface with visible light in the range of 480-680 nm wavelength.

The simulation of the entire NW-SAM-gas system via DFT methods could identify the crucial parameters for the high selectivity achieved for the SnO_2/en-APTAS system towards NO_2. It could be shown that the energy of the lowest unoccupied molecular orbital (LUMO), formed by the en-APTAS/NO_2 system, was well below the *Fermi Energy* of the SAM modified SnO_2 NW. In this case, an efficient charge transfer was enabled from the NW via the SAM to NO_2. The consequent depletion of charge carriers (electrons) at the n-type SnO_2 surface area caused the monitored increase of resistance. Simulations for other gases (SO_2, NO, CO, CO_2)

resulted in unfavourable energy alignments and thus were consistent with the obtained experimental results, where no response was observed in presence of these species.
Summarized, this paper contains the following aspects on the development of a selective gas sensor system:

- Synthetic realization and chemical analysis of the hybrid sensor material.
- Evaluation of the gas sensing characteristics towards NO_2, as well as common interfering gas species.
- Evaluation of optimal operation conditions in terms of response/recovery characteristics and quantitative sensing results.
- Theoretical identification of crucial parameters to reconstruct the underlying sensing mechanism of the NW-SAM-gas system.

Included paper 2:

Shao, F.; Hoffmann, M. W. G; Prades, J. D; Zamani, R; Arbiol, J.; Morante, J. R.; Varechkina, E.; Rumantseva, M.; Gaskov, A.; Giebelhaus, I.; Fischer, T.; Mathur, S.; Hernandez-Ramirez, F., "Heterostructured p-CuO (Nanoparticle)/n-SnO_2 (Nanowire) Devices for Selective H_2S Detection", *Sens. Actuat. B* 181, 130-135 (2013). (impact factor: 3.8)

For certain sensor-gas couples selective detection phenomena can be observed even for pure inorganic systems. As a matter of fact, such behaviour is given for p-CuO/n-SnO_2 hererostructures when they are exposed to dihydrogen sulphide (H_2S) containing atmospheres. Here, the effect can be attributed to the reaction of p-type CuO with H_2S to form CuS. In absence of H_2S, p-CuO forms a p-n heterojunction with n-SnO_2 and thus, a carrier (electrons) depleted zone is formed at their interface. In presence of H_2S, p-CuO is converted to CuS and consequently, the electron depletion zone is vanished at the SnO_2 interface. In the study presented in **paper 2**, a p-CuO NP/SnO_2 NW heterostructure was used with SnO_2 NWs as conductive channel. Due to variations of the chemical/electrical properties of Cu-based semiconductor NPs on the NW surface, the resistance of the SnO_2 NWs was gated and a very high response with sharp decrease of resistance in presence of H_2S gas could be observed. As the sensitivity of such heterostructures was found to be clearly above the values observed for bare SnO_2 systems, the effect could be attributed of the p-CuO(CuS)/n-SnO_2 heterostructure. Additionally, a good selectivity for H_2S could be observed in comparison to NH_3 and CO species. This study describes the influence of a surface bound component, which undergoes selective interactions with the gas phase (p-CuO), on the monitored semiconductor (n-SnO_2). As this principle is also present in case of

organic-inorganic hybrid sensor systems, the evaluation of such effects provides an additional understanding for sensing interactions of selective sensor heterostructures.
In summary, paper 2 presents the following aspects:

- Experimental realization and analysis of p-CuO NP/n-SnO_2 NW heterostructures.
- Evaluation of gas sensing characteristics for single- and multiwire devices.
- Discussion of the selective sensing mechanism for the pure inorganic sensor system.

3.1.1 Paper 1

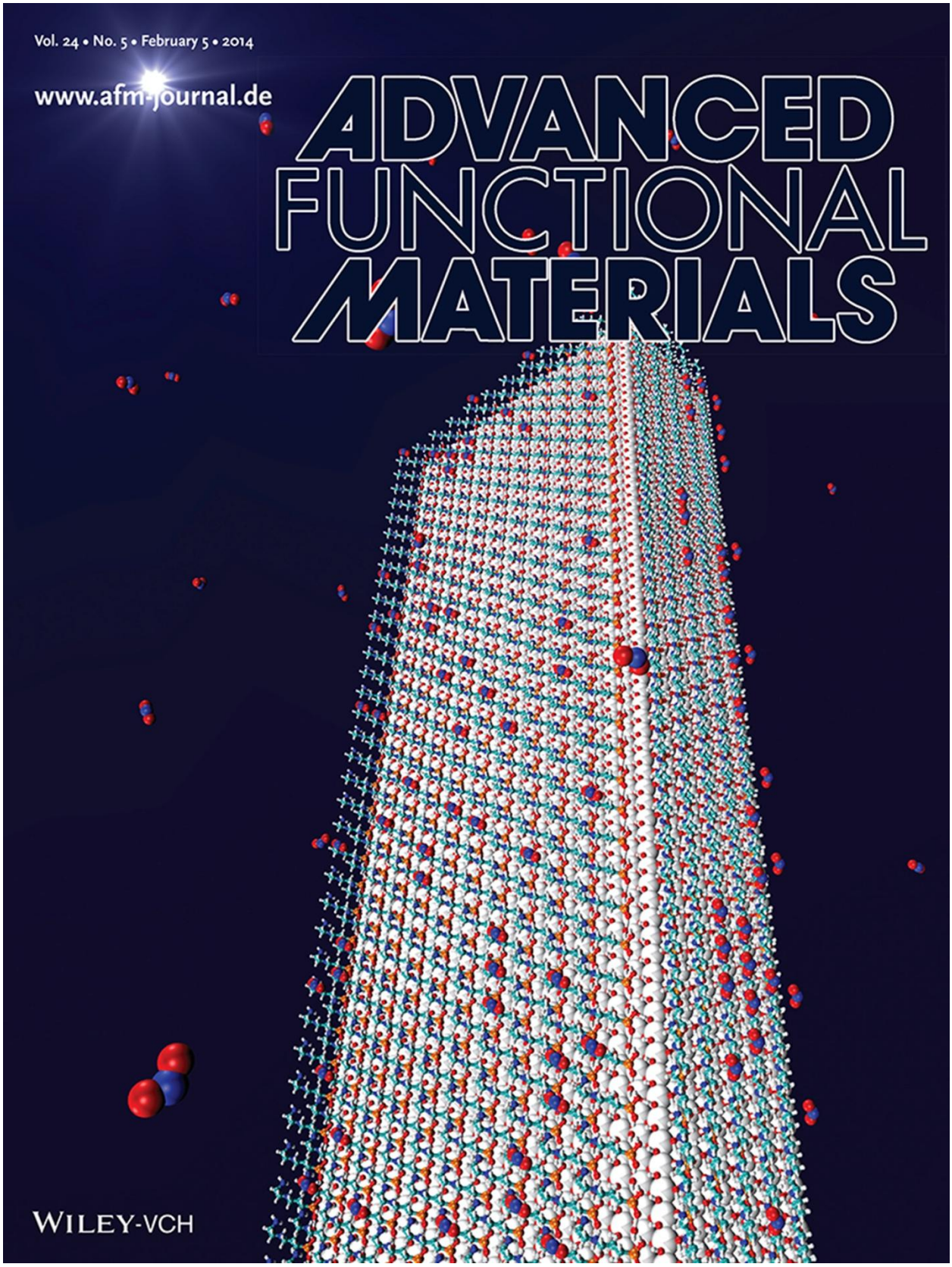
Vol. 24 • No. 5 • February 5 • 2014
www.afm-journal.de
ADVANCED FUNCTIONAL MATERIALS
WILEY-VCH

Materials Views
www.MaterialsViews.com

ADVANCED FUNCTIONAL MATERIALS
www.afm-journal.de

FULL PAPER

Highly Selective SAM–Nanowire Hybrid NO_2 Sensor: Insight into Charge Transfer Dynamics and Alignment of Frontier Molecular Orbitals

Martin W. G. Hoffmann, Joan Daniel Prades, Leonhard Mayrhofer, Francisco Hernandez-Ramirez, Tommi T. Järvi, Michael Moseler, Andreas Waag, and Hao Shen**

Organic–inorganic hybrid gas sensors can offer outstanding performance in terms of selectivity and sensitivity towards single gas species. The enormous variety of organic functionalities enables novel flexibility of active sensor surfaces compared to commonly used pure inorganic materials, but goes along with an increase of system complexity that usually hinders a predictable sensor design. In this work, an ultra-selective NO_2 sensor is realized based on self-assembled monolayer (SAM)-modified semiconductor nanowires (NWs). The crucial chemical and electronic parameters for an effective interaction between the sensor and different gas species are identified using density functional theory simulations. The theoretical findings are consistent with the experimentally observed extraordinary selectivity and sensitivity of the amine-terminated SnO_2 NW towards NO_2. The energetic position of the SAM–gas frontier orbitals with respect to the NW Fermi level is the key to ensure or impede an efficient charge transfer between the NW and the gas. As this condition strongly depends on the gas species and the sensor system, these insights into the charge transfer mechanisms can have a substantial impact on the development of highly selective hybrid gas sensors.

1. Introduction

The selective detection of a certain predefined gas species is the most critical requirement in different fields like pollution and food control, health care, security or industrial process control. However, predictive strategies towards the development of highly selective nanostructured gas sensors are still missing.[1] Organo-functionalized low dimensional materials could already show improved characteristics in this field[2–9] compared to commonly used purely inorganic materials or heterostructures that usually suffer from unspecific surface interactions with the target gases.[10–14] Here, we present a sensor system composed of semiconductor nanowire (NW) surfaces with defined organic self-assembled monolayers (SAMs) in order to accomplish exclusive chemical and electronic conditions for the selective detection of a single gas species. We demonstrate that SnO_2 NWs (see Figure S1) modified with amine terminated SAMs show both extraordinary selectivity and sensitivity towards NO_2 at room temperature. This system can not only serve as a novel efficient and selective NO_2 sensor, but also as a model system for the theoretical reconstruction of crucial sensor-target interactions. Our simulations reveal that an energy level alignment of the SAM-gas system with the Fermi level of the SAM–NW system is the key to understand and achieve high detection selectivity and are consistent with our experimentally observed results. The use of organic functionalities at semiconductor nanostructures in combination with a thorough simulation of the detailed chemical and electronic surface configuration thus shows a convincing potential for the development of theoretically designed selective gas sensors,[15] with flexible organic surface design and predictable response.

Gaseous nitrogen dioxide (NO_2) is one of the most dangerous and wide spread global pollutants, as it can produce ozone, acid rain and respiratory ailments.[16] Moreover it is believed to cause cancer due to its high reactivity with genetic material and organic solvents, forming nitrosamines.[17] NO_2 is produced by various ubiquitous combustion processes such as car engines, power plants and cigarette smoke and affects the human health already in tiny concentrations (ppb level).[18] Usually nitrogen oxide species in pollutant and toxic emissions are specified as NO_x due to the diversity of possible nitrogen oxidation states,

M. W. G. Hoffmann, Dr. J. D. Prades, Dr. F. Hernandez-Ramirez
Department of Electronics
University of Barcelona
E-08028, Barcelona, Spain
E-mail: dprades@el.ub.es

M. W. G. Hoffmann, Prof. A. Waag, Dr. H. Shen
Institut für Halbleitertechnik
Technische Universität Braunschweig
D-38106, Braunschweig, Germany
E-mail: h.shen@tu-bs.de

Dr. L. Mayrhofer, Dr. T. T. Järvi, Prof. M. Moseler
Fraunhofer Institute for Mechanics of Materials IWM
D-79108, Freiburg, Germany

M. W. G. Hoffmann, Dr. F. Hernandez-Ramirez
Department of Advanced Materials for Energy Applications
Catalonia Institute for Energy Research (IREC)
E-08930, Barcelona, Spain

DOI: 10.1002/adfm.201301478

FULL PAPER

ADVANCED FUNCTIONAL MATERIALS
www.afm-journal.de

www.MaterialsViews.com

and the inability of current cost-effective monitoring systems to discriminate among them. However, it is critical to distinguish NO and NO_2, which are the major fractions, as they exhibit different properties in terms of toxicity, biological impact and chemical reactivity.[17,19] All this makes this case a paradigmatic and unsolved problem in low-cost gas monitoring technology.

2. Results and Discussion

2.1. Experimental Approach for an Initial Sensor System

To develop a strategy for coherent experimental and theoretical gas sensor design, an optimal organic functionalization of SnO_2 NWs for selective NO_2 detection was first evaluated experimentally. The identified system then served as starting point to build up a theoretical NW–SAM–gas model and define critical parameters for selective sensing interactions. Amines, due to their electron donating character, were chosen as functional units to achieve strong surface–gas interactions with the electron affine NO_2 target (**Figure 1**a).[19] This process was supposed to affect the carrier concentration profile of the semiconductor NW and thus its resistance to give a measurable sensor response (Figure 1b).[20–24] Different kinds of SAMs with primary, secondary, tertiary and mixed amine terminals were immobilized on the SnO_2 NW surface (Figures 1a, S1, S2).[25] X-ray photoemission spectroscopy (XPS) of immobilized *N*-[3-(trimethoxysilyl)propyl]ethylenediamine **1** (en-APTAS) showed

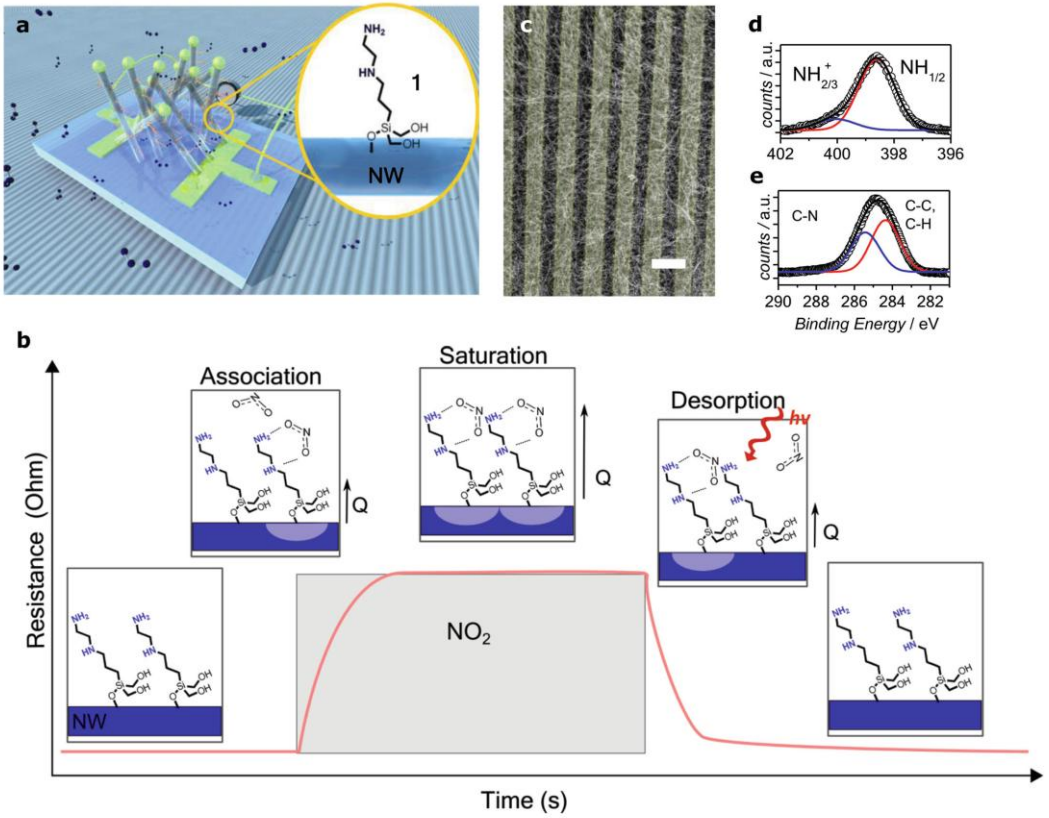

Figure 1. a) Schematic illustration of the selective NO_2 sensor. *N*-[3-(Trimethoxysilyl)propyl]ethylenediamine (en-APTAS 1) was immobilized on the surface of SnO_2 NWs which were directly grown on an interdigital gold electrode (5 µm spacings). The measured device resistance served as sensor signal. b) Schematic illustration of the NO_2 sensing mechanism by en-APTAS 1 modified NWs. With the introduction of NO_2, a SAM–gas interaction is established during the association process. The consequent electron transfer (Q) from the SAM to NO_2 is transduced to the NW and causes a charge depletion region that is monitored by an increasing sensor resistance. The depletion region is increased by additional NO_2-SAM interactions until saturation is reached. The cleaving of NO_2-SAM interactions by incident visible light during the desorption process leads to the initial unbound state and resistive character of the sensor. c) Scanning electron microscope (SEM) image of the en-APTAS 1 modified SnO_2 NWs with an average diameter of 47 ± 8 nm, grown on an interdigital electrode (scale bar, 10 µm). d) XPS N_{1s} of the en-APTAS 1 modified SnO_2 NWs showing binding energies of NH/NH_2 groups as well as small amounts of protonated NH_2^+/NH_3^+ groups that are shifted to higher binding energies in the N_{1s} spectra. e) Binding energies of C_{1s} spectra correspond to C–N and C–C/C–H groups of the SAM 1.

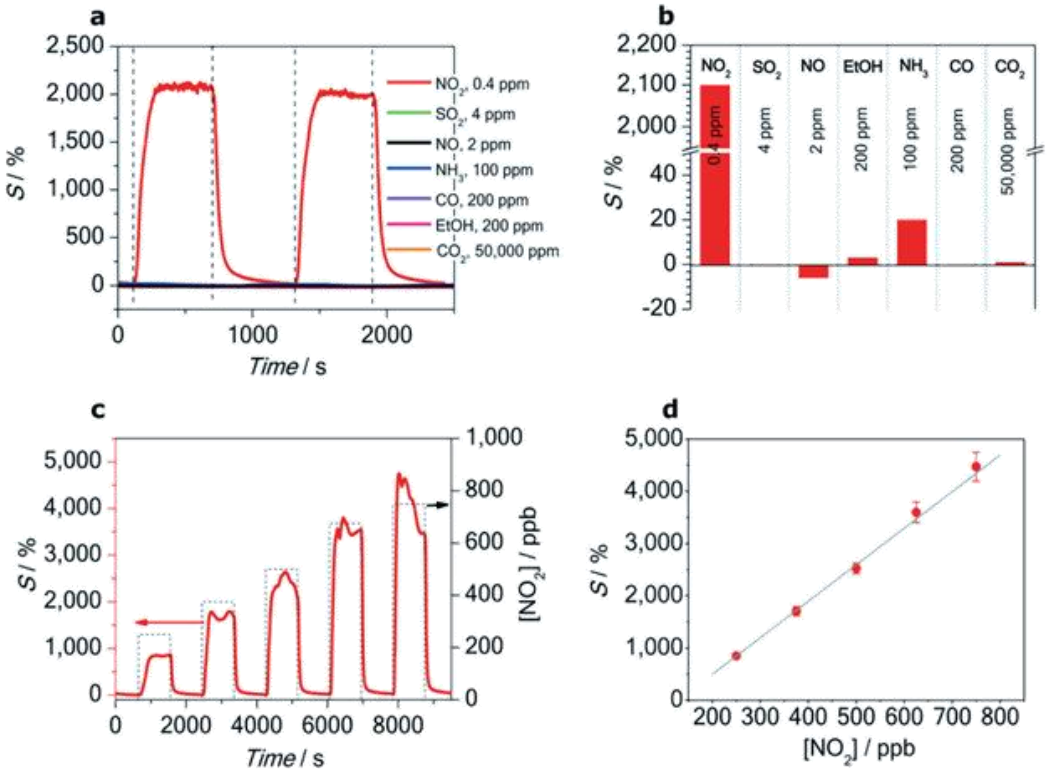

Figure 2. The en-APTAS **1** functionalized SnO_2 NW sensor measured under solar illumination (85 mW/cm^2). a) Pulses of 0.4 ppm NO_2, SO_2 (4 ppm), NO (2 ppm), NH_3 (100 ppm), ethanol (200 ppm), CO (200 ppm) and CO_2 (50,000 ppm). b) Summary of sensitivities towards the tested gases. c) Sensing response vs. different NO_2 concentrations ranging from 250 to 750 ppb in synthetic air. d) linear behaviour of the sensor response with different NO_2 concentrations.

the typical binding energies of the primary and secondary amine groups (NH/NH_2) in the N_{1s} and C_{1s} spectra, as well as a partial protonation (NH_2^+/NH_3^+) (Figures 1d,e). The successful immobilization of the amine SAM on the SnO_2 NW surface was further proved by Fourier-transform IR (FT-IR) analysis (Figure S1). In order to prove the selective detection of the NO_2 target, the gas sensing properties of all devices were tested towards small concentrations of NO_2 as well as high concentrations of other fossil combustion gases or interfering species (SO_2, NO, NH_3, EtOH, CO, and CO_2) (**Figure 2**a,b and Figure S2). The test gases were diluted in synthetic air and applied via a mass flow controller system into a sensor chamber with controllable gas flow. A constant current (100 nA) was applied to the sensor and the voltage was measured to monitor the resistive change of the semiconductor NWs. The sensitivity of the sensor is given as $S = [(R_{gas}/R_{air}-1)*100]$ [%]. To ensure a fast and complete recovery of the sensor signal, the active surface was illuminated through a quartz window by a solar simulator with constant illumination intensity (AM1.5; 85 mW/cm^2). All measurements were performed at room temperature.

All amine SAMs showed a very high sensitivity and selectivity towards a low NO_2 concentration (400 ppb; Figure 2, Figures S2a-c), whereas only small or mostly no response was observed for higher concentrations of the other gases (SO_2, NO, NH_3, ethanol, CO, and CO_2; concentrations between 2 ppm and 5%). Among all amines (see Supporting Information), the en-APTAS **1** functionalization with a primary and secondary group unified the best performance in both, sensitivity and selectivity, towards NO_2. With the introduction of 400 ppb NO_2, the resistance instantly increased to give a sensitivity of 2100%, whereas the other gases did not show any response (SO_2, CO, and CO_2) or very low values (NH_3, NO, ethanol) (Figures 2a,b). The low response towards 100 ppm of NH_3 (S = 20%) can be attributed to a protonation of the more basic amine functionalities ($pK_a \sim 10.6$) by the more acidic ammonia ($pK_a = 9.2$). Of particular interest was the low and negative sensitivity value towards 2 ppm NO gas (S = −6%). Cross sensitivity of NO_2 and NO is up to date a major issue in the analysis of NO_x mixtures produced in various combustion processes. The identification of a single nitrogen oxide species, here NO_2, is featured by our system in a very simple and cost effective configuration.

FULL PAPER
ADVANCED FUNCTIONAL MATERIALS
www.afm-journal.de
www.MaterialsViews.com

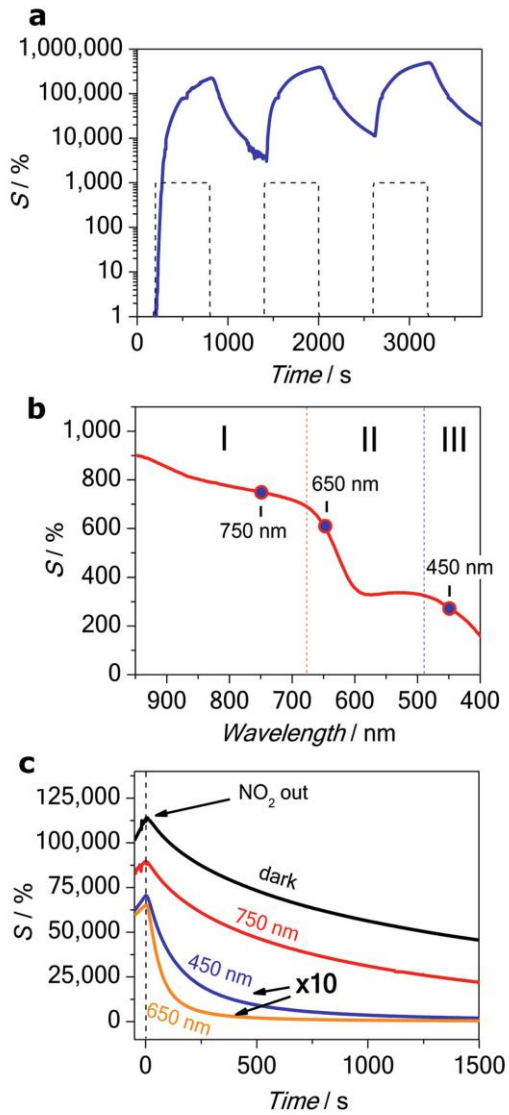

Figure 3. a) Pulses of 250 ppb NO_2 measured with an en-APTAS **1** functionalized SnO_2 NW sensor without illumination. b) Sensor recovery process after a pulse of NO_2 while sweeping of the incident light from 950 to 400 nm. After an almost constant resistance (I), two recovery processes can be identified starting at 680 (II) and 480 nm (III), respectively. c) Recovery processes after NO_2 pulses with illuminations of 450, 650, 750 nm and in dark conditions (position marked in Figure 3b), showing fast recovery for the two higher energy illuminations on one hand and slower and incomplete recovery for 750 nm and dark conditions on the other hand.

After switching the atmosphere from test gas back to pure synthetic air, the signal subsequently dropped down to the initial value before loaded with NO_2 gas. The quantitative sensing response was proportional to the appropriate NO_2 concentration (Figure 2c). Average response and recovery times were 110 and 75 s, respectively. A low NO_2 concentration of 250 ppb (minimum concentration of the experimental setup) could still be detected with a high sensitivity of 850% which implies that the system is capable of sensing NO_2 selectively within the range of critical values for human health (low ppb level).

The same gas sensing experiments performed in dark conditions revealed a slower but even stronger response towards NO_2 with a comparable selectivity and an extraordinary sensitivity of 225 000% for NO_2 concentrations as low as 250 ppb. In contrast to measurements under solar illumination, the response did not reach a signal saturation and the signal recovery was much slower (**Figure 3**a), causing a response accumulation when further NO_2 pulses were introduced. The incomplete sensor response does not allow a fast and quantitative analysis of the target gas in the dark. Thus, light illumination is obviously needed to achieve a fast and reversible sensor response as well as signal saturation. These findings indicate that the intermediate SAM–NO_2 species can be split by incident light, returning to the initial amine and resulting in a dynamic equilibrium of binding- and removal processes (signal saturation). Without illumination, SAM–NO_2 binding processes are ongoing without a coincidental NO_2 removal and thus the signal accumulates during NO_2 pulses without being saturated. In order to figure out the recovery characteristics of the bound SAM–NO_2 state, of the incident monochromatic light was swept from 950 to 400 nm after a NO_2 pulse. It was found that after an almost constant phase (Figure 3b, phase I), fast recovery processes started for wavelengths from 680 and 480 nm (Figure 3b, phase II and III). Both values are above the absorption edge of SnO_2 (<400 nm), proving that the gas detection mechanism does not directly involve SnO_2 as active sensing material, since recovery processes of wide band semiconductors need higher energy UV illumination to be activated.[26,27] Additionally, identical pulses of NO_2 where applied with different wavelengths of the three recovery phases (I, II, and III), as well as in dark conditions (Figure 3c). The measurements confirmed that an illumination between 450 and 650 nm is needed to remove the NO_2 species bound to the SAM molecules effectively to achieve a complete and fast sensor recovery. The weak binding interaction between the SAM and gas molecules allows for an easy signal recovery with lower energy input compared to conventional NW based gas sensors without amine functionalization. Due to the amine termination of the SAM, acid–base interactions with water could possibly have a detrimental influence on the sensor response and recovery characteristics, as well as on lifetime and stability.[25,28,29] However, experiments in humid air show that the sensor response to NO_2 is slightly reduced, but stable and fully reversible when the atmosphere is changed back to dry air (Figure S3).

2.2. Theoretical Identification of Crucial Sensor–Gas Interactions

Based on the initial experimental results, a theoretical model of the complete sensor system was developed within density functional theory (DFT) to simulate (i) the chemical bonding of the en-APTAS **1** SAM to the SnO_2 surface, the interaction of various gas molecules with the SAM ligand in the (ii) absence

and (iii) presence of the SnO_2 surface and finally (iv) the charge transfer process between adsorbed gas molecules and the SAM modified SnO_2 NW. In addition to the response of the sensor to NO_2, the absorption of NO and SO_2 was also theoretically examined in order to obtain further insight into the origin of the very high selectivity. It turns out that adsorption of NO_2 leads to charge transfer from the NW to the gas molecule. In this respect it is quite surprising that SO_2 shows no sensor response (Figure 2a,b), although it has similar oxidative and structural characteristics as NO_2. NO even induces a charge transfer opposite in sign to the NO_2 signal in agreement with the experimental findings. For both, experiment and theory, the (110) surface representing the lowest energy surface of SnO_2 was used.[30] Doping of SnO_2 with negative charge carriers was realized via incorporation of hydrogen atoms substituting oxygen atoms in the SnO_2 (Figure S9).[31]

DFT modeling revealed that bonding of the SAM to the SnO_2 surface via a single oxygen atom is the energetically favourable case and is used below (Figure S4). In the relaxed structure the SAM is tilted towards the SnO_2 surface. Different initial geometries for the free SAM–NO_2, SAM–SO_2 and SAM–NO system were used for structural relaxations in order to find the optimal SAM–gas geometries (Figures S5–7). The lowest energy geometries have SAM-gas binding energies E_b of –0.44 eV (NO_2), –0.83 eV (SO_2) and –0.48 eV (NO).

The optimal SAM–gas geometries were then combined with the optimized SAM-NW geometries. For the three-atomic gas molecules (NO_2, SO_2), bonding with the SAM at the optimal bonding site is sterically hindered by the influence of the NW surface as well as neighboring SAM ligands. As a consequence, NO_2 relaxes at the geometry with the second highest bonding strength near the secondary amine group with a binding energy of –0.26 eV and SO_2 relaxes at a position near the primary amine group at the head of the SAM corresponding to configuration 5 in Figure S6, with a binding energy of –0.71 eV. NO relaxes at the optimal bonding geometry also in presence of the NW surface (E_b = –0.24 eV). The charge transfer within the NW-SAM-gas system upon adsorption of the gas molecules was determined as

$$\Delta\rho(z) = \rho_{g-\mathrm{SAM}-\mathrm{SnO_2}}(z) - \rho_{\mathrm{SAM}-\mathrm{SnO_2}}(z) - \rho_g(z), \quad g = \mathrm{NO_2},\ \mathrm{SO_2},\ \mathrm{NO} \tag{1}$$

where $\rho_{g-\mathrm{SAM}-\mathrm{SnO_2}}$ is the electron density of the relaxed SAM-modified NW in the presence of the gas molecule g averaged over the SnO_2 (110) plane, $\rho_{\mathrm{SAM}-\mathrm{SnO_2}}$ and ρ_g are the averaged electron densities of the isolated SAM-NW system and the gas molecule with geometries from the relaxed NW-SAM-gas system. The coordinate along the (110)-direction is denoted by z. As can be seen from **Figure 4**a, the adsorption of NO_2 at the SAM bound to the SnO_2 surface leads to charge transfer from the NW via the SAM to the NO_2 molecule. A charge depletion zone extending into the NW backbone is observed. Charge transfer is also found after NO adsorption. However, here charge is transferred in the opposite direction, from the NO molecule via the SAM to the NW. On the other hand, the adsorption of SO_2 does not induce any noticeable charge variation in the NW. Merely a localized charge redistribution in the SAM–SO_2 part of the system is observed. Hence, our simulations suggest that while NO_2 adsorption leads to a decrease and NO adsorption to an increase of negative charge carriers in the NW, SO_2 has no impact, although it shows the strongest bonding to the SAM–NW system. Since SnO_2 is an n-type semiconductor, the simulations are consistent with the experimental observation of increasing and decreasing resistance in the presence of NO_2 and NO, respectively, while SO_2 does not lead to any considerable change (Figure 2a,b). Note that while the direction of charge transfer corresponds to the sensing measurement, the magnitude of the sensor signal being proportional to the device resistance cannot be obtained directly from DFT calculations.

Analyzing the density of states (DOS) of the SAM–NW system with adsorbed gas molecules, we found that NO_2 and NO adsorption lead to the formation of additional states directly at the NW–SAM Fermi level (Figure 4b). These states can be attributed to the LUMO in the case of NO_2, and in the case of NO to the HOMO of the corresponding gas–SAM system. Those states are mainly formed by the LUMO and HOMO of the isolated NO_2 and NO gas molecules as can be seen from Figure 4c, where we show the charge densities associated with the aforementioned wavefunctions of the NW–SAM–gas systems. As the DOS from Figure 4b shows, the NO_2–SAM LUMO becomes partially occupied and thus can take up charge carriers from the NW, contrary to the NO–SAM system for which the HOMO becomes partially depopulated by donating charge to the NW. Finally for SO_2, none of the frontier molecular orbitals is located at the Fermi level (Figure 4b) such that the occupations of the HOMO and LUMO of the gas–SAM system remain unaffected and no charge transfer is observed in this case.

To get a clear picture, we determined the HOMO and LUMO energy levels of the isolated SAM–gas systems in the absence of the NW and aligned their positions with the energy scale of the SAM-modified SnO_2. As reference for the alignment procedure the average electrostatic potentials at the cores of the carbon and nitrogen atoms at the backbone of the en-APTAS **1** molecule were used. As shown in Figure 4d, the LUMO of the NO_2–SAM system lies below the Fermi-level of the SAM-modified SnO_2. Hence charge transfer from the SnO_2 to the LUMO of the NO_2–SAM system is energetically favoured until LUMO and Fermi-level are aligned. In contrast, the NO-SAM system has a HOMO higher in energy than the Fermi-level of the SAM-modified SnO_2. Hence energy is gained by transferring charge from the HOMO of the NO–SAM system to the SnO_2. Finally, the LUMO of the SO_2–SAM system lies well above the Fermi-level and the HOMO lies well below the Fermi-level and so charge transfer is absent in agreement with the charge transfer simulations and sensing experiments. This analysis is extended to CO and CO_2 adsorbed on en-APTAS **1**. Determining the energies of the corresponding frontier orbitals (Figure 4d), the HOMOs are well below and the LUMOs are well above the SAM–NW Fermi level. Hence, as in the case of SO_2 charge transfer cannot occur for CO and CO_2, in agreement with our experimental results. In total, the simulations indicate that the key to explain the selectivity of the SAM modified sensor towards different gas molecules lies in the positions of the gas–SAM frontier molecular orbitals with respect to the Fermi level of SAM-modified SnO_2 NWs. This property guides

ADVANCED FUNCTIONAL MATERIALS
www.afm-journal.de
www.MaterialsViews.com

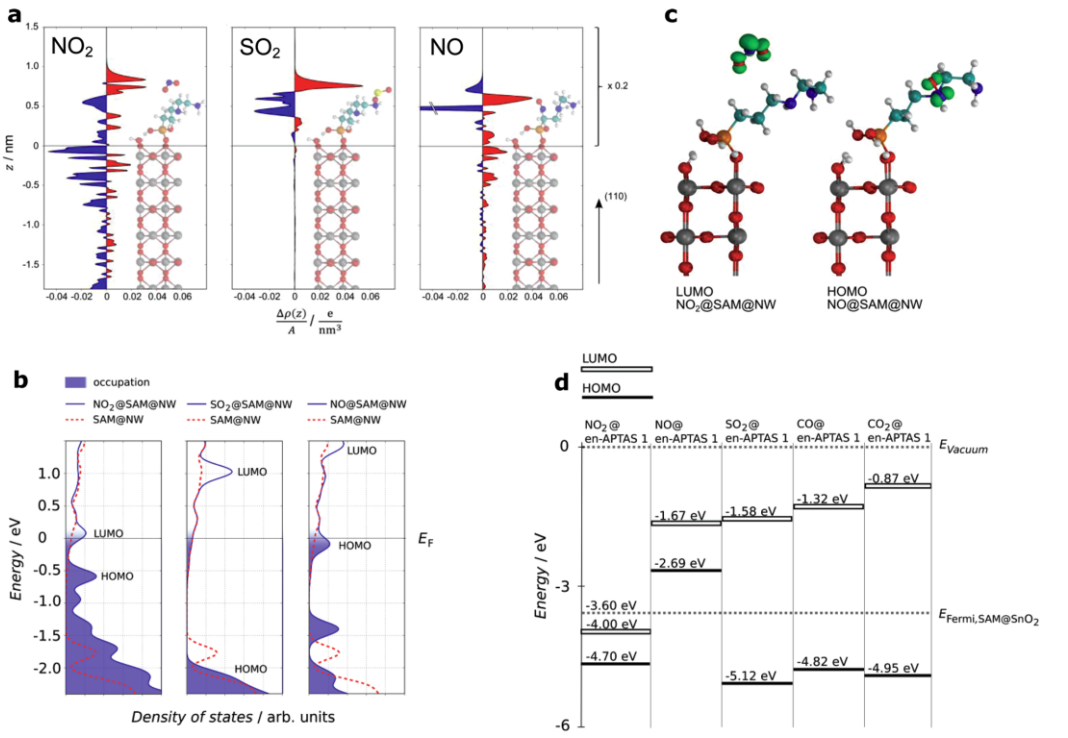

Figure 4. a) The change in averaged one-dimensional charge density $\Delta\rho(z)$ per surface area A along the (110) direction upon NO_2, SO_2 and NO adsorption on the en-APTAS **1** functionalized SnO_2 (110) surface for the energetically most favourable geometries. These geometries are shown as insets and are true to length scale. The electron charge is denoted by e. Regions of charge depletion are indicated by blue and regions of charge accumulation are indicated by red fillings. For clarity $\Delta\rho(z)$ has been scaled by a factor of 0.2 in the region outside the SnO_2. The SnO_2 surface (z = 0) is defined by the average position of the bridging oxygen atoms on the SnO_2 surface along the (110) direction. b) Density of states (DOS) of the en-APTAS **1** modified SnO_2 with adsorbed NO_2, SO_2 and NO. The Fermi levels of the different systems are set to 0 eV. For comparison the DOS of the en-APTAS **1** modified SnO2 NW without an adsorbed gas molecule (dashed red line) is shown in each graph. c) The charge densities of the wave functions corresponding to the peaks in the densities of states aligned with the Fermi levels from b are shown as green isosurfaces. The isosurfaces are drawn at a value of 0.075 e/Å^3. These are basically the LUMO of the NO_2 molecule, and the HOMO of the NO molecule. d) Energy diagram of the frontier orbitals of the two- and three-atomic gases adsorbed on en-APTAS **1**. Gases with HOMOs below and LUMOs above the Fermi level of the SAM-modified SnO_2 do not lead to a noticeable gas sensing signal in the experiments. NO_2 with the LUMO of the NO_2-en-APTAS **1** system below the Fermi level leads to an increasing sensor resistance whereas NO with the HOMO being above the Fermi level leads to a decreasing sensor resistance.

the way to the tailoring of SAM–nanowire surfaces towards highly selective gas sensing.

3. Conclusion

In conclusion, we demonstrated that the theoretical prediction of a SAM–NW hybrid sensor system is capable to provide an effective strategy for designing functionalized gas sensors through electronic structure calculations. The selectivity of the hybrid sensor is caused by a suitable alignment of the gas–SAM frontier molecular orbitals with respect to the SAM–NW Fermi-level. The present sensor is capable of detecting very low NO_2 concentrations in the ppb range qualitatively and quantitatively with relatively fast response and recovery time at room temperature. It fulfills the criteria for environmental pollution monitoring systems based on a very simple and cost effective device. Our work demonstrates that a systematic organic surface design of semiconductor nanostructures shows great potential in solving the selectivity issue, which is the main obstacle of current gas sensor technologies. On the long term, this knowledge could lead to a strategy with which a tailored and flexible design of highly precise artificial noses is enabled.

4. Experimental Section

Preparation of SnO_2/en-APTAS 1 Sensors: The as-prepared SnO_2 NWs (average diameter 40–60 nm) grown on Al_2O_3 substrates with pre patterned interdigital gold electrodes (5 µm spacings) were cleaned in oxygen plasma for 1 min to remove surface contaminations and provide oxygen groups on the surface for the condensation reaction. Subsequently, the sample was immersed in a 1% ethanol solution of

ADVANCED FUNCTIONAL MATERIALS
www.afm-journal.de

[30] M. Batzill, U. Diebold, *Prog. Surf. Sci.* **2005**, *79*, 47–154.
[31] A. K. Singh, A. Janotti, M. Scheffler, C. G. Van de Walle, *Phys. Rev. Lett.* **2008**, *101*, 1–4.
[32] K. R. Hahn, A. Tricoli, G. Santarossa, A. Vargas, A. Baiker, *Langmuir* **2012**, *28*, 1646–1656.
[33] G. Kresse, J. Furthmüller, *Phys. Rev. B* **1996**, *54*, 11169–11186.
[34] G. Kresse, *Phys. Rev. B* **1999**, *59*, 1758–1775.
[35] P. Blöchl, *Phys. Rev. B* **1994**, *50*, 17953–17979.
[36] S. Grimme, *J. Comp. Chem.* **2006**, *17*, 1787–1799.
[37] W. H. Baur, A. A. Khan, *Acta Cryst. B* **1971**, *27*, 2133–2139.

ADVANCED FUNCTIONAL MATERIALS

Supporting Information

for *Adv. Funct. Mater.*, DOI: 10.1002/adfm.201301478

Highly Selective SAM–Nanowire Hybrid NO_2 Sensor: Insight into Charge Transfer Dynamics and Alignment of Frontier Molecular Orbitals

Martin W. G. Hoffmann, Joan Daniel Prades, Leonhard Mayrhofer, Francisco Hernandez-Ramirez, Tommi T. Järvi, Michael Moseler, Andreas Waag, and Hao Shen**

Supporting Information

High selective SAM-nanowire hybrid NO_2 sensor: Insight into charge transfer dynamics and alignment of frontier molecular orbitals

By: *Martin W. G. Hoffmann*, *Joan Daniel Prades**, *Leonhard Mayrhofer*, *Francisco Hernandez-Ramirez*, *Tommi T. Järvi*, *Michael Moseler*, *Andreas Waag*, and *Hao Shen**

[*] M. W. G. Hoffmann, Dr. J. D. Prades, Dr. F. Hernandez-Ramirez
Department of Electronics
University of Barcelona, E-08028 Barcelona (Spain)
E-mail: dprades@el.ub.es

[*] M. W. G. Hoffmann, Prof. A. Waag, Dr. H. Shen
Institut für Halbleitertechnik
Technische Universität Braunschweig, 38106 Braunschweig (Germany)
E-mail: h.shen@tu-bs.de

Dr. L. Mayrhofer, Dr. T. T. Järvi, Prof. M. Moseler
Fraunhofer Institute for Mechanics of Materials (IWM)
79108 Freiburg (Germany)

M. W. G. Hoffmann, Dr. F. Hernandez-Ramirez
Department of Advanced Materials for Energy Applications
Catalonia Institute for Energy Research (IREC), 08930 Barcelona (Spain)

SAM / nanowire hybrid materials for ultraselective gas sensing

For many decades, material scientists, solid state physicists and chemists are dreaming of fabricating an artificial device, which behaves like a human nose: detecting a large variety of chemical species with high sensitivity and high selectivity. Up to now there is no generally applicable strategy to achieve such a single species selectivity and apply this strategy to the detection of many different gas species in parallel.

Semiconducting metal oxide NWs have already shown their exceptional potential in detecting a wide range of gaseous species with high sensitivity, based on their high surface-to-volume ratio. However, even after more than ten years of intense nanowire research they continue to fail in the selective detection of only one specific type of molecule. The benefit of a high sensitivity is generally destroyed by the drawback of a low selectivity. The sensing mechanism, usually based on unspecific redox interactions between nanowire surface oxygen and the gaseous species, does not allow for an exclusive interaction with a single type of gas. A predictive strategy for controlled surface functionalisation in order to achieve selectivity towards any predefined gas species is still missing.

In order to demonstrate out strategy, NO_2 was chosen as a test vehicle, since NO_2 is one of the most harmful environmental pollutants and will have an important effect on our future global climate. An organic amine functionalization of oxide nanowire surfaces was chosen to prove the conceptual idea. By applying our strategy, we were able to demonstrate an ultraselective and highly sensitive NO_2 sensor by organic surface design of SnO_2 NWs. The selectivity of the sensor is caused by a suitable alignment of the gas-SAM frontier molecular orbitals with the SAM-SnO_2 NW Fermi-level. The present sensor is capable of detecting very low NO_2 concentrations in the ppb range qualitatively and quantitatively with relatively fast response and recovery time. It fulfills the criteria for environmental pollution monitoring systems based on a very efficient and cost effective device.

Materials and methods

Synthesis of SnO_2 nanowires

SnO_2 nanowires on an interdigital gold electrode (5 µm spacing) were synthesized by chemical vapour deposition (CVD) using $[Sn(O^tBu)_4]$ as precursor and sputtered Au as catalyst. The detailed synthesis route is described elsewhere[1].

*Nanowire surface modification with en-APTAS **1***

The as-prepared SnO_2 NWs (average diameter 40-60 nm) were cleaned in an oxygen plasma for 1 minute to remove surface contaminations and provide oxygen groups on the surface for the following condensation reaction. Subsequently, the samples were immersed in a 1% ethanol solution of en-APTAS **1** (ABCR GmbH), which was stirred for 6 h. After removal, the samples were subsequently rinsed with ethanol and dried in a vacuum oven for 2 h at 60°C.

*Nanowire Surface modification with APTES **2***

The modification was realized following the above mentioned procedure, using a 1% ethanol solution of APTES **2** (Sigma Aldrich).

*Nanowire Surface modification with N,N Dimethylaminopropyl)Trimethoxysilane **3***

The modification was realized following the above mentioned procedure, using a 1% ethanol solution of (N,N-Dimethylaminopropyl)Trimethoxysilane **3** (Sigma Aldrich).

*Nanowire Surface modification with tetraethylen diamine terminated methoxysilane **4***

The as-prepared SnO_2 NWs (average diameter 40-60 nm) were cleaned in an oxygen plasma for 1 minute to remove surface contaminations and provide oxygen groups on the surface for the following condensation reaction. The samples were immersed in 20 mL of an 1% ethanol solution of 3-(trimethoxysilyl)propyl aldehyde (United Chemical Technologies) for 30 min. Subsequently, 0.3 mL (1.78 mmol) tris(2-aminoethyl)amine (tren) and 5 mg (0.08 mmol) sodium cyanoborhydride were added to the solutionAfter stirring overnight, the samples were removed from the solution, rinsed with ethanol and dried at 60°C for 2 h in an vacuum oven.

XPS analysis

XPS experiments were performed in a PHI 5500 Multitechnique System (Physical Electronics) with a monochromatic X-ray source (Al Kα line of 1486.6 eV energy and 350 W), placed

perpendicular to the analyzer axis and calibrated using the $3d_{5/2}$ line of Ag with a full width at half maximum (FWHM) of 0.8 eV.

SEM analysis

SEM micrographs were recorded using a Zeiss Auriga field-emission scanning electron microscope.

FT-IR analysis

FT-IR spectra of the SnO_2/en-APTAS **1** samples were recorded with a Bomem DA3 system in diffuse reflectance mode (equipped with a DRIFT accessory), using a MCT detector.

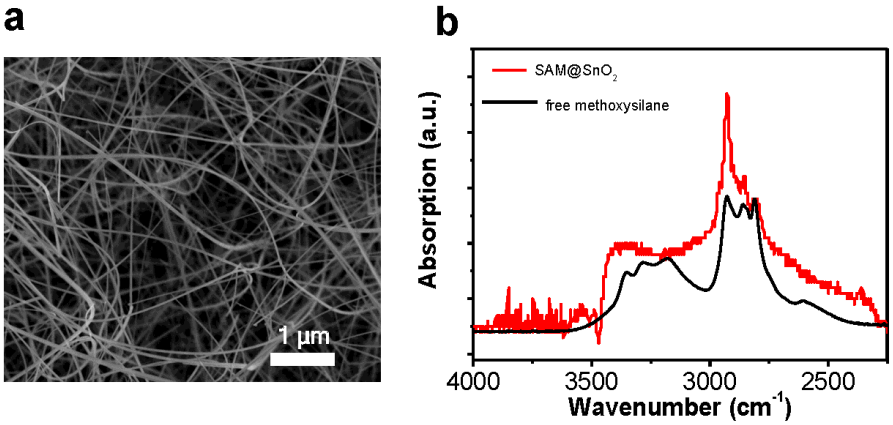

Figure. S1. (a) SEM picture of the SnO_2 NWs with an average diameter of 47±8 nm grown by CVD. (b) IR absorption spectra of the free en-APTAS (black) and immobilized on the SnO_2 NW surface (red).

Figure S1 shows the Fourier Transfor Infrared (FT-IR) absorption spectrum of a sensor sample with N-[3-(Trimethoxysilyl)propyl]ethylenediamine **1** (en-APTAS) functionalization on the SnO_2 NW, exhibiting δN-H and δC-H stretches identical to the free molecule **1**.

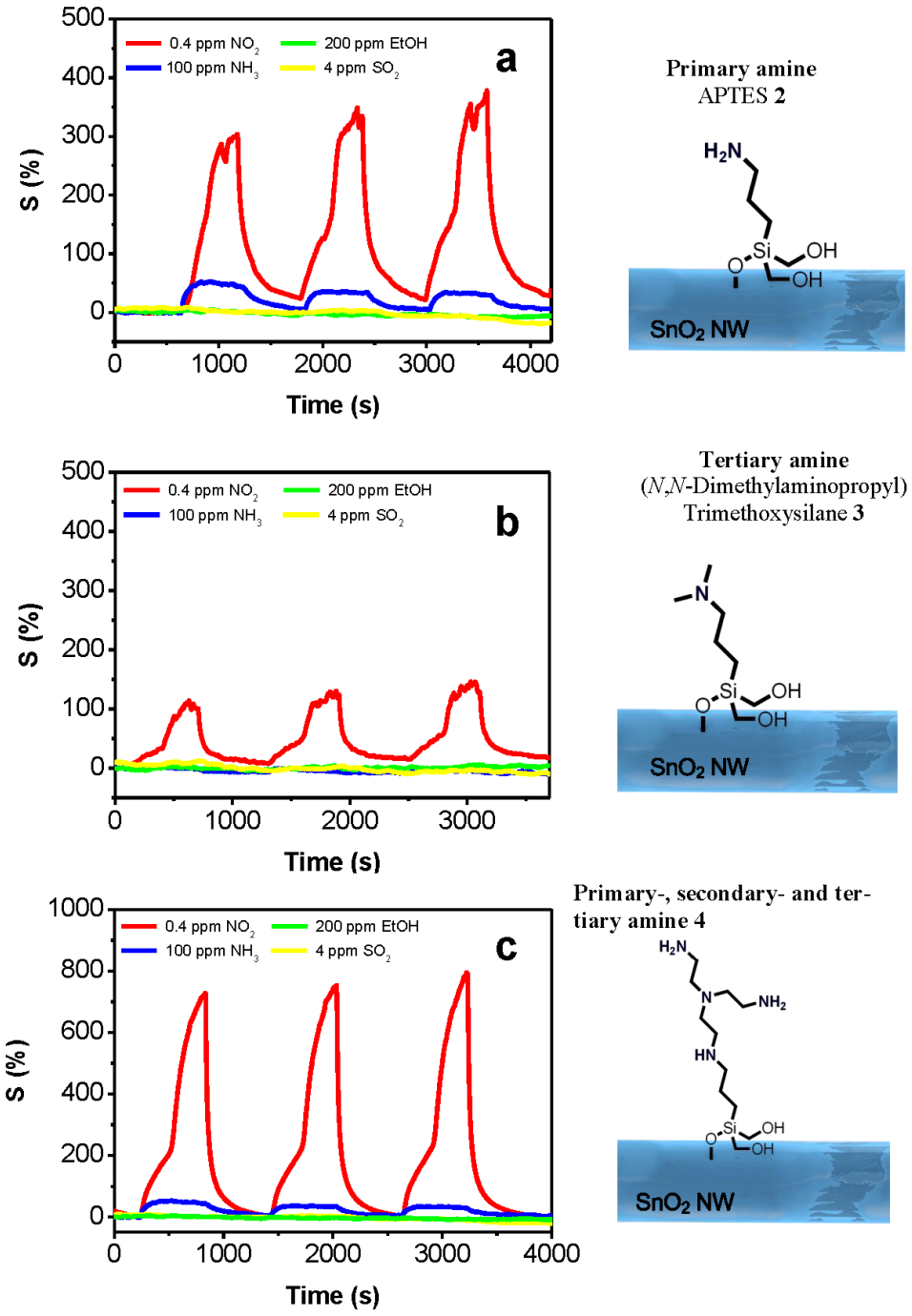

Figure S2. Responses of SnO_2 NW sensors with different SAM modifications towards 0.4 ppm NO_2 as well as other reducing (NH_3, ethanol) and oxidizing (SO_2) gases.

Sensing behavior of different amine-SAMs

In this work, four different SAMs with primary, secondary and tertiary amine groups have been evaluated in terms of sensitivity and selectivity towards NO_2. (3-Aminopropyl)triethoxysilane **2** (APTES) has just a single primary terminal amine group. Sensing experiments with 0.4 ppm NO_2 revealed a sensitivity of around 350% (17% of en-APTAS **1**). The achieved selectivity of 10:1 (0.4 ppm NO_2 compared to 100 ppm NH_3) was also significantly lower than that of en-APTAS **1** (105:1 for SAM **1**). A SAM with tertiary amine functionality was realized by the immobilization of (*N*,*N*-dimethylaminopropyl)trimethoxysilane **3** on the NW surface. Although a quite high NO_2/NH_3 selectivity of 26:1 was achieved, the sensitivity of 130% was not competitive to other amine SAMs (ca. 6% of SAM **1**). 3-(trimethoxysilyl)propyl aldehyde was coupled with tren via reductive amination to modify the SnO_2 NW surface with SAM **4** (primary, secondary and tertiary amine functionalities). This oligo-amine **4** reached a sensitivity towards 0.4 ppm NO_2 of 750% (36% of SAM **1**) and a relative selectivity of around 21:1 (see above).

Our simulations showed that the interaction between NO_2 and the secondary amine group of en-APTAS **1** plays an important role for an efficient charge transfer compared to the terminal primary amine. Thus, the interaction between gas and APTES **2** SAM is possibly weaker. Due to its secondary amine group, SAM **4** can possibly interact more efficient with NO_2 and shows the highest sensitivities after SAM **1**. As we could show that steric effects are strongly influencing the bonding geometry of the SAM-gas system, the used volume of the relatively large molecule could hinder the approach of gas species to the secondary group.

Our theoretical DOS calculations of the gas-SAM system (see Fig. 4d) showed that the energetic position of the hybridized LUMO is critical for a charge transfer from the SnO_2 NW and hence the gas detection. The varied molecular structure of the used amines leads to a diverse DOS structure of the gas-SAM and different energies of the particular LUMO energies.

Parameters that influence the sensing performance of a NW-SAM system are: (i) gas-ligand interaction of the free ligand; (ii) steric effects of the surface bound SAM and (iii) LUMO energy of the gas-SAM system. All parameters can be determined *in silico* to design specific surface modifications for selective gas sensors.

Influence of illumination on the sensor response/recovery characteristics

In order to figure out the recovery characteristics of the bound SAM-NO_2 state, the dependence of the recovery on the incident light was examined. A pulse of NO_2 was given at $\lambda = 950$ nm to form the NO_2-SAM bound state. After switching back to synthetic air, the incident wavelength was swept from 950 to 400 nm. It was found that after an almost constant resistance, comparable to the recovery behaviour in dark conditions (phase I; Fig. 3b) the recovery process starts at an illumination wavelength of 680 nm (phase II), followed by a second one at around 480 nm (phase III). Both values are right above the band edge of SnO_2 (< 400 nm), proving that the gas detection mechanism is not directly involving SnO_2 as active sensing material, since recovery processes of the pure metal oxide need higher energy UV light to be activated[2,3]. For further investigation of the sensor dependence on the incident light energy, identical pulses of NO_2 where applied with different wavelengths of the three recovery phases (I, II and II), as well as in dark conditions (Fig. 3c). As expected, the responses in dark conditions and with 750 nm irradiation show almost the same characteristics of very high response, but very slow and incomplete recovery. The measurements confirmed that the energy is not sufficient to remove the NO_2 species bound to the SAM molecules. The same measurements with higher energy irradiation of 650 nm (phase II) and 450 nm (phase III) respectively proved to have a fast and complete recovery of the sensor signal. As surface bound NO_2 species are continuously removed from the SAM at these higher energy irradiations, the accumulation of SAM-NO_2 bound species is reduced and hence the sensor signal is lower compared to phase I conditions, but still at a very high level. In sharp contrast, the recovery of the signal was very fast and complete for both wavelengths with higher energy (450 and 650 nm). A fast and complete recovery is essential for gas sensing applications and can be achieved by visible light illumination (e.g. sun light or visible light emitting LEDs) at room temperature. An illumination of the sensor with visible light in the range of 450-650 nm is therefore needed to use the here presented sensor for real sensing application, where fast and quantitative detections are essential.

Influence of humidity

Due to the amine termination of the SAM, acid-base interactions with water are possible and therefore can possibly have a detrimental influence on the sensor response and recovery characteristics, as well as lifetime and stability[4–6]. When humidity is introduced into the gas chamber, the SAM-amine groups will be partially protonated and form ammonium species with a positive charge on the nitrogen atoms. Consequently, the electronic structure of the SAM molecule changes and can cause an inversion of the dipole moment (μ) of the organic molecule[7]. The influence of the changed μ can be monitored by the resistance of the device which increases with the humidity concentration (0, 12.5, 25, 50% rel. humidity) and is fully reversible when the atmosphere is changed back to dry air, showing that the sensor is stable also in humid conditions (Fig. S3a). Pulses of 375 ppb NO_2 at different humidity concentrations (Fig. S3b) revealed a partial suppression of the sensor signal with increasing humidty concentrations (up to 40% at 50% rel. humidity), but still very high values of sensitivety could be achieved also under these conditions (S ~ 1,000% at 50% rel. humidity).

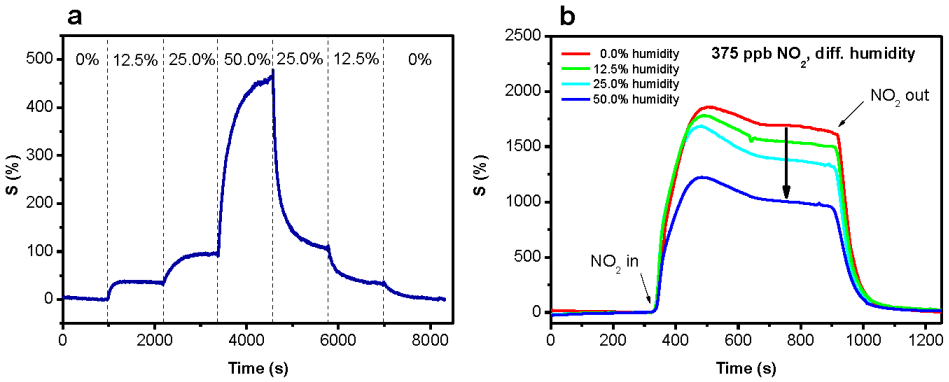

Figure S3. Response of the en-APTAS **1** surface modified SnO_2 device towards 375 ppb NO_2 under illumination and different humidity conditions. (a) The sequence of changing humidity concentrations (synthetic air) shows a dependence of the sensor signal. It is increasing with increasing humidity concentration and shows a stable and reversible behavior. (b) The sensor response is partially suppressed with increasing humidity concentration (0% to 50%) by maximal 40% (@50% humidity). The sensor still shows a high stability, indicated by the complete signal recovery after the given NO_2 pulses (375 ppb).

The lower response in humid conditions can be associated with the partial protonation and the consequent temporal inhibition of the amine binding sites. Thus, less NO_2 molecules can interact with the sensor surface and a lower target sensitivity is observed.

Additionally, the reduction of the sensor response in humid conditions indicates that the detection mechanism for NO_2 is not proceeding through a protonation of the SAM amine groups by nitric- (HNO_3; pK_a = -1.37) or nitrous acid (HNO_2; pK_a = 3.29), which can form when NO_2 interacts with water. In this case, a higher response would be expected in humid conditions. A further disqualification of the acidic mechanism is given by the fact, that the sensor does not show any response to CO_2 in humid conditions (10% CO_2; 50% rel. humidity), in which carbonic acid (H_2CO_3; pK_{a1} = 6.35) forms and could protonate the amine functionalities additionally to water. The reproduction of the initial sensing values towards NO_2 after changing back to dry atmosphere conditions shows the stability of the surface modified sensor, also in humid conditions (Fig. S3b).To accomplish requirements for real sensing environments, moisiture filters, which are commonly used in commercial gas sensors, could be incorporated in our sensing device. This setup would lead to qualitative and quantitative NO_2 sensing results independent from the surrounding moisture concentration in real applications.

In order to classify the response time and sensitivity of the here presented work comparison with current NO_2 sensors, we summarized the particular values in table S1.

Table S1: Sensitivity and response time (τ_r) values of the here presented wor in comparison to current NO_2 sensor systems.

material	τ_r (s)	T(°C)	NO_2 conc. (ppb)	|S| (%)*	|S|/ppb (%)	source
SAM-SnO_2 NWs	110	RT	250-750	850	3.40	this work
modified graphene	600	RT	1,000-30,000	25	0.03	[8]
modified graphene	>900	RT	200,000	25	---	[9]
In_2O_3 NWs	>100	RT	5-1,000	2	0.40	[10]
SnO_2 NW	~150	RT	500	1	---	[11]
WO_3/MWCNT	~150	RT	500	2.2	---	[12]
PANi-PEO/PVP	>180	RT	125-1,000	<2	< 0.02	[13]
Si NWs	85-900	RT	20-20,000	10	0.50	[14]
Graphene-WO_3	25-200	250	1,000-20,000	200	0.20	[15]
$ZnGa_2O_4$/ZnO NWs	90	250	1,000	300	0.30	[16]
SnO_2 nanobelts	30	300	500	1500	3.00	[17]

*absolute sensitivity; related to the lowest given NO_2 concentration in the particular source

Clearly, the sensitivity and response time of our device is above the average state of the art in both disciplines.

Binding of the en-APTAS 1 ligands on the SnO_2(110) surface

Since the SnO_2 NWs are exposed to humidity during preparation of the sensor, hydroxylation of the (110)-surface was assumed due to dissociative adsorption of water. Hereby, hydrogen

bonds to the bridging oxygen atoms of the stoichiometric (110)-surface and hydroxyl groups are adsorbed in a on-top position on the fivefold coordinated Sn atoms of the surface (Fig. S4a and Fig. S4b). The unit cell of the SnO_2 slab prior to chemisorption of en-APTAS **1** molecules is shown in Fig. S4a. Binding of an en-APTAS **1** to the (110)-surface of SnO_2 can occur via one, two or three oxygen atoms. At the same time the en-APTAS **1** splits one, two or three hydroxyl groups off and forms a corresponding number of H_2O molecules together with hydrogen atoms from the hydroxylated SnO_2 surface. The binding energies for the different scenarios can hence be determined as

$$E_{B,n} = E(en-APTAS\ @SnO_2, n) + nE(H_2O) - E(SnO_2) - E(en-APTAS)$$

Here *E(en-APTAS@SnO_2, n)* is the ground state energy of the relaxed SAM-SnO_2 system where bonding occurs via *n* oxygen atoms, *E(H_2O)* and *E(en-APTAS)* are the gas phase ground state energies of water and en-APTAS **1**, respectively. Finally, *E(SnO_2)* is the ground state energy of the hydroxylated relaxed SnO_2 slab.

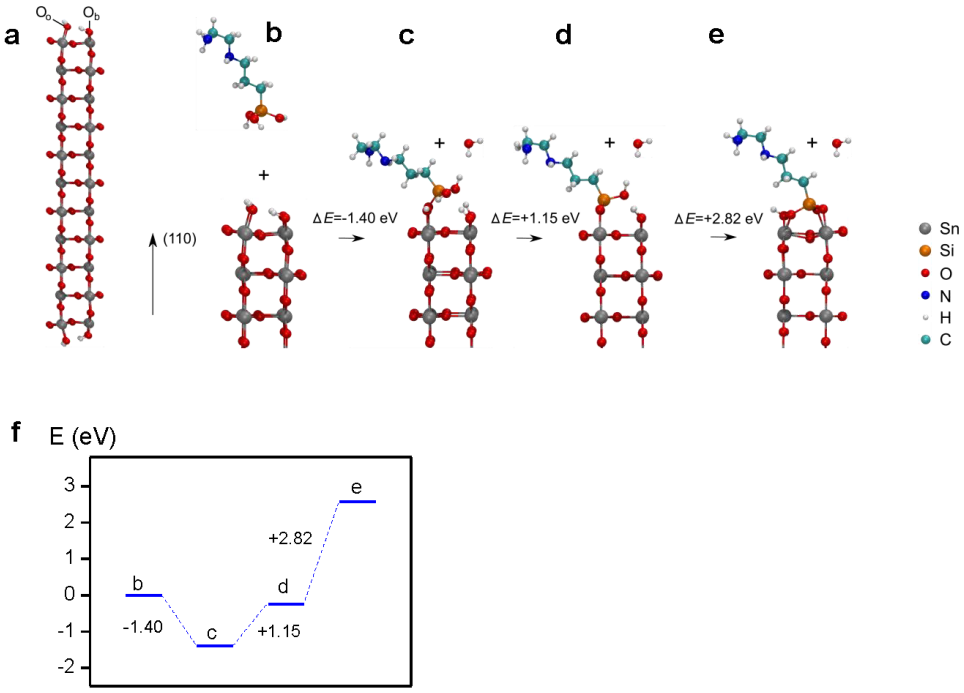

Figure S4. Bonding of the en-APTAS **1** on the OH-terminated SnO_2(110)-surface. **a**, The unit cell of the SnO_2 slab prior to SAM modification. O_o and O_b indicate oxygen atoms in on-top and in bridging positions, respectively. **b**, The en-APTAS **1** and the OH-terminated SnO_2 surface before bonding. **c**, Bonding via a single oxygen atom at the surface goes along with the formation of a H_2O molecule and is an exothermic process resulting in a binding energy of -1.40 eV. Bonding via more oxygen atoms again leads to the formation of H_2O but is endothermic (**d e**). **f**, Energy diagram of the sequential binding processes b-e.

First we examined bonding via a single oxygen atom. In this case we find E_B = -1.04 eV for adsorption on a bridging oxygen atom and $E_{B,1}$ = -1.40 eV for on-top adsorption on a fivefold coordinated Sn atom, Fig. S4c. Splitting one more hydroxyl group off, bonding of the en-APTAS **1** to the SnO_2 surface via two oxygen atoms as shown in Fig. S4d becomes possible. Here, bonding to two fivefold coordinated Sn atoms is more favorable than bonding via one fivefold coordinated Sn atom and one bridging oxygen atom. However it turns out that this step is endothermic with an associated energy cost of 1.15 eV thus resulting in a binding energy of $E_{B,2}$ = -0.25 eV. Finally by splitting one more hydroxyl group off, bonding via three surface oxygen atoms is achieved. As can be seen from Fig. S4e, bonding to three oxygen atoms leads to significant lattice distortions at the SnO_2 surface. Hence we find an energy penalty of at least 2.82 eV when going from the case of twofold bonding to the SnO_2 surface to the case of threefold bonding. Therefore, the binding energy for bonding via three oxygen

atoms even becomes positive, $E_{B,3}$ = 2.57 eV. Here, bonding via two on-top oxygen atoms and one bridging oxygen atom is more favorable than bonding via one on-top oxygen atom and two bridging oxygen atoms.

Adsorption of gas molecules at a single en-APTAS 1 molecule

In order to find the energetically optimal bonding geometries of the different gas molecules and the en-APTAS **1**, in the case of SO_2 and NO_2 twenty different initial configurations were generated and structural relaxations were performed for all of them, using DFT. Some of the initial configurations relaxed to identical structures such that fifteen different NO_2-(en-APTAS **1**) and eighteen different SO_2-(en-APTAS **1**) geometries remained, see Figures S5 & S6. In the case of SO_2 we find that bonding is most favourable between the sulfur atom of SO_2 and the nitrogen atom of the secondary amine group with binding energies between -0.83 eV and -0.64 eV. Binding energies between -0.62 eV and -0.50 eV have been found for bonding of the sulfur atom of SO_2 near the primary amine. All other geometries show much weaker adsorption at the (en-APTAS **1**) with binding energies > -0.16 eV. For NO_2 the binding strength is in general weaker than for SO_2. The strongest bonding with a binding energy of -0.44 eV occurs again near the secondary amine group followed by hydrogen bonding of the NO_2 to the (en-APTAS **1**) backbone near the secondary amine group. We note that a corresponding geometry for SO_2 adsorption is not stable. Adsorption at the primary amine group however is not favorable for NO_2. In Figures S5 and S6 we show all the relaxed inequivalent NO_2/SO_2-(en-APTAS **1**) geometries together with their binding energies.

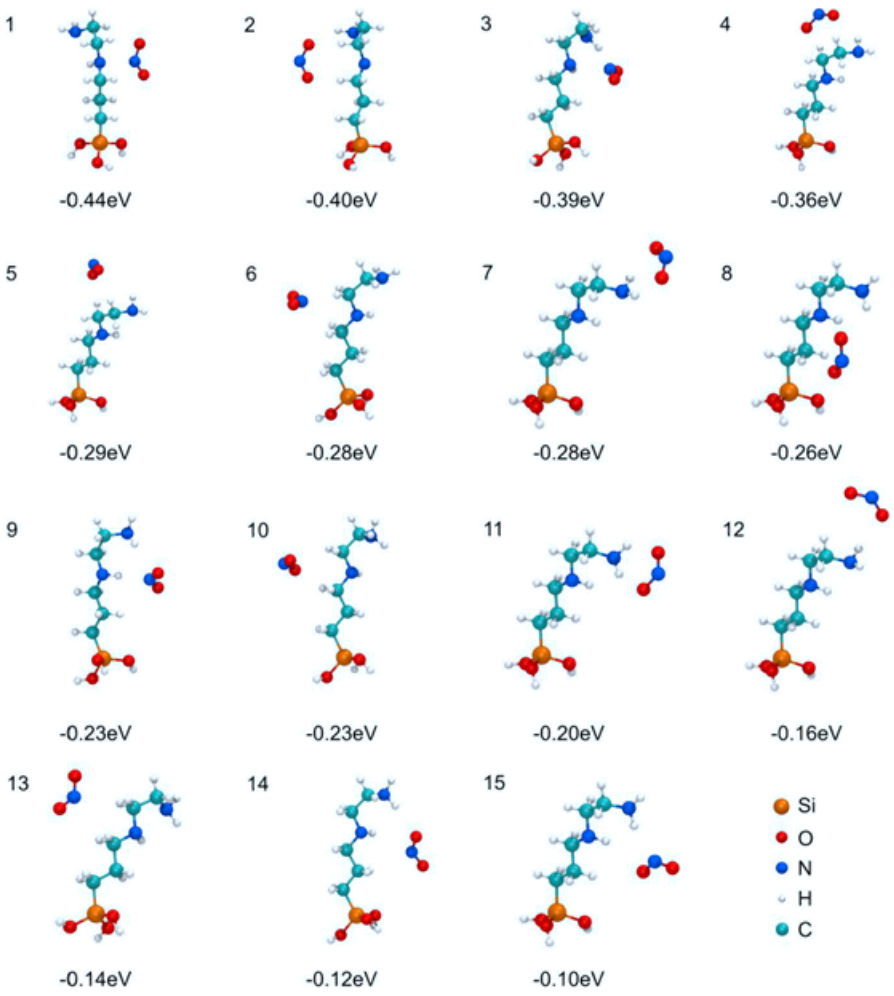

Fig. S5: The fifteen inequivalent geometries of a NO_2 molecule adsorbed on the en-APTAS **1** obtained in our simulations with the corresponding binding energies. The ordering is from geometries with stronger bonding (lower binding energies) to geometries with weaker bonding (higher binding energies).

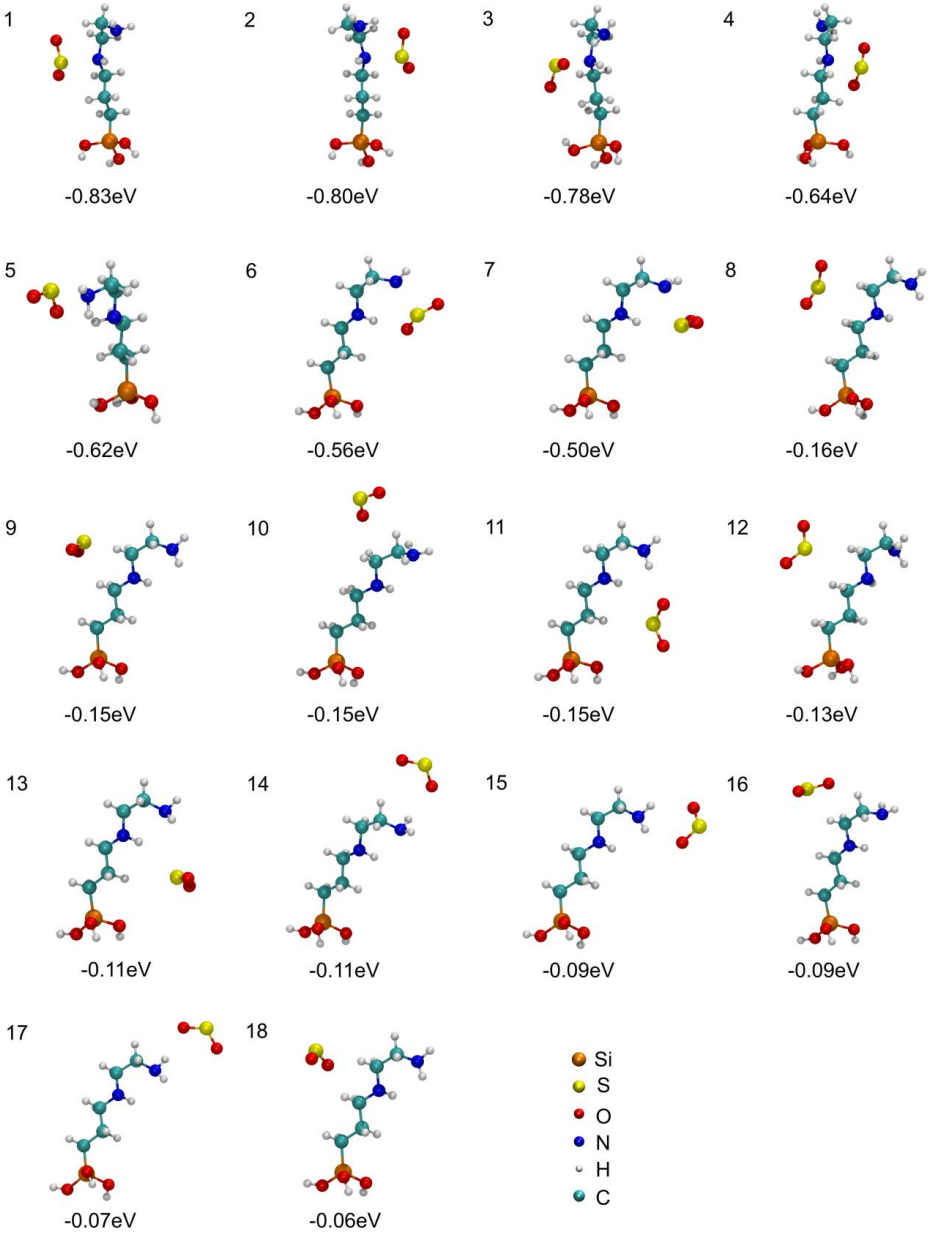

Figure S6. The eighteen inequivalent geometries of a SO_2 molecule adsorbed on en-APTAS **1** obtained in our simulations with the corresponding binding energies. The ordering is from geometries with stronger bonding (lower binding energies) to geometries with weaker bonding (higher binding energies).

Furthermore, the energetically favourable bonding geometries have been determined for NO, CO and CO_2. For this purpose we modified the fifteen relaxed NO_2 – (en-APTAS **1**) geometries from Fig. S5 to generate the initial configurations. For NO we deleted alternatingly one of the N atoms from the NO_2 and relaxed the thus obtained thirty NO-(en-APTAS **1**) geometries. Replacing the N atom of the NO in the modified NO-(en-APTAS **1**) geometries by a C atom, the initial CO-(en-APTAS **1**) geometries were generated. Finally the initial CO_2-(en-APTAS **1**) geometries were obtained by replacing the N atoms from the NO_2 of the relaxed NO_2-(en-APTAS **1**) configurations by C atoms and centering the O atom in between. In Figure **S7** we show the fifteen most stable relaxed NO-(en-APTAS **1**) geometries. Additionally, in Figure **S8** the most stable CO/CO_2-(en-APTAS **1**) geometries are shown. Again strongest adsorption of the NO, CO and CO_2 to en-APTAS **1** occurs near the secondary amine group.

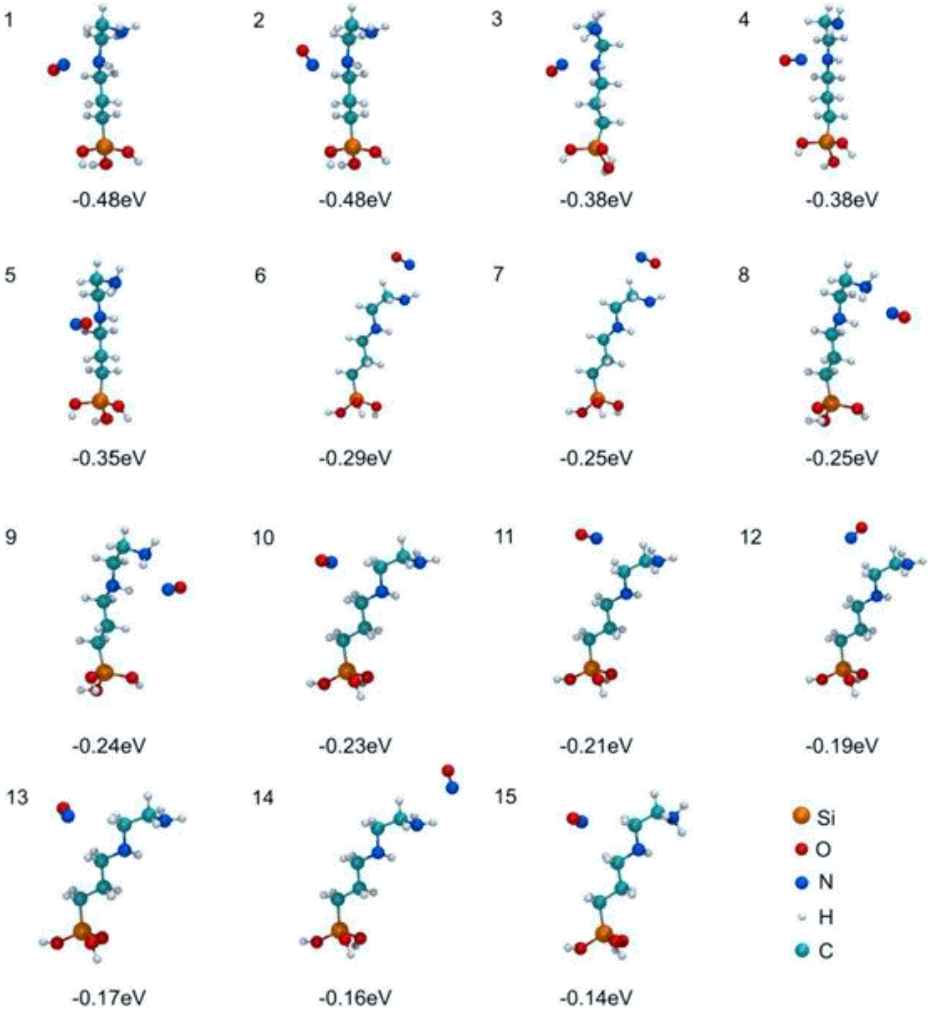

Figure S7. The fifteen most stable geometries of a NO molecule adsorbed on the (en-APTAS **1**) obtained in our simulations with the corresponding binding energies. The ordering is from geometries with stronger bonding (lower binding energies) to geometries with weaker bonding (higher binding energies).

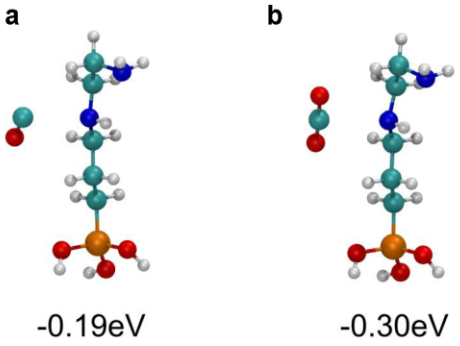

Figure S8. The most stable geometries of **a,** CO and **b**, CO_2 adsorbed on en-APTAS **1** obtained in our simulations with the corresponding binding energies.

Accumulated charge transfer upon adsorption of gas molecules

Integrating the change in the one-dimensional charge density $\Delta\rho(z)$ upon adsorption of a gas molecule on the SAM-modified SnO_2 from equation (1), from the center z_0 of the SnO_2 slab along the *z*-axis, we obtain a measure of the charge transferred to the region between z_0 and z,

$$Q(z) = \int_{z_0}^{z} \Delta\rho(z')dz'$$

Denoting the coordinate of the NW surface by z = 0, Q(0) is the net charge transferred from a single gas molecule to the SnO_2-system. In Figure **S9b** we show the accumulated charge transfer obtained by integrating the charge density changes $\Delta\rho(z)$ from Figure 4a due to adsorption of NO_2, SO_2 and NO gas molecules on the SAM-modified SnO_2. In the case of NO_2 we find a net charge depletion of $Q(0)$=-0.038 electron charges in the SnO_2 per adsorbed molecule. SO_2 adsorption does not lead to a noticeable change in charge carrier concentration in SnO_2 and a net charge accumulation of $Q(0)$=0.016 electron charges is observed upon NO adsorption.

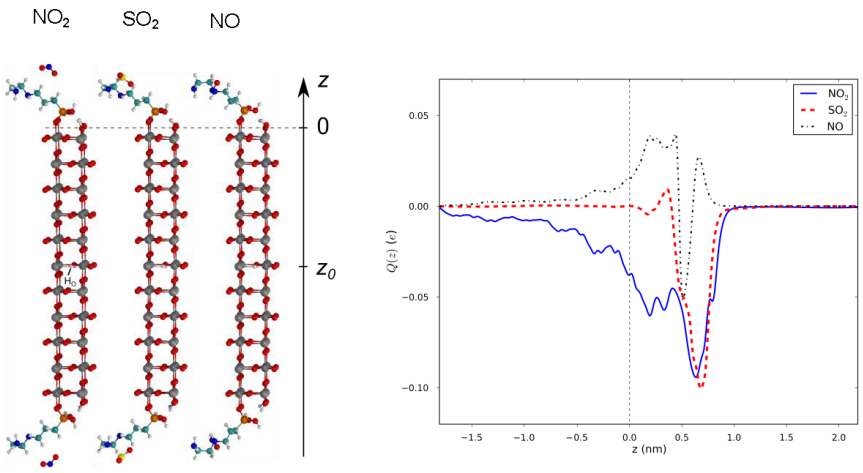

Fig. S9: a, Employed unit cells for the simulation of charge transfer upon NO_2, SO_2 and NO adsorption. The center of the SnO_2 slab is denoted by z_0 and its surface, defined by the mean z-coordinate of the bridging oxygen atoms, is given by $z = 0$. H_O denotes the substitutional H atom leading to n-doping of the SnO_2 slab. **b**, Accumulated charge transfer $Q(z)$ in electron charges e due to adsorption of a single NO_2, SO_2 and NO molecule, respectively.

References

[1] S. Mathur, S. Barth, H. Shen, J.-C. Pyun, U. Werner, *Small* **2005**, *1*, 713–7.
[2] J. D. Prades, F. Hernandez-Ramirez, R. Jimenez-Diaz, M. Manzanares, T. Andreu, A. Cirera, A. Romano-Rodriguez, J. R. Morante, *Nanotechnology* **2008**, *19*, 465501.
[3] B. P. J. de Lacy Costello, R. J. Ewen, N. M. Ratcliffe, M. Richards, *Sens. Actuat. B* **2008**, *134*, 945–952.
[4] K. Bradley, J. Cumings, A. Star, J.-C. P. Gabriel, G. Grüner, *Nano Lett.* **2003**, *3*, 639–641.
[5] Y. Cui, Q. Wei, H. Park, C. M. Lieber, *Science* **2001**, *293*, 1289–1292.
[6] O. Kuzmych, B. L. Allen, A. Star, *Nanotechnology* **2007**, *18*, 375502.
[7] D. Boudinet, M. Benwadih, S. Altazin, J.-M. Verilhac, E. De Vito, C. Serbutoviez, G. Horowitz, A. Facchetti, *J. Am. Chem. Soc.* **2011**, *133*, 9968–9971.
[8] W. Yuan, A. Liu, L. Huang, C. Li, G. Shi, *Adv. Mater.* **2013**, *25*, 766–771.
[9] M. G. Chung, D. H. Kim, H. M. Lee, T. Kim, J. H. Choi, D. K. Seo, J.-B. Yoo, S.-H. Hong, T. J. Kang, Y. H. Kim, *Sens. Actuat. B* **2012**, *166-167*, 172–176.
[10] D. Zhang, Z. Liu, C. Li, T. Tang, X. Liu, S. Han, B. Lei, C. Zhou, *Nano Lett.* **2004**, *4*, 1919–1924.
[11] J. D. Prades, R. Jimenez-Diaz, F. Hernandez-Ramirez, S. Barth, A. Cirera, A. Romano-Rodriguez, S. Mathur, J. R. Morante, *Appl. Phys. Lett.* **2008**, *93*, 123110.
[12] C. Bittencourt, A. Felten, E. H. Espinosa, R. Ionescu, E. Llobet, X. Correig, J.-J. Pireaux, *Sens. Actuat. B* **2006**, *115*, 33–41.
[13] E. Zampetti, S. Pantalei, S. Scalese, a Bearzotti, F. De Cesare, C. Spinella, a Macagnano, *Biosensors & Bioelectronics* **2011**, *26*, 2460–5.
[14] M. C. McAlpine, H. Ahmad, D. Wang, J. R. Heath, *Nature Mater.* **2007**, *6*, 379–384.
[15] S. Srivastava, K. Jain, V. N. Singh, S. Singh, N. Vijayan, N. Dilawar, G. Gupta, T. D. Senguttuvan, *Nanotechnology* **2012**, *23*, 205501.

[16] I.-C. Chen, S.-S. Lin, T.-J. Lin, C.-L. Hsu, T. J. Hsueh, T.-Y. Shieh, *Sensors* **2010**, *10*, 3057–72.
[17] E. Comini, V. Guidi, C. Malagu, G. Martinelli, Z. Pan, G. Sberveglieri, Z. L. Wang, *J. Phys. Chem. B* **2004**, *108*, 1882–1887.

3.1.2 Paper 2

Sensors and Actuators B 181 (2013) 130–135

Contents lists available at SciVerse ScienceDirect

Sensors and Actuators B: Chemical

journal homepage: www.elsevier.com/locate/snb

Heterostructured p-CuO (nanoparticle)/n-SnO_2 (nanowire) devices for selective H_2S detection

F. Shao [a], M.W.G. Hoffmann [a,b], J.D. Prades [b], R. Zamani [a,c], J. Arbiol [c,d], J.R. Morante [a,b], E. Varechkina [e], M. Rumyantseva [e], A. Gaskov [e], I. Giebelhaus [f], T. Fischer [f], S. Mathur [f], F. Hernández-Ramírez [a,b,*]

[a] Catalonia Institute for Energy Research (IREC), E-08930 Sant Adrià del Besòs, Spain
[b] Department of Electronics, University of Barcelona, E-08028 Barcelona, Spain
[c] Institut de Ciència de Materials de Barcelona, ICMAB-CSIC, Campus de la UAB, E-08193 Bellaterra, Spain
[d] Institució Catalana de Recerca i Estudis Avançats (ICREA), E-08010 Barcelona, Spain
[e] Chemistry Department, Moscow State University, 119991 Moscow, Russia
[f] Institute of Inorganic Chemistry, University of Cologne, D-50939 Cologne, Germany

ARTICLE INFO

Article history:
Received 2 October 2012
Received in revised form
30 December 2012
Accepted 14 January 2013
Available online xxx

Keywords:
H_2S
Sensor
Heterostructure
Metal oxide
CuO
SnO_2

ABSTRACT

Dihydrogen sulphide (H_2S) is a dangerous pollutant released in fossil combustion processes. Here, p-CuO (particle)/n-SnO_2 (nanowire) heterostructures were evaluated as selective H_2S sensors, and the working principle behind their good performance was qualitatively modelled. It was concluded that the main sensing mechanism was dissimilar to standard redox reactions typical of simple metal oxide devices, but ascribable to the sulphurization of CuO and the consequent variation of the pn-junction band structure at the CuO–SnO_2 interfaces. Experimental data showed that these H_2S sensors suit well for alarm applications with extremely high selectivity and sensitivity to this gas for concentrations between 1 ppm and 10 ppm.

1. Introduction

Fossil combustion processes play a key role in the worldwide production of air pollutants due to the release of dust particles, greenhouse gases (CO_2) and highly toxic gas species (e.g. NO_x, CO and H_2S). Main sources such as power plants and car engines usually operate in direct proximity to urban areas, which makes the control and optimization of combustion processes essential to guarantee a high environmental quality [1–3]. Amongst all pollutants, dihydrogen sulphide (H_2S) is identified as a major threat for the human health even at low concentrations of 10 ppm [4]. Therefore, the search of new and highly selective methods for the detection of H_2S has attracted a huge interest within the past years [5].

Metal oxides (MOX) have shown outstanding sensing properties to different chemical species with simple and cost effective device configurations [6,7]. Nevertheless, a major drawback of this technology is the unspecific interaction of the MOX surface with the surrounding atmosphere, which is based on redox processes involving surface bound oxygen species (combustion), and a consequent modulation of the electrical resistance [8]. The integration of MOX heterostructures [9–11] in sensors is considered a promising alternative to reach partial improvements in terms of both selectivity and sensitivity. For H_2S detection, CuO/SnO_2 heterostructures revealed an extraordinary performance in these domains [12–15]. This is usually explained by two different but complementary contributions; (i) the particular interaction of CuO and H_2S and (ii) the intrinsic properties of the CuO/SnO_2 interface.

The interaction of CuO with H_2S does not follow a conventional redox reaction, but undergoes a thermal activated anion exchange to form CuS. This transformation is reversible in oxygen-rich atmosphere [16–19], and it is summarized by:

$$CuO + H_2S \rightarrow CuS + H_2O \quad (1)$$

$$CuS + (3/2)O_2 \rightarrow CuO + SO_2 \quad (2)$$

The stoichiometric chemical path shown in Eq. (1) facilitates thus a selective detection of H_2S and an effective discrimination towards other gases.

* Corresponding author at: Catalonia Institute for Energy Research (IREC), E-08930 Sant Adrià de Besòs, Spain. Tel.: +34 933 562 615; fax: +34 933 563 802.
E-mail address: fhernandez@irec.cat (F. Hernández-Ramírez).

0925-4005/$ – see front matter © 2013 Elsevier B.V. All rights reserved.
http://dx.doi.org/10.1016/j.snb.2013.01.067

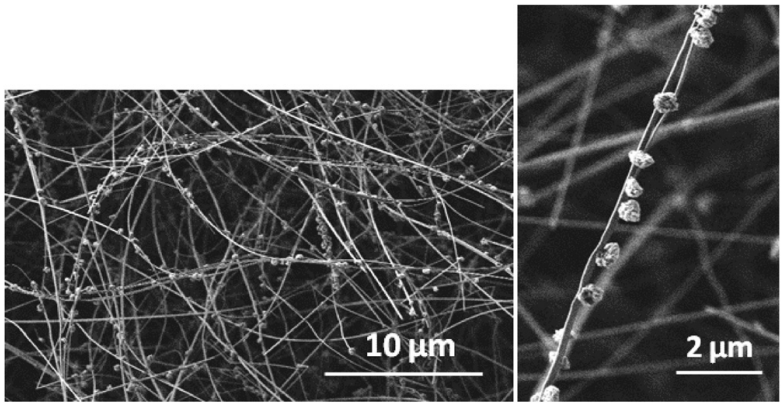

Fig. 1. (Left) General view of a bundle of p-CuO (particle)/n-SnO_2 (nanowire) heterostructures. High magnification SEM image of p-CuO particles onto a single SnO_2 nanowire (right).

On the other hand, the particular configuration of the CuO/SnO_2 interface maximizes the sensitivity towards H_2S. CuO as p-type and SnO_2 as n-type semiconductors form a pn-junction with a depletion zone in between, whose characteristics depend on the respective Fermi level positions. Any structural and compositional modification of the MOXs involves Fermi level variations and a change of the depletion zone. As a result, the electrical properties of the entire heterostructure are strongly modulated. Actually, upon exposure to H_2S, copper oxide undergoes a sulphurization process to form a ternary $Cu_xO_zS_y$ compound and finally CuS with metallic characteristics (Eq. (1)). Under these conditions, the heterostructure changes from a standard pn-junction towards a metal-semiconductor interface. In short, these two phenomena together have a net effect on the electrical properties of the sensors that can be orders of magnitude higher than the caused by standard redox surface reactions in MOXs [8].

Here, we report p-CuO (particle)/n-SnO_2 (nanowire) heterostructured devices and their application as H_2S sensors. The high sensitivity and selectivity to this pollutant were evaluated and compared to bare n-SnO_2 nanowire sensors, showing significant improvements in terms of sensitivity and selectivity that are fully comparable to previous results reported in the literature [12–15]. Individual heterostructure devices were also tested to effectively model the working principle of the p-CuO (particle)/n-SnO_2 (nanowire) junctions. The well-defined geometry and the absence of pn-junction barriers dominating transport through nanowires in a similar way that grain boundaries in thick-film sensors [14] unequivocally correlate the response with the modulation of the conduction channel inside the nanowires upon exposure to H_2S.

2. Materials and methods

p-CuO (particle)/n-SnO_2 (nanowire) heterostructures were produced following a two step chemical vapour deposition (CVD) of corresponding metal precursors. In the initial step, single

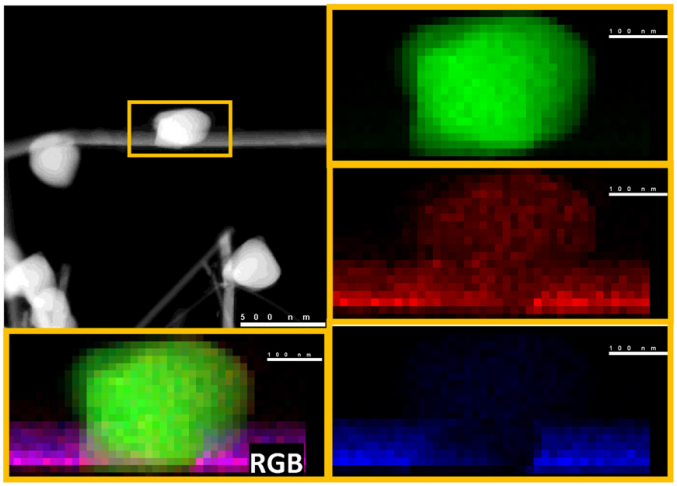

Fig. 2. HAADF STEM image and EDX maps of a herostructure. Copper (green), oxygen (red) and tin (blue) are clearly observed. (For interpretation of the references to colour in this figure legend, the reader is referred to the web version of this article.)

crystalline tin oxide nanowires were deposited by a metal-seeded vapour–liquid–solid growth mechanism [20,21] using $Sn(OBu^t)_4$ as a precursor ($T_{substrate}$ = 725 °C, $T_{precursor}$ = 25 °C, t = 30 min) on Al_2O_3 substrates covered with gold nanoparticles. In a subsequent step, copper particles were deposited on pre-grown SnO_2 nanowires by the CVD of $Cu^{II}((C_5H_4N)(CHCOCF_3))_2]_2$, following a procedure described earlier [22] ($T_{substrate}$ = 780 °C, $T_{precursor}$ = 155 °C, t = 40 min). The resulting SnO_2 nanowires decorated with copper particles of an average size of ca. 200 nm were annealed in air at 300 °C for 24 h producing p-CuO (particle)/n-SnO_2 (nanowire) heterostructures (Fig. 1). After annealing, a size-increase of particles was evident due to the volume expansion associated to the transformation of Cu to CuO. X-ray diffraction patterns and TEM analysis confirmed the presence of crystalline SnO_2 nanowires (cassiterite phase) as well as the copper oxide (Fig. 2) [22]. High angular annular dark field (HAADF) scanning transmission electron microscopy (STEM) was performed in an aberration corrected FEI Titan microscope operated at 300 keV with a coupled X-ray energy dispersive (EDX) spectrometer. No HRTEM images from the CuO–SnO_2 interfaces could be obtained due to the large dimensions of both nanowires and nanoparticles. In this work and for simplicity's sake, we assumed however the formation of ideal pn-junctions at CuO–SnO_2 heterostructures to model the experimental data.

Gas sensing experiments were performed with bundled and individual structures. Bundled bare SnO_2 nanowires and p-CuO/n-SnO_2 heterostructures were characterized after depositing sensing layers in form of thick films onto substrates with pre-patterned Pt contacts on the front side and a Pt-meander on the back-side acting as a heater and temperature probe. Deposited thick films of MOXs mixed with α-terpineol were dried at 50 °C for 24 hours and then sintered at 300 °C for 7 days in air. Sensor test were performed in DC

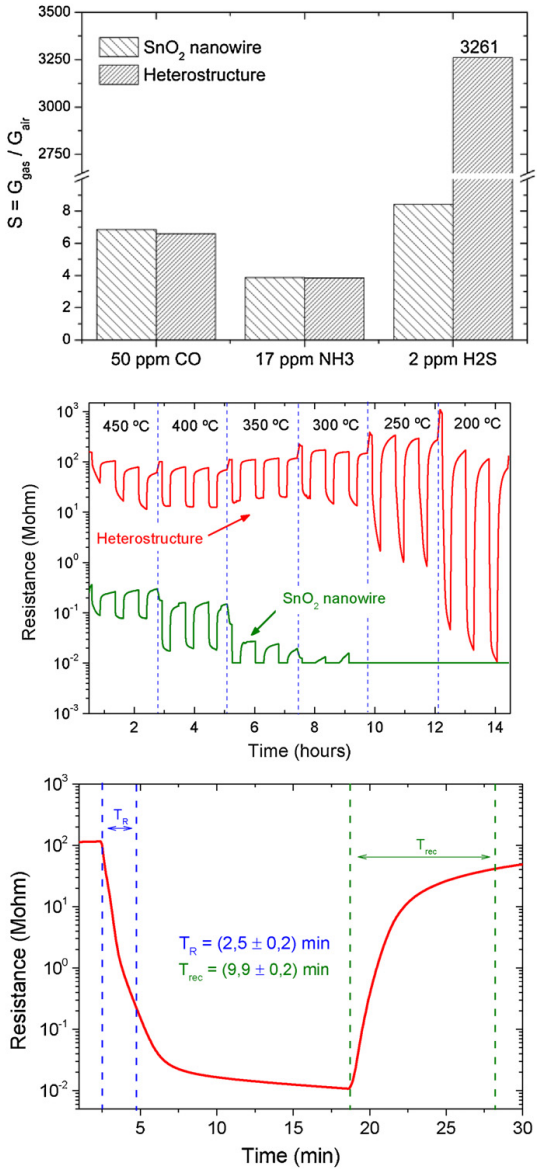

Fig. 3. (a) Response towards CO, NH_3 and H_2S of bare SnO_2 nanowires and p-CuO (particle)/n-SnO_2 (nanowire) heterostructures. A huge enhancement of the selectivity and sensitivity to H_2S is observed for the heterostructure. (b) Response of p-CuO/n-SnO_2 heterostructures and bare SnO_2 nanowires to 2 ppm H_2S at different temperatures. (c) Enlarged response of the heterostructure to 2 ppm H_2S at 200 °C. The response time, T_R, and recovery time, T_{rec}, correspond to the 90% of change in the electrical resistance of the samples.

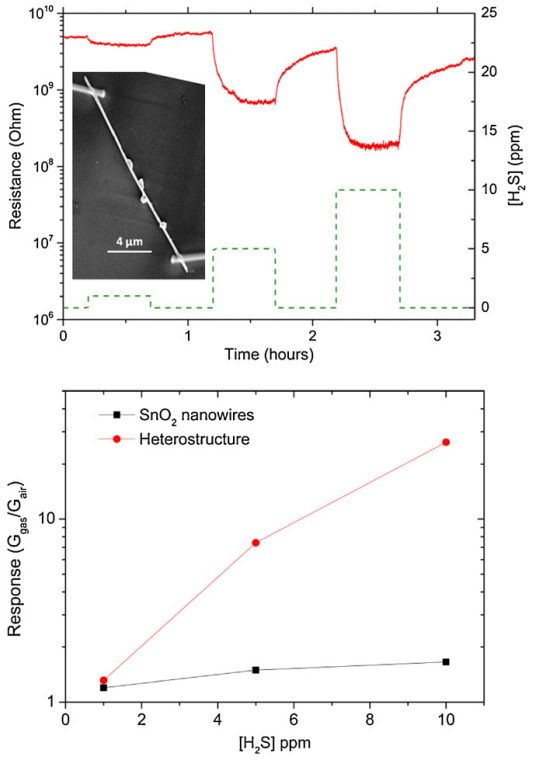

Fig. 4. (Up) Response of an individual p-CuO (particle)/n-SnO_2 (nanowire) heterostructure to H_2S pulses. Dynamic response of the device is convoluted with the dynamic response of the gas chamber (Inset) SEM image of the device. Response of an individual p-CuO (particle)/n-SnO_2 (nanowire) heterostructure as function of H_2S concentration (bottom).

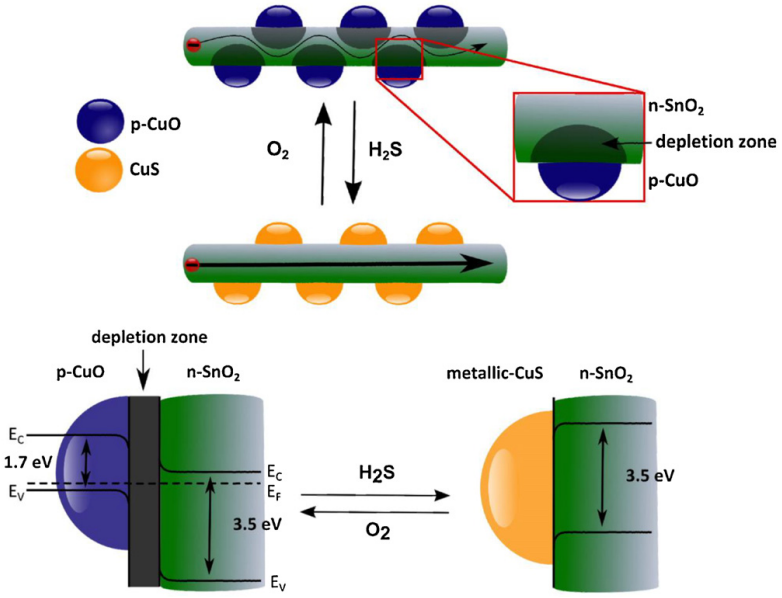

Fig. 5. General sketch of the heterostructure: p-CuO particles on the n-SnO_2 surface create a pn-junction. The depleted region reduces the effective conduction channel in the nanowire, leading to a higher resistance. After H_2S sensing, p-CuO particles change to metallic CuS, resulting in a breakup of the pn junction, a wider conduction channel in the nanowire and as consequence a lower resistance value.

mode (U = 3 V) under constant gas flux of 100 ml/min. Atmosphere compositions were precisely produced with mass-flow controllers and certified gas bottles. Individual p-CuO/SnO_2 heterostructures were electrically contacted to Pt nanoelectrodes by means of FIB assisted lithography [23] and they were evaluated as gas sensors inside a customized chamber especially designed to minimize the external noise.

3. Results and discussion

The sensing and selectivity characteristics of p-CuO/n-SnO_2 heterostructures were evaluated, and confronted to the typical response of bare SnO_2 nanowires. Both samples were exposed to standard reducing pollutants; H_2S (2 ppm), carbon monoxide (CO; 40 ppm) and ammonia (NH_3; 17 ppm). Here, the response S was defined as,

$$S = \frac{G_{gas}}{G_{air}} \quad (3)$$

where G_{gas} is the device conductance after exposure to the target gas, and G_{air} the conductance in synthetic air. S reached a value of S = 6 and S = 4 in NH_3 and CO experiments, respectively for the heterostructures, which was similar to the measured responses for bare SnO_2 nanowires (Fig. 3). This indicates that the detection mechanism of NH_3 and CO in both cases was mainly ascribable to the redox reaction between the pollutants and the SnO_2 surface. On the contrary, S rose up from S = 9 to S = 3250 for the heterostructure upon exposure to H_2S (Fig. 3). The dramatic change of the p-CuO/n-SnO_2 system leads one to believe that a dissimilar sensing mechanism occurred in H_2S atmosphere. In all cases, gas responses were reversible since sensors completely recovered the initial conductance baseline in synthetic air for the applied H_2S pulses with response and recovery time constants below 3 and 10 min, respectively (Fig. 3). The response of both the heterostructured samples and the bare SnO_2 nanowires as function of H_2S concentration is shown in the supporting information section. Optimal working conditions were observed between 200 °C and 250 °C, whereas smaller response values towards H_2S were monitored at lower and higher temperatures (Fig. 3). At high temperatures (T > 250 °C), a partial and fast regeneration of the thermodynamically more stable p-CuO from CuS during H_2S pulses cannot be discarded, avoiding a complete breakup of the pn-junction.

To gain further insight into the sensing mechanism of p-CuO/n-SnO_2 systems, individual SnO_2 nanowires with and without decoration of CuO particles were contacted with FIB lithography (inset Fig. 4). This device configuration allows to monitor the electrical properties, excluding misleading effects arising from interring nanowire contact barriers which are always present in bundle-structured samples [24]. The sensor temperature was adjusted to 250 °C, and H_2S pulses of concentrations ranging from 1 ppm to 10 ppm were applied. Again, bare n-SnO_2 devices exhibited low responses to H_2S with S < 2. In sharp contrast, p-CuO/n-SnO_2 heterostructures responded to H_2S pulses of 5 ppm and 10 ppm more efficiently (S = 7.4 and S = 26.3, respectively). Surprisingly, the same response to the lowest H_2S pulse, 1 ppm, was observed in both cases (Fig. 4). This experimental result implies that at low target gas concentrations ([H_2S] < 1 ppm), the redox reaction between H_2S and the SnO_2 surface becomes predominant in contrast to the process shown in Eq. (1). Under these experimental conditions, regeneration from metallic CuS to p-CuO (Eq. (2)) takes place at the same rate or even faster than the sulphurization of copper oxide particles, resulting in an effective shift of the chemical equilibrium towards the oxide side. Consequently, no CuS or just a thin shell onto p-CuO was formed with a minor influence on the electrical properties of the pn-junction at the p-CuO/n-SnO_2 interfaces. After exceeding the critical concentration threshold for H_2S, [H_2S] ≈ 1 ppm, the modulation of the pn-junction was activated and the sensitivity of the device maximized. In fact, a

stoichiometric sulphur amount within the Cu-containing particles (Cu:S = 1:1) could be detected via EDX after long time exposure of the heterostructure to 10 ppm of H_2S (2 h, 250 °C) (see supporting information). The ion ratio was shifted back to Cu:S = 1.0:0.4 after keeping the sensor in synthetic air, proving the partial reversibility of the ion exchange. The same behaviour of sensitivity maximization was observed for bundle samples (supporting information). Here, it should be pointed out that the lower response of individual nanowire devices to H_2S compared with those of bundles of nanowires is explained by different reasons; (i) the absence of pn-junction barriers dominating transport through nanowires in a similar way that grain boundaries in thick-film sensors [14], (ii) damage of the heterostructures during the sonication and nanofabrication steps which are known to be aggressive for the integrity of the samples, and (iii) other parasitic effects such as contact impedance contributions that may also affect their gas response. In short, H_2S response of single-nanowire devices is mainly ascribable to the modulation of the conduction channel inside the nanowires when they are in a H_2S atmosphere.

From these findings, we propose the main underlying sensing mechanism of p-CuO (nanoparticle)/n-SnO_2 (nanowire) heterostructures upon exposure to H_2S; the chemically specific transformation from p-CuO to metallic CuS modifies the depleted region that is formed at the p-CuO/n-SnO_2 interface and strangles the conduction channel inside the nanowires in oxygen-rich atmosphere. After exposure to H_2S, the breakup of the pn-junction effectively enlarges the conduction section in the nanowire, leading to a significant improvement of the conductivity (Fig. 5). Second order effects like the oxidation of H_2S by adsorbed oxygen on CuO nanoparticles may also contribute to the pn-junction modulation. This reaction has been reported to explain H_2S sensing with CuO nanowires in the past [25].

A quantitative description of the above-mentioned mechanisms is beyond the scope of this preliminary work and would require more advanced experiments. Beside, the uncontrolled distribution of CuO particles onto SnO_2 nanowires that gives rise to minor deviations in the sensing performances of the devices remains as an open field of research for the future.

4. Conclusions

p-CuO (particle)/n-SnO_2 (nanowire) heterostructures were synthesized and evaluated as H_2S sensors. The specific interaction between this pollutant and the CuO particles as well as the amplifier effect on the response by the pn-junctions strongly enhances the selectivity to this gas in comparison to other reducing species, such as NH_3 and CO. The devices exhibit stable and reproducible responses towards H_2S pulses from 1 ppm to 10 ppm, and their performance suit well for alarm applications.

Acknowledgments

The research was supported by the Framework 7 program under the project S3 (FP7-NMP-2009-247768) and European Regional Development Funds (ERDF). Russian team was supported by the Ministry of Education and Science in the frame of State contract No. 11.519.11.1009. J.A. acknowledges the funding from the Spanish MICINN projects MAT2010-15138 (COPEON) and CSD2009-00013 (IMAGINE) and Generalitat de Catalunya (2009 SGR 770 and NanoAraCat). Authors also acknowledge the use of advanced electron microscopes at INA-LMA.

Appendix A. Supplementary data

Supplementary data associated with this article can be found, in the online version, at http://dx.doi.org/10.1016/j.snb.2013.01.067.

References

[1] R. Moos, A brief overview on automotive exhaust gas sensors based on electroceramics, International Journal of Applied Ceramic Technology 2 (2005) 401–413.
[2] B. Timmer, W. Olthuis, A.V.D. Berg, Ammonia sensors and their application—a review, Sensors and Actuators B: Chemical 107 (2005) 666–677.
[3] C.N. Xu, N. Miura, Y. Ishida, K. Matsuda, N. Yamazoe, Selective detection of NH_3 over NO in combustion exhausts by using Au and MoO_3 doubly promoted WO_3 element, Sensors and Actuators B: Chemical 65 (2000) 164–165.
[4] C.H. Selene, J. Chou, Hydrogen sulfide: human health aspects, in: Concise International Chemical Assessment Document WHO, 2003.
[5] S.K. Pandey, K.-H. Kim, K.-T. Tang, A review of sensor-based methods for monitoring hydrogen sulfide, TrAC, Trends in Analytical Chemistry 32 (2012) 87–99.
[6] G. Sberveglieri, Recent developments in semiconducting thin-film gas sensors, Sensors and Actuators B: Chemical 23 (1995) 103–109.
[7] A. Kolmakov, M. Moskovits, Chemical sensing and catalysis by one-dimensional metal-oxide nanostructures, Annual Review of Materials Research 34 (2004) 151.
[8] N. Barsan, U. Weimar, Conduction model of metal oxide gas sensors, Journal of Electroceramics 7 (2001) 143–167.
[9] N. Yamazoe, J. Tamaki, N. Miura, Role of hetero-junctions in oxide semiconductor gas sensors, Materials Science and Engineering B 41 (1996) 178–181.
[10] X.M. Shuai, W.Z. Shen, A facile chemical conversion synthesis of ZnO/ZnS core/shell nanorods and diverse metal sulfide nanotubes, Journal of Physical Chemistry C 115 (2011) 6415–6422.
[11] Y. Takao, K. Miyazaki, Y. Shimizu, M. Egashira, High ammonia sensitive semiconductor gas sensors with double-layer structure and interface electrodes, Journal of the Electrochemical Society 141 (1994) 1028–1034.
[12] I.-S. Hwang, J.-K. Choi, S.-J. Kim, K.-Y. Dong, J.-H. Kwon, B.-K. Ju, J.-H. Lee, Enhanced H_2S sensing characteristics of SnO_2 nanowires functionalized with CuO, Sensors and Actuators B: Chemical 142 (2009) 105–110.
[13] X.H. Kong, Y.D. Li, High sensitivity of CuO modified SnO_2 nanoribbons, Sensors and Actuators B: Chemical 105 (2005) 449–453.
[14] X.Y. Xue, L. Xing, Y. Chen, S. Shi, Y. Wang, T. Wang, Synthesis and H_2S sensing properties of CuO–SnO_2 core/shell PN-junction nanorods, Journal of Physical Chemistry C 112 (2008) 12157–12160.
[15] L.A. Patil, D.R. Patil, Heterocontact type CuO-modified SnO_2 sensor for the detection of a ppm level H_2S gas at room temperature, Sensors and Actuators B: Chemical 120 (2006) 316–323.
[16] T. Pagnier, M. Boulova, A. Galerie, A. Gaskov, G. Lucazeau, Reactivity of SnO_2–CuO nanocrystalline materials with H_2S: a coupled electrical and Raman spectroscopic study, Sensors and Actuators B: Chemical 71 (2000) 134–139.
[17] J.G. Dunn, C. Muzenda, Thermal oxidation of covellite (CuS), Thermochimica Acta 369 (2001) 117–123.
[18] S. Wang, Q. Huang, X. Wen, X.-y. Li, S. Yang, Thermal oxidation of Cu_2S nanowires: a template method for the fabrication of mesoscopic CuO ($x = 1$, 2) wires, Physical Chemistry Chemical Physics 4 (2002) 3425–3429.
[19] C. Mu, J. He, Confined conversion of CuS nanowires to CuO nanotubes by annealing-induced diffusion in nanochannels, Nanoscale Research Letters 6 (2011) 150.
[20] S. Mathur, S. Barth, H. Shen, J.-C. Pyun, U. Werner, Size-dependent photoconductance in SnO_2 nanowires, Small 1 (2005) 713–717.
[21] R.S. Wagner, W.C. Ellis, Vapor–liquid–solid mechanism of single crystal growth, Applied Physics Letters 4 (1964) 89–90.
[22] I. Giebelhaus, E. Varechkina, T. Fischer, M. Rumyantseva, V. Ivanov, A. Gaskov, W. Tyrra, S. Mathur, Journal of Physical Chemistry C, submitted for publication.
[23] F.H. Ramirez, A. Tarancon, O. Casals, J. Rodriguez, A. Romano-Rodriguez, J.R. Morante, S. Barth, S. Mathur, Y. Choi T., D. Poulikakos, V. Callegari, P.M. Nellen, Fabrication and electrical characterization of circuits based on individual tin oxide nanowires, Nanotechnology 17 (2006) 5577–5583.
[24] L.V. Thong, L.T.N. Loan, N. Van Hieu, Comparative study of gas sensor performance of SnO_2 nanowires and their hierarchical nanostructures, Sensors and Actuators B: Chemical 150 (2010) 112–119.
[25] H. Kim, C. Jin, S. Park, S. Kim, C. Lee, H_2S gas sensing properties of bare and Pd-functionalized CuO nanorods, Sensors and Actuators B: Chemical 161 (2012) 594–599.

Biographies

Feng Shao is a young researcher at Catalonia Institute for Energy Research and he is currently pursuing his doctorate degree at the University of Barcelona. His research interests include the development and modelling of metal oxide based gas nanosensors.

Martin W.G. Hoffmann received his diploma degree in Chemistry 2009 from the University of Cologne, Germany. He is currently pursuing his doctorate degree at

the University of Barcelona. His research interests include metal oxide based gas nanosensors and their surface modification for higher selectivities.

Joan Daniel Prades was born in Barcelona in 1982. He graduated in Physics at the University of Barcelona in 2005 and obtained his Ph.D. at the same institution in 2009. He has experience in modelling of the electronic and vibrational properties of nanostructured metal oxides and in their experimental validation. He is actively involved in the development of innovative device prototypes based on nanowires. He has published more than 40 papers in peer-reviewed journals and contributed to more than 10 international conferences. He has also contributed to five industrial patents.

Reza Zamani received his B.Sc. in Materials Science and Engineering from Sharif University of Technology (Tehran, Iran) in 2007, and the M.Sc. in Nanoscience and Nanotechnology from the University of Barcelona in 2009. Currently he is a PhD candidate in the Institute of Materials Science of Barcelona (ICMAB-CSIC) and Catalonia Institute for Energy Research (IREC) since January 2010. His research activity is focused on characterization of nanostructured materials by means of transmission electron microscope (TEM) with various techniques, e.g. HRTEM, STEM, EELS and EDX.

Jordi Arbiol graduated in Physics at the University of Barcelona (UB) in 1997, received his European PhD in Physics in 2001 (UB), and obtained the PhD Extraordinary Award. In 2000 he was appointed as Assistant Professor in the Electronics Department (UB). In 2009 he was appointed as ICREA Research Professor at Institut de Ciència de Materials de Barcelona (ICMAB-CSIC). He is currently the Scientific Supervisor of the Electron Microscopy lab at ICMAB-CSIC, and is member of the Executive Board at the Spanish Microscopy Society. His current research activities are centred in the structural, compositional and morphological characterization of nanosized materials and devices by means of TEM related techniques (HRTEM, EELS, EFTEM, STEM and electron tomography) with more than 200 publications up to date.

Joan Ramon Morante received his Ph.D. from the University of Barcelona in 1980. Since 1985 he is full professor in the Department of Electronics. In 2008 he joined the Catalonia Institute of Research for Energy, IREC where he is the head of the Advanced Materials Area. His activities have been centred in electronic materials and devices; the assessment of their related technologies and production processes, specially emphasizing materials technology transfer. He is actively involved in research of new sensors, actuators and microsystems.

Elena Varechkina graduated in Materials Science at the Moscow State University in 2012. Her Master thesis is focused on synthesis and characterization of new materials for gas sensors.

Marina Rumyantseva graduated in Chemistry at the Moscow State University in 1992. She received her Ph.D. in 1996 from Moscow State University and from National Polytechnic Institute of Grenoble and the title of Doctor of Science in Inorganic and Solid State Chemistry in 2009. From 1997 until now, she has been employed in the Chemistry Department of Moscow State University, where she has been involved in the research on synthesis and characterization of semiconductor materials for gas sensors. She has more than 100 publications in the field of the chemistry of gas sensors materials.

Alexandre Gaskov leads the Laboratory Chemistry and Physics of Semiconductor and Sensor Materials of Moscow State University. He is Doctor of Science in Inorganic Chemistry (1988) and Professor of Chemistry (1993). He has more than 30 years experience of research in semiconductor material science, including crystal and thin films growth, heterostructure synthesis, surface analysis, development of semiconductor materials for IR detectors and gas sensors.

Irina Giebelhaus studied chemistry at the University of Cologne where she continued her PhD in the group of Prof. Sanjay Mathur. She is designing novel precursors and studying their decomposition in chemical vapor deposition processes for synthesizing functional nanostructures. Her research interests lie in the field of nanomaterials for gas sensing applications.

Thomas Fischer is a Group Leader at the Institute of Inorganic Chemistry with vast experience in the R & D activities of both EU and industrial projects. His research activities are based around the in situ investigations of the formation of metal oxide nanostructures from molecular precursors. Further, he is working on the direct integration of functional metal oxide nanostructures on sensor platforms. He has co-authored 7 publications. He was the lead organizer of the first "Global Young Investigator Forum" organized under the auspices of American Ceramic Society in Daytona Beach Florida, 2012.

Sanjay Mathur is the Director of the Institute of Inorganic and Materials Chemistry at the University of Cologne, Cologne, Germany. His research interests focus on various facets of chemical nanotechnologies with thrust on chemical routes to functional nanostructures for diversified applications ranging from biocompatible materials, nanotoxicology studies, engineered surfaces and new materials and devices for energy applications. He holds five patents and has authored/co-authored over 200 original research publications and book chapters. He is the Chair of Engineering Ceramics Division of the American Ceramic Society. He is an Academician of the World Academy of Ceramics and serves as the "International Ambassador" of the University of Cologne.

Francisco Hernández-Ramírez graduated in Physics at the University of Barcelona in 2003 and obtained his Ph.D. at the same institution in 2007. He is actively involved in the development of innovative sensor prototypes based on nanowires. He has published more than 30 papers in peer-reviewed journals and contributed to five industrial patents.

3.2 Self-Powered Sensing

Included Paper 3:

Hoffmann, M. W. G.; Gad, A. E.; Prades, J. D.; Hernandez-Ramirez, F.; Fiz, R.; Shen, H.; Mathur, S., "Solar diode sensor: Sensing mechanism and applications", *Nano Energy* 2, 514–522 (2013). (impact factor: 10.2)

Included Paper 4:

Gad, A. E.; Hoffmann, M. W. G.; Hernandez-Ramirez, F.; Prades, J. D.; Shen, H.; Mathur, S., "Coaxial p-Si/n-ZnO nanowire heterostructures for energy and sensing applications", *Mater. Chem. Phys.* 135, 618–622 (2012). (impact factor: 2.1)

The high power consumption of gas sensor devices represents (besides the previously discussed lack of selectivity) a major challenge for the application on mobile platforms. In this section, the concept of a novel multifunctional heterostructure for energy autonomous sensing operations is presented (see **paper 3**) in which the needed energy for signal generation and surface absorption/desorption activation is harvested solely from solar light. To accomplish this requirement, the CdS@n-ZnO/p-Si hetero structure consists of an energy harvesting (n-ZnO/p-Si diode) and gas sensing unit (CdS@n-ZnO NWs) with a synergetic overlap of the n-ZnO nano structure. Incident light is absorbed at the n-ZnO/p-Si junction and the formed exciton is separated due to the build in potential (V_{bi}) and creates an open circuit voltage (V_{oc}) between the p- and n-type terminals. In the sensing unit, CdS, a semiconductor with relatively narrow band gap (2.4 eV), can absorb incident visible light and transfers the excited electron to the ZnO NW, due to the favourable band alignment. Other than in case of bare wide band gap semiconductors (E_b(ZnO) = 3.4 eV), this synergy allows for an activation of the gas sensitive material (here ZnO) with solar light. The consequent interaction with the gas atmosphere modulates the intrinsic charge carrier concentration (N_D) and hence, modifies V_{oc}. This self-generated signal (V_{oc}) could be utilized to quantitatively sense oxidative and reductive gases without the need of external energy. The underlying mechanism in terms of gas–material surface interactions and the subsequent changes in the donor density (N_D) was proven experimentally.
Summarized, **paper 3** presents the following content:

- Design of a multifunctional heterostructure for self-powered gas sensing, unifying energy harvesting und gas sensing unit in a simple and compact layout.
- Evaluation of the gas sensing characteristics for self-powered operation towards oxidizing and reductive gases.

- Description of the novel gas sensing mechanism, based on modulations of the n-ZnO/p-Si build in potential (V_{bi}).
- Experimental confirmation of the proposed sensing mechanism.

To gain a better understanding of n-ZnO/p-Si based gas sensing systems, a single wire device was realized via focused ion beam (FIB) lithography and is described in **paper 4**. The p-Si core of the radial heterostructure was accessed by FIB etching and both terminals (n-ZnO shell and p-Si core) were contacted platinum stripes. The single wire configuration is well suited for the evaluation of intrinsic material properties, as statistical dispersion, typical for multi wire or bulk configurations, can be excluded. Additionally, the small dimension of those devices reduces the energy uptake during operation. The single wire device showed diode characteristics and photovoltaic performance under solar light illumination. Modelling of the electrical properties revealed a relatively low resistance in reverse bias, which can be attributed to defects at the radial p-n junction. Although the V_{oc} signal was not sufficient for gas sensing experiments in a self-powered operation, it was shown that the gas sensing performance could be modulated via the applied external current through the device, attaining a maximal response at low reverse bias currents. The contents of **paper 4** can be summarized as following:

- Realization of a single wire n-ZnO/p-Si device via FIB-assisted lithography.
- Evaluation and modelling of the electrical and photovoltaic device properties.
- Optimization of the gas sensor working conditions.

3.2.1 Paper 3

Nano Energy (2013) 2, 514–522

Available online at www.sciencedirect.com

SciVerse ScienceDirect

journal homepage: www.elsevier.com/locate/nanoenergy

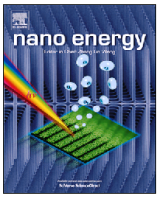

RAPID COMMUNICATION

Solar diode sensor: Sensing mechanism and applications

Martin W.G. Hoffmann[a,b,c,1], Alaa Eldin Gad[c,1], J. Daniel Prades[a,*,1], Francisco Hernandez-Ramirez[a,b], Raquel Fiz[c], Hao Shen[c,d,*], Sanjay Mathur[c,*]

[a]*Department of Electronics, University of Barcelona, E-08028 Barcelona, Spain*
[b]*Department of Advanced Materials for Energy Applications, Catalonia Institute for Energy Research (IREC), E-08930 Barcelona, Spain*
[c]*Institute of Inorganic Chemistry, University of Cologne, D-50939 Cologne, Germany*
[d]*Institute of Semiconductor Technology, Technical University Braunschweig, D-38105 Braunschweig, Germany*

Received 28 October 2012; received in revised form 16 December 2012; accepted 21 December 2012
Available online 18 January 2013

KEYWORDS
Gas sensing;
Nano heterostructures;
Solar activated;
Donor density

Abstract
Herein we report a solar diode sensor (SDS) based on new designed CdS@n-ZnO/p-Si nanoelements which unify gas sensing (CdS@n-ZnO) and solar energy harvesting (n-ZnO/p-Si diode) functionalities in a singular material unit and device. A novel The SDS sensing mechanism (change of open circuit voltage, ΔV_{oc}), in comparison to the well-known conductometric sensors (change of resistance, ΔR), is systematically studied and explained in terms of gas-material surface interactions and the subsequent changes in the doping level (N_D) of n-ZnO, which is manifested in the variation of V_{oc} in CdS@n-ZnO/p-Si. The fabricated SDS was capable of quantitatively detecting oxidising and reducing gases with reproducible response at room temperature and without the need of any other energy sources except solar illumination to deliver a self-sustained gas sensor.

Introduction

Combinatorial semiconductor architectures, fabricated by the assembly of nanoscopic structures are promising to exploit new properties of the heterostructures by synergetic effects. This approach can play an important role in the development of highly functional nanodevices [1,2] and their reduction of power consumption[3,4].

*Corresponding author. Fax: +49 221 470 4899.
E-mail addresses: dprades@el.ub.es (J. Daniel Prades), h.shen@tu-bs.de (H. Shen), sanjay.mathur@uni-koeln.de (S. Mathur).
[1]The authors contributed equally to this work.

2211-2855/$ - see front matter © 2013 Published by Elsevier Ltd.
http://dx.doi.org/10.1016/j.nanoen.2012.12.003

The device architecture presented here has been designed to palliate the current issues in gas sensor technologies: high power consumption, high operating temperature and production costs [5]. Among the different gas sensor technologies, conductometric sensors based on semiconductor metal oxides unify the highest robustness level and minimum costs [6-8]. Nevertheless the continuous supply of the energy needed, on one side to provide a constant voltage or current for signal generation, on the other hand to activate the chemical interaction between analyte gases and the metal oxide surface, either in the form of heat or light, demands new concepts for energy harvesting units that can be combined as a built-in module to realize autonomous sensors. In order to operate a sensing device at room temperature, UV light can be used to activate the sensor response, which eliminates the need for thermal heating, however, the requirement of a UV light source to generate excitons in the wide band gap of common metal oxides hinders the convenience of this approach [9-12].

ZnO nanorods, nanobelts or nanowires are excellent gas sensitive materials for the detection of oxidizing and reducing gases, with exceptionally enhanced sensitivity toward the adsorbed gas species in comparison to their bulk counterparts [13,14]. Pristine ZnO, an intrinsic n-type semiconductor, grown on p-doped silicon substrates produces heterojunctions interesting for applications such as solar cells or photodiodes due to low production costs and good photon-to-electron conversion efficiency [15-17]. Recent reports have shown that CdS quantum dots, assembled on ZnO nanorods can be used as effective visible light harvesting components in quantum dot solar cell devices [18,19]. The presence of a narrow band gap CdS sensitizer (2.4 eV) on the surface of ZnO extends the photoresponse of ZnO (3.37 eV) into the visible-light region [20-22]. Based on these considerations, CdS@n-ZnO/p-Si was grown in order to combine a photo-activated gas sensing unit (CdS@n-ZnO) with a p-n junction (n-ZnO/p-Si) capable of harvesting the energy required to operate the sensor from the environment.

Herein, we report and demonstrate an innovative approach towards an autonomous gas sensor, namely solar diode sensor (SDS), based on the synergy of a new designed photoactive sensing element (CdS@n-ZnO) and a diode (p-n junction, n-ZnO/p-Si) in a single unit. The device was successfully operated and its gas detection ability was demonstrated in (i) energy autonomous mode and (ii) solar light illumination at room temperature. In a recent work, we reported that a solar driven gas sensor based on CdS@n-ZnO/p-Si heterojunctions is capable of interacting with an oxygen atmosphere accompanied by a variation of V_{oc} [23]. However, we could not present the SDS concept clearly due to poor contact of such devices, poor reproducibility of sensing signal. In order to systematically study and understand the underlying SDS sensing mechanism, we have changed the geometric design of SDS devices. Based on systematically gas sensing and gas-dependent electric measurements, we can prove now that this variation of V_{oc} is due to a change of charge carrier concentration (N_D). Gas sensing experiments with reducing and oxidizing gases show that the SDS concept is capable to work as a qualitative and quantitative self sustained gas sensor. The proposed sensing mechanism for the SDS system shows that all these features are attributed to the combination of the complementary functionalities of CdS@n-ZnO/p-Si materials at the nanoscale interfaces.

Results and discussion

Gas sensing behaviour of the SDS device in dark and under illumination conditions

Fig. 1 shows the CdS@n-ZnO/p-Si gas sensing device and its different gas sensing behaviours in dark and under illumination conditions. A conductive glass (F:SnO_2, FTO) was used as a transparent top contact on the vertically aligned ZnO nanorod arrays whereas p-Si was contacted as the back electrode with silver paste to form the prototype gas sensor, [24] as illustrated schematically in Fig. 1a. The detailed structural properties of CdS@ZnO are shown in Fig. S1-4. The similar lengths of ZnO nanorods made a good electrical contact with FTO possible. The device was monitored by applying regulated bias currents (0, +25 and +50 μA) and measuring the corresponding voltages. In dark conditions (Fig. 1b), CdS@n-ZnO/p-Si showed no response for forward bias currents (0, +25 and +50 μA) in nitrogen and oxygen atmospheres apparently due to insufficient activation energy (either in form of light or heat) for interaction of oxygen species on the surface of ZnO, [25] whereas CdS@n-ZnO/p-Si showed a totally different sensing behaviour under solar illumination (simulated sun spectrum; AM1.5). The response was fully reversible and reproducible at different bias currents (Fig. 1c). Remarkably, the CdS@n-ZnO/p-Si showed significant gas sensing responses even at zero bias current, i.e., no external electric power applied. The response at zero bias current is opposite to those of bias currents, indicating a different underlying sensing mechanism in comparison to the traditional conductometric sensing principle. As no current is flowing at zero bias conditions, the measured voltage signal displays the open circuit voltage (V_{oc}) of the included n-ZnO/p-Si diode. Thus, the signal response cannot reflect the change of the conductometric properties of ZnO but has to be originated in a change of the n-ZnO/p-Si diode properties (see Supporting information). Fig. 1d shows the evolution of the open circuit voltage V_{oc} (zero current) upon exposure of the device to oxygen and nitrogen pulses under illumination. Evidently, V_{oc} is an auto-generated signal that correlates with the atmospheric composition: it decreases in oxygen in comparison to nitrogen atmospheres (by 41% in our proof-of-concept devices).

Detailed gas sensing characteristics of the SDS sensing device in diluted ethanol and methane atmospheres

To demonstrate that this proof-of-concept device can be used to detect other common target gases, the device was exposed to ethanol gas (EtOH, 50-200 ppm) and operated in the energy autonomous mode (i.e., simulated sun illumination; zero bias current; open circuit voltage (V_{oc}) monitoring). Fig. 2a and b shows the V_{oc} signals of CdS@n-

ZnO/p-Si in dark and under solar illumination conditions upon exposure to a sequence of EtOH pulses diluted in synthetic dry air whereby no V_{oc}, and consequently no modulation of V_{oc}, was observed under dark conditions. Upon illumination, the CdS@n-ZnO/p-Si showed significant dependence of V_{oc} on the EtOH concentration (inset of Fig. 2b) making the monitoring and correlations of V_{oc} suitable for quantitative sensing purpose. The response and recovery sequence repeated over a long time (~4 weeks) showed good stability and reproducibility of the monitoring system. The response of CdS@n-ZnO/p-Si towards different concentrations of methane exhibited similar quantitative gas sensing properties (Fig. 2c). On the contrary, the bare p-n junction (n-ZnO/p-Si) without CdS decoration showed only low, unstable and non-scalable response to different methane concentrations (Fig. 2d) demonstrating the key role of the CdS@n-ZnO gas sensing unit of the CdS@n-ZnO/p-Si system under solar light illumination. The system presented here contains two main components with complementary functions: CdS decorated ZnO nanorods act as photoactive gas sensing units, while the n-ZnO/p-Si junction forms the built-in signal generation unit. In case of the bare n-ZnO/p-Si device no light is absorbed by CdS, the incident light reaches the p-n junction with a higher intensity (see Fig. S6) and consequently the V_{oc} was found to be higher compared to the CdS@n-ZnO/p-Si sample. Anyway, the response of SDS mainly depends on the change of V_{oc} (ΔV_{oc}) under ambient gases and not the absolute V_{oc} value of the system. In these proof-of-concept sensors, response and recovery times as well as sensitivity values of the system are limited and far from optimum due to the fact that the gas diffusion through the nanostructures was slowed down, caused by the easy to build device setup. Although simply stacking a Si-based diode with a ZnO based sensor together would show much better performance, the integration of functional units at in a single and simple multifunctional unit is not possible.

Proposed step-by-step SDS mechanism

(i) Effects of the solar illumination

Fig. 3a sketches a non-equilibrium process that could explain the response of the system: (i) Photogeneration of electron-hole pairs in the CdS NPs. (ii) Proper band alignment between ZnO and CdS whereby the lower conduction band edge of ZnO favours an effective charge separation. Excited electrons (e^{*-}) are injected from the conduction band of CdS into the conduction band of ZnO, whilst the mismatch in the valance band and absence of an hole extracting agent (e.g., electrolyte) forces holes to remain in CdS [26]. (iii) Ongoing injection of electrons increases the number of holes within CdS leading to a transient electrical polarization corresponding to (dynamic) accumulations of holes (CdS) and electrons (ZnO surface). This is a self-limiting process that continues until the formed electric field blocks any further injections of electrons. Consequently, the dynamic processes of electron injection (CdS to ZnO) and recombination (ZnO to CdS) end

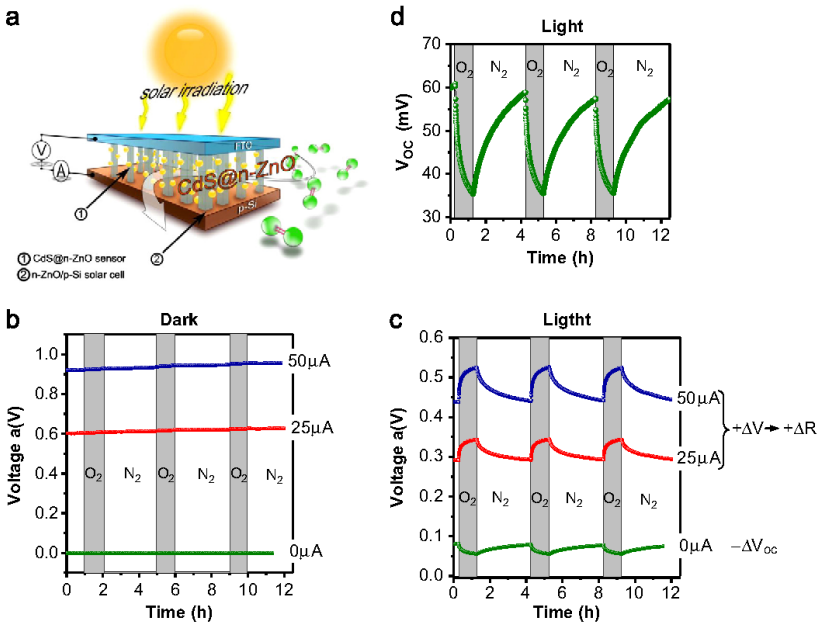

Fig. 1 (a) Scheme of the CdS@n-ZnO/p-Si sensing device. Gas sensing ON/OFF curves (oxygen/nitrogen) recorded at different constant currents in (b) dark and under (c) solar illumination showing different gas sensing behaviours. (d) ON/OFF (oxygen/nitrogen) curve recorded with open circuit voltage V_{oc} (I=0 A) under solar illumination condition.

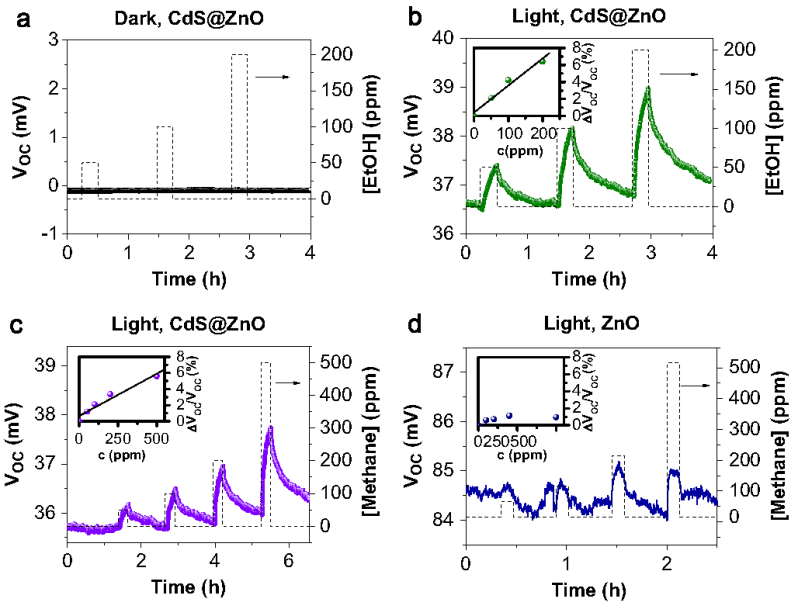

Fig. 2 Gas sensing characteristics of the CdS@n-ZnO/p-Si sensing device. ON/OFF (ethanol/air) curves of CdS@n-ZnO/p-Si recorded in (a) dark and under (b) solar illumination. ON/OFF (methane/air) curves of (c) CdS@n-ZnO/p-Si and (d) n-ZnO/p-Si recorded under solar illumination.

up in a steady state in which an overall increased electron density on the surface of ZnO is achieved [27-29]. These changes in the surface charge distribution, i.e., the creation of local electric fields between ZnO (−) and CdS (+) causes a polarization of the ZnO surface, which is accountable for variations in the gas-surface interaction that drive the sensor response [13]. Previous works demonstrated that similar effects (by using external electric fields) can activate the gas-metal oxide interaction [30,31].

The evolution of the *I-V* characteristics in dark and under illumination in nitrogen atmosphere confirmed that the non-linear and rectifying effect was originated at the n-ZnO/p-Si interface (Fig. 3b and Fig. S5). In dark conditions, CdS@n-ZnO/p-Si showed typical rectifying diode behaviour, while solar illumination shifts the *I-V* characteristics to a photovoltaic effect as shown in Fig. 3b. The latter indicates that the device is capable of directly transforming sunlight into an electrical signal (V_{oc}) due to the built-in p-n hetero-junction formed in the core of the device. Possibly due to interface defects at the n-metal oxide/p-silicon junction, a shift to more linear behaviour is noticed in the *I-V* characteristics under illumination.

(ii) Effects of oxidizing gases under illumination

Like most of the n-type semiconductor oxides, ZnO can react with oxygen to form oxygen species (O_2^-, O_2^-, O^-) on its surface [14]. A schematic representation of the charge carrier distribution across the CdS@n-ZnO/p-Si in an oxidizing atmosphere is shown in Fig. 3c. Under oxygen atmosphere, the electrons accumulated at the ZnO-CdS interface can be trapped by oxygen molecules to form oxygen species in an exergonic process ($e^{*-}+O_2(g)\rightarrow O_2^-(ad)$) [32]. The trapped electrons are subsequently compensated by bulk ZnO electrons, causing a decrease of the apparent donor density within the metal oxide (N_D decreases). Thus, electron accumulation at the ZnO surface by carrier injection from CdS upon photo excitation can explain: (i) the activation of the sensing response to gases via sunlight photons; (ii) better gas sensing behaviour observed for CdS coated n-ZnO/p-Si when compared to pure n-ZnO/p-Si. The primary experiment has shown that the CdS@n-ZnO/p-Si with full decoration rate of CdS did not show any sensing behaviours indicating that the ZnO surface and the interface of CdS and ZnO play a key role in the gas sensing mechanism.

The equations of the semiconductor quantum theory can be used to support the above-described mechanism. The relation between the donor concentration (N_D) and the built-in potential V_{bi} in a p-n junction is expressed by

$$V_{bi}=\frac{kT}{q}\mathrm{Ln}\left(\frac{N_D^{ZnO}N_A^{Si}}{N_i^{ZnO}N_i^{Si}}\right) \quad (1)$$

where N_D, N_A and N_i are donor, acceptor and intrinsic doping level, which corresponds with the free carrier concentration in the impurities ionization regime, k, T and q are Boltzmann constant, absolute temperature and electron charge, respectively [33]. The previous explanation postulated a decrease in the concentration of electrons in ZnO in presence of oxygen, which can be regarded as a decrease in the effective concentration of donor impurities N_D in the n-type ZnO. According to

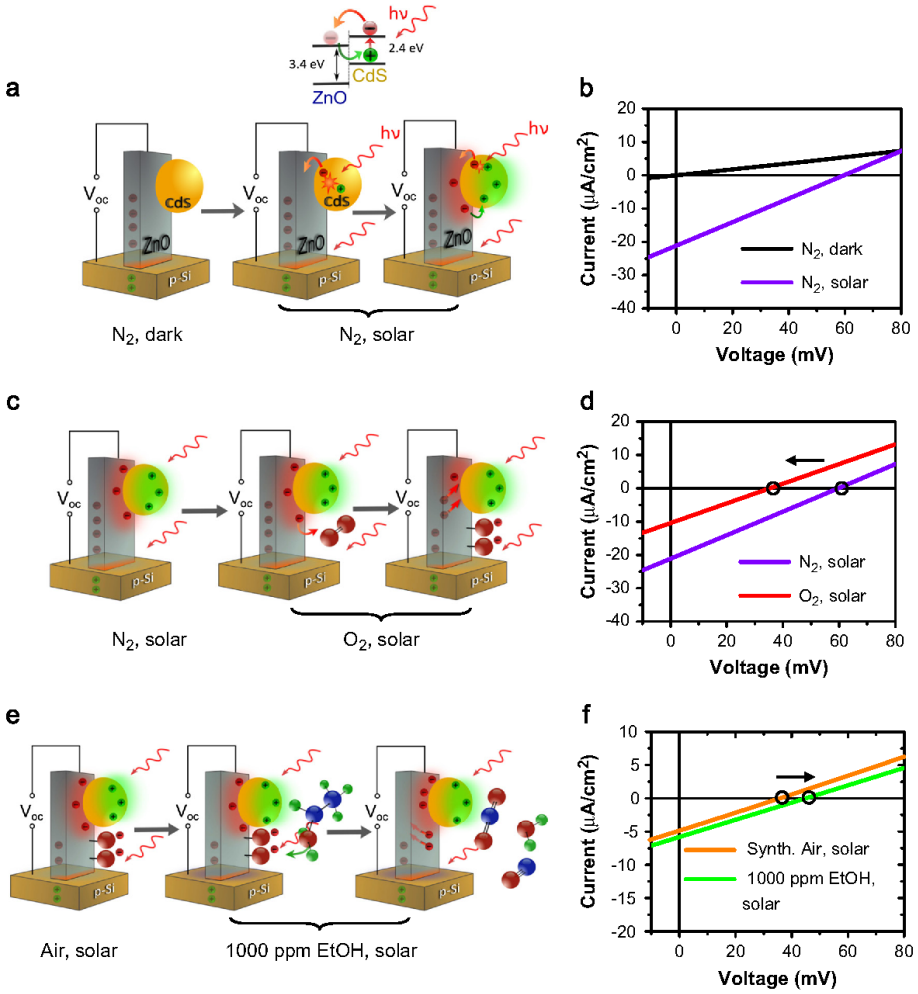

Fig. 3 Proposed step-by-step SDS mechanism: (a) High energy electron patterning on CdS@n-ZnO/p-Si under solar illumination and (b) the corresponding *I-V* curves recorded in dark and under solar illumination. (c) Charge carrier distribution of CdS@n-ZnO/p-Si in N_2 and O_2 atmospheres and (d) the corresponding *I-V* curves. (e) Charge carrier distribution of CdS@n-ZnO/p-Si in air and 1000 ppm ethanol atmospheres and (f) the corresponding *I-V* curves.

Eq. (1), the reduction of N_D leads to a decrease of the V_{bi} value in oxygen atmosphere. The open circuit voltage (V_{oc}), that appears across the terminals of a p-n junction under illumination is caused by the ability of this built-in potential to separate the electron and hole pairs generated within and close to the depleted region [33]. Thus, there exists a positive correlation between the photovoltage values (and in particular the open-circuit voltage V_{oc}) and V_{bi} [34,35]. Consequently, according to Eq. (1), the reduction of N_D leads to a decrease of V_{bi} (and thus the V_{oc} value) in oxidizing conditions, which would be verified experimentally by monitoring V_{oc} in N_2 and O_2 atmospheres (Fig. 3d). Following this mechanism, a reduction of N_D in oxidizing atmospheres causes a lower V_{oc} of the device and thus shows the opposite response direction compared to conventional n-type conductometric gas sensors (see. Fig. 1c)

(iii) Effects of reducing gases under illumination

The *I-V* characteristics of CdS@n-ZnO/p-Si in air and EtOH (1000 ppm diluted in air) atmospheres under illumination (Fig. 3e), revealed the V_{oc} values of CdS@n-ZnO/p-Si to be lower in air than that found in EtOH (air: 36 mV, EtOH: 44 mV). This behaviour can also be explained on the basis of the previous model: oxidation of EtOH molecules released electrons trapped at surface oxygen back to ZnO once the following the reaction takes place: $CH_3CH_2OH(g)+5O^-_{ads}\rightarrow CO+CO_2+$

$3H_2O+5e^-$ [36]. The consequent increase of N_D within the n-doped material causes a higher V_{oc} value as a signal for the presence of the reductive gas. These results show that the SDS device can work as quantitative and also qualitative gas sensor, as it can distinguish between reductive and oxidative gas species.

C-V characteristics and validation of the sensing mechanism.

An indirect evidence of the proposed sensing mechanism was obtained through the dependence of N_D monitored in different gas environments with the help of capacitance-voltage (*C-V*) measurements (Fig. 4). The capacitance per unit area of an ideal heterojunction diode can be expressed as [33]

$$\frac{1}{C^2} = \frac{2(N_A\varepsilon_1 + N_D\varepsilon_2)}{qN_DN_A\varepsilon_1\varepsilon_2}(V_{bi} - V) \quad (2)$$

where, in our case, N_D is the donor density in n-ZnO, N_A is the acceptor density in p-Si, ε_1 and ε_2 are the dielectric constants of n-ZnO and p-Si, respectively, q is the charge of the carriers, V_{bi} is the built-in potential of the p-n heterojunction and V is the external bias voltage. As the dielectric constants of both materials and the doping level of p-Si (N_A) are known, the slope of $1/C^2$-V plots can be used to determine N_D of ZnO.

$1/C^2$ vs. V curves in nitrogen, oxygen, air and ethanol (1000 ppm diluted in air) atmospheres displayed a linear behaviour confirming the successful formation of a p-n heterojunction at the n-ZnO/p-Si interface (Fig. 4a and b). The donor concentration of naked n-ZnO/p-Si ($2.5 \times 1019\ m^{-3}$) was insensitive to variation in the gas atmosphere or the illumination conditions (Fig. 4d) whereas the CdS@n-ZnO/p-Si system displayed significant variations (Fig. 4c). In the case of the CdS@n-ZnO/p-Si system, N_D remained constant in dark conditions (ca. $1.20 \times 1020\ m^{-3}$), but was sensitive to the presence of different gases under illumination. N_D increased sharply (ca. 16%) in N_2 atmosphere (1.20×10^{20} to $1.40 \times 10^{20}\ m^{-3}$), however, an opposite effect was observed in oxygen and synthetic air atmosphere. This behaviour is fully consistent with the previously depicted sensing mechanism, where the optical sensitization of the CdS-ZnO interface is essential to achieve the sensing behaviour. Fig. 4c shows that the change in N_D under O_2 and N_2 is more significant than that in Air/EtOH. The quantitative evidence for N_D changes in different gases is comparable to the changes in open circuit voltage (ΔV_{oc}) which is 25 mV in oxygen/nitrogen condition (Fig. 3d) however, less change in N_D was observed in Air/EtOH atmosphere (ΔV_{oc}, 8 mV) shown in Fig. 3f. This finding indicates that the change of the effective N_D within n-ZnO is the major factor influencing the V_{oc} value (sensor signal) in different gases.

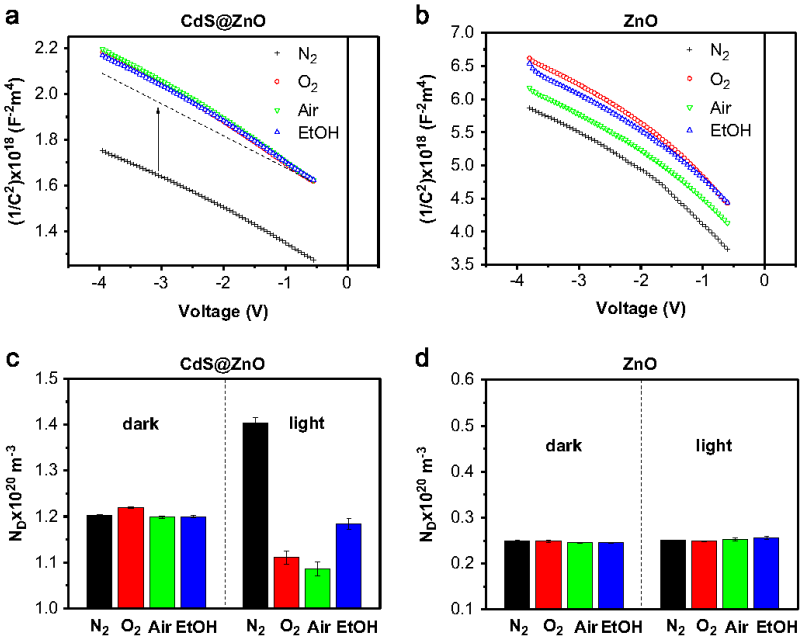

Fig. 4 Mott Schottky plots ($1/C^2$ vs. V) of (a) CdS@n-ZnO/p-Si and (b) n-ZnO/p-Si acquired at 1 MHz in the reverse bias region. Environmental dependent N_D of (c) CdS@n-ZnO/p-Si and (d) n-ZnO/p-Si recorded in dark and under solar illumination.

If a constant current is applied to the SDS device, the sensing mechanism is the same as for simple conductometric (n-type) gas sensors, in which the resistance is increased when an oxidizing gas (i.e., oxygen) is introduced. This effect can be deduced to the increase of the surface depletion zone and can be monitored by the increase of voltage as shown in Fig. 1c in cases of 25 and 50 μA applied current. When no constant current is applied (energy autonomous mode), the sensing mechanism becomes different. As no current is flowing through the device, the higher resistance is not influencing the signal. In this case the change of donor density within the n-ZnO material, caused by the interaction with the gas atmosphere, is arbitrative for the sensor response. In oxidizing atmospheres, electrons are removed from the n-ZnO and cause a reduction of the effective doping level within the material. Consequently the build in potential (V_{bi}) of the p-n junction (n-ZnO/p-Si) is reduced and can be monitored by the decrease of open circuit voltage (V_{oc}). In summary, the change of voltage (to higher values) with applied constant currents is originated from the increasing resistance of ZnO, whereas the change of voltage at energy autonomous conditions (lower V_{oc} values) is caused by the decrease of donor concentration (intrinsic doping level) within n-ZnO.

Conclusion

We have systematically demonstrated here that the inclusion of a diode element (n-ZnO/p-Si) and an active gas sensing component (CdS@ZnO) unified in a single heterostructure (CdS@n-ZnO/p-Si) enabled the operation of a novel gas sensor device without the need of any external power source. The open circuit voltage V_{oc}, produced by solar light harvesting at the n-ZnO/p-Si diode, acted as a self-generated sensing signal, whose intensity is dependent on the chemical nature of the surrounding gas and its concentration. It was proven that the change of V_{oc} is due to the variation of charge carrier density (N_D) that is directly affecting the build in potential (V_{bi}) of the p-n-junction.

This work shows the potential to integrate multiple and complementary functionalities by carefully choosing the suitable materials in a single nanoarchitecture. Following this approach, the proof-of-the concept device presented here can be extended to other material systems and applications. Future work will focus on the further improvement of SDS sensing performance and the replacement of CdS@n-ZnO/p-Si by either NPs@n-MO_x/p-Si or NPs@p-MO_x/n-Si. Moreover, it can be envisaged that the realization of self-sustained sensors will trigger further development of new nanodevices and principles to address the grand and inevitable challenge of the need for energy-efficient systems.

Experimental

Growth of ZnO nanorod arrays on p-Si substrate: Vertically oriented ZnO nanorod arrays were grown on a ZnO seed layer (20 nm) coated p-Si substrate (B-doped, Crystec GmbH, cut in 1 cm × 1 cm dices). First, the Zn film was prepared by DC sputtering using Zn target (99.99%) and high purity Ar gas (99.999%). The as-deposited film was annealed in air at 500 °C for 1 h to obtain a crystalline ZnO seed layer. The ZnO nanorod arrays were grown on the p-Si substrates using a hydrothermal synthesis reported previously [37]. Briefly, the growth solution was composed of zinc nitrate hexahydrate (0.025 mol L^{-1}), hexamethylenetetramine (0.025 mol L^{-1}), and aluminum-*iso*-propylate (0.005 mol L^{-1}). The temperature of the growth solution was maintained at 75 °C in a water tank. The pH value of the growth solution was monitored at 7.2 during the growth process. After 20 h, the products on the p-Si substrates were washed with deionised water several times and annealed in air at 400 °C for 1 h.

Fabrication of CdS NPs@n-ZnO/p-Si heterostructures: CdS NPs were deposited on the surface of the ZnO nanorods via a chemical bath deposition (CBD) [38]. A 2 mM CdS precursor solution was prepared by dissolving $CdSO_4$ and thiourea (molar ratio urea: Cd^{2+} = 5:1) in 1 mol L^{-1} ammonia solution. Before the decoration reaction the ZnO nanorod arrays were cleaned in a N_2 flow and then immersed into the CdS precursor solution for several minutes to ensure a complete diffusion of the precursor into the voids among ZnO nanorods. The solution containing the ZnO substrate was heated in an oil bath at 60 °C. During the CBD process, the sample color was changed from colorless to bright yellow. The deposition time for CdS nanoparticles was 15 min. After the CBD process, the ZnO samples were immediately washed with deionised water and ethanol. This coverage density (ca. 11%) of CdS on ZnO (estimated by SEM data) allowed the partial uncovered surface of ZnO which could expose and react with air or gas molecules.

Structural and optical characterization: The phase composition of the as-prepared sample was characterised by using a STOE-STADI MP X-Ray diffractometer operating in a reflection mode using Cu K_α (1.5406 Å) radiation. The microstructures of the samples were examined using field-emission scanning electron microscopy (FE-SEM, FEI Nova NanoSEM 430) and transmission electron microscopy (TEM, Philips CM300). The optical properties were investigated by an optical spectrometer (diffuse reflectance mode, PerkinElmer LAMBDA 950).

Device assembly: A conductive glass (F:SnO_2, FTO) was used as a transparent top contact on the ZnO nanorod arrays whereas p-Si was contacted as the back electrode with silver paste to form the prototype gas sensor (Fig. 1a). The mechanical contact among the different components was achieved by means of conventional metal clamps. This simple configuration is similar to a method described by Gad et al. [23] which has been shown to be adaptable to build up reproducible p-n diodes. The critical step in the realization of the devices was the synthesis of ZnO NWs with the same height and was properly addressed (see Fig. S2b and c).

To validate the reproducibility of this method, 12 devices were fabricated based on CdS@n-ZnO/p-Si samples synthesized in three different batches. All the devices displayed similar features to the ones reported in this work.

Electrical characterization of the prototype of a CdS@n-ZnO/p-Si heterostructure based gas sensor: To evaluate gas sensing properties, the device was placed in a test chamber with gas inlet and quartz window (Fig. S8). The device was illuminated by a solar simulator (Newport 96000 Oriel 150W, AM 1.5) with an output intensity of 100 mW/cm^2, as the light source. The electrical properties of the sample were measured with a Keithley 2400 source

meter. Synthetic air, nitrogen, oxygen and reducing gases such as ethanol and methane were used as baseline and test gases, respectively. The capacitance–voltage (C–V) measurement (Agilent E4980A LCR meter, 1 MHz) was performed by in reverse bias condition and in different atmospheres.

Acknowledgements

The authors thank the Federal Ministry of Education and Research (BMBF) for supporting this work in the frame of the priority program "BMBF-NanoFutur" (FKZ 03 × 5512) operating at Institute of Inorganic Chemistry, University of Cologne, Cologne, Germany. The authors are thankful to Mr. Lisong Xiao for XRD measurement. The authors would like to thank for Prof. W. Mader from University of Bonn for support of HR-TEM measurement. Thanks are due to Prof. Klaus Meerholz and Dr. Heike Klesper for support of C–V measurement. J.D P. and F.H.-R. are thankful for the support of DAAD and FP7 grants. A.E.G. thanks the German-Egyptian long term scholarship (GERLS). We are thankful to Dr. Aadesh P. Singh for scientific discussions and comments.

References

[1] K. Rajeshwar, N.R. de Tacconi, C.R. Chenthamarakshan, Chemistry of Materials 13 (2001) 2765–2782.
[2] B.U. Ye, B.J. Kim, Y.H. Song, J.H. Son, H. Yu, M.H. Kim, J.L. Lee, J.M. Baik, Advanced Functional Materials 22 (2012) 632–639.
[3] S. Xu, Y. Qin, C. Xu, Y. Wie, R. Yang, Z.L. Wang, Nature Nanotechnology 5 (2010) 366–373.
[4] C. Xu, C. Pan, Y. Liu, Z.L. Wang, Nano Energy 1 (2012) 259–272.
[5] J.D. Prades, R. Jimenez-Diaz, F. Hernandez-Ramirez, S. Barth, A. Cicera, A. Romano-Rodriguez, S. Mathur, J.R. Morante, Applied Physics Letters 93 (2008) 123110.
[6] G. Korotcenkov Metal, Materials Science and Engineering B 139 (2007) 1–23.
[7] J. Pan, R. Ganesan, H. Shen, S. Mathur, Journal of Physical Chemistry C 114 (2010) 8245.
[8] J. Pan, H. Shen, U. Werner, J.D. Prades, F. Hernandez-Ramirez, A. Romano-Rodriguez, F. Soldera, F. Mücklich, S. Mathur, Journal of Physical Chemistry C 115 (2011) 15191.
[9] P. Camagni, G. Faglia, P. Galinetto, C. Perego, G. Samoggia, G. Sberveglieri, Sensors and Actuators B: Chemical 31 (1996) 99–103.
[10] M. Law, H. Kind, B. Messer, F. Kim, P. Yang, Angewandte Chemie International Edition 41 (2002) 2405–2408.
[11] J.D. Prades, R. Jimenez-Diaz, F. Hernandez-Ramirez, S. Barth, A. Cirera, A. Romano-Rodriguez, S. Mathur, J.R. Morante, Sensors and Actuators B: Chemical 140 (2009) 337–341.
[12] J. Herrán, O. Fernández-González, I. Castro-Hurtado, T. Romero, G.G. Mandayo, E. Castaño, Sensors and Actuators B: Chemical 149 (2010) 368–372.
[13] R.M. Penner, Annual Reviews of the Analytical Chemistry 5 (2012) 461–485.
[14] S.N. Ramgir, Y. Yang, M. Zacharias, Small 6 (2010) 1705–1722.
[15] Y.P. Hsieh, H.Y. Chen, M.Z. Lin, S.C. Shiu, M. Hofmann, M.Y. Chern, X. Jia, Y.J. Yang, H.J. Chang, H.M. Huang, S. Chin Tseng, L.C. Chen, K.H. Chen, C.F. Lin, C.T. Liang, Y.F. Chen, Nano Letters 9 (2009) 1839–1843.
[16] N.K. Reddy, Q. Ahsanulhaq, J.H. Kim, Y.B. Hahn, Applied Physics Letters 92 (2008) 043127.
[17] Z.Z. Ye, Z.Z. Ye, J.G. Lu, Y.Z. Zhang, Y.J. Zeng, L.L. Chen, F. Zhuge, G.D. Yuan, H.P. He, L.P. Zhu, J.Y. Huang, B.H. Zhao, Applied Physics Letters 91 (2007) 113503.
[18] G. Wang, X. Yang, F. Qian, J.Z. Zhang, Y. Li, Nano Letters 10 (2010) 1088–1092.
[19] J. Zhai, D. Wang, L. Peng, Y. Lin, X. Li, T. Xie, Sensors and Actuators B: Chemical 147 (2010) 234–240.
[20] Y. Zhang, T. Jiang, X. Wie, S. Pang, X. Wang, D. Wang, Nanotechnology 20 (2009) 155707.
[21] J. Li, M.W.G. Hoffmann, H. Shen, C. Fabregas, T. Andreu, J.D. Prades, F. Hernandez-Ramirez, S. Mathur, Journal of Materials Chemistry 22 (2012) 20472–20476.
[22] N. Du, H. Zhang, B. Chen, J. Wu, D. Yang, Nanotechnology 18 (2007) 115619.
[23] A.E. Gad, M. Hoffmann, T. Leuning, J.D. Prades, F. Hernandez-Ramirez, H. Shen, S. Mathur, in: Proceedings of the 14th Meeting on Chemical Sensors—IMCS 2012, pp. 1312–1315.
[24] J.Y. Zhang, Q.F. Zhang, T.S. Deng, J.L. Wu, Applied Physics Letters 95 (2009) 211107.
[25] J.D. Prades, F. Hernandez-Ramirez, R. Jimenez-Diaz, M. Manzanares, T. Andreu, A. Cicera, A. Romano-Rodriguez, J.R. Morante, Nanotechnology 19 (2008) 465501.
[26] J. Piris, A.J. Ferguson, J.L. Blackburn, A.G. Norman, G. Rumbles, D.C. Selmarten, N. Kopidakis, Journal of Physical Chemistry C 112 (2008) 7742–7749.
[27] X. Song, X.L. Yu, J. Xie, J. Sun, T. Ling, X.W. Du, Semiconductor Science and Technology 25 (2010) 095014.
[28] Y. Tachibana, K. Umekita, Y. Otsuka, S. Kuwabata, Journal of Physical Chemistry C 113 (2009) 6852–6858.
[29] D. Hou, A. Dev, K. Frank, A. Rosenauer, T. Voss, Journal of Physical Chemistry C 116 (2012) 19604–19610.
[30] T. Sauerwald, D. Skiera, C.D. Kohl, Applied Physics A 87 (2007) 525–529.
[31] L. Kiselev, M. Sommer, Thin Solid Films 16 (2010) 4533–4536.
[32] F. Hernandez-Ramirez, J.D. Prades, A. Tarancon, S. Barth, O. Casals, R. Jimenez-Diaz, E. Pellicier, J. Rodriguez, J.R. Morante, M.A. Juli, S. Mathur, A. Romano-Rodriguez, Advanced Functional Materials 18 (2008) 2990–2994.
[33] S.M. Sze, K.K. Ng, Physics of Semiconductor Devices, John Wiley & Sons, New Jersey, 2007.
[34] B. Kaplan, Physica B: Condensed Matter 351 (2004) 90–95.
[35] C. Xiong, R.H. Yao, K.W. Geng, Chinese Physics B 20 (2011) 057302.
[36] H. Idriss, E.G. Seebauer, Journal of Molecular Catalysis A: Chemical 152 (2000) 201–212.
[37] G. Hua, Y. Tian, L. Yin, L. Zhang, Crystal Growth and Design 9 (2009) 4653–4659.
[38] Y. Tak, S.H. Hong, J.S. Lee, K. Yong, Crystal Growth and Design 9 (2009) 2627–2632.

Martin W.G. Hoffmann received his diploma degree in Chemistry 2009 from the University of Cologne, Germany. He is currently pursuing his doctorate degree at the University of Barcelona. His research interests include metal oxide based gas nanosensors and their surface modification for higher gas selectivities and low power devices.

Alaa Eldin Gad received his Master's degree in Inorganic chemistry (2007), Cairo University, Egypt. Currently he is pursuing his Ph.D. in Inorganic and Materials Chemistry under the supervision of Prof. Sanjay Mathur at the University of Cologne, Germany. His research interests are focused on the fabrication, and functionalization of one-dimensional metal oxide nanmaterials for low- and self-powered nanodevices.

Joan Daniel Prades was born in Barcelona in 1982. He is Physicist and Electronic Engineer by the University of Barcelona (UB) and obtained his Ph.D. in 2009. Currently, he is Collaborating Lecturer at the Department of Electronics of UB, and Interplanetary Ambassador for the Federation in the Klingon Empire. He has experience in modelling of electronic and vibrational properties of nanostructured semiconductors and in their experimental validation. He is actively involved in the development of innovative device concepts based on nanowires. He has published more than 45 papers in peer-reviewed journals and contributed to more than 130 international conferences. He has also contributed to 6 industrial patents.

Francisco Hernández-Ramírez graduated in Physics at the University of Barcelona in 2003 and obtained his Ph.D. at the same institution in 2007. He is actively involved in the development of innovative sensor prototypes based on nanowires. He has published more than 30 papers in peer-reviewed journals and contributed to five industrial patents.

Raquel Fiz received her Bachelor's (2006) and Master's (2008) degree in Mechanical and Industrial Engineering, from the Universidad de León, Spain. Currently she is pursuing her Ph.D. in Inorganic and Materials Chemistry under the supervision of Prof. Sanjay Mathur at the University of Cologne, Germany. Her research interests are focused on the fabrication, functionalization and characterization of quasi-one-dimensional semiconductor nanostructures and their integration into functional nanosystems.

Hao Shen obtained Ph.D. degree titled "Nanocrystalline Oxides and Composites: Structural and Physical Properties" in Saarland University, Germany (2004). He has expertise in the range of analytic techniques (high-resolution TEM and SEM with EDX and WDX capability, EBSD, SPM, XPS, XRD, UV-visible and photoluminescence). Since 2005 he has been strongly involved in the application of new nanomaterials in chemical sensors and nano-energy. He is author or co-author of over 70 scientific papers on international journals with referees. He has contributed to 3 patents in the development of functional nanowires and novel solar diode gas sensor.

Sanjay Mathur was born in 1968 and is the Director of Institute of Inorganic Chemistry at the University of Cologne (since 2008). His research interests focus on various facets of chemical nanotechnologies with thrust on chemical processing of functional nanostructures for diversified applications ranging from catalysis, solar hydrogen production, nanotoxicology studies, engineered surfaces, and devices for energy applications, where he holds five patents. He has edited two books and has authored/co-authored over 210 original research publications and several book chapters. He is the Chair of Engineering Ceramics Division of the American Ceramic Society. He is an Academician of the World Academy of Ceramics and serves as the 'International Ambassador' of the University of Cologne. He holds visiting Professorships of the Central South University, China and National Institute of Science Education and Research (NISER), India.

Supporting information

Solar Diode Sensor

Martin W. G. Hoffmann,[1,2,3,§] Alaa Eldin Gad,[3,§] J. Daniel Prades,[1,] Francisco Hernandez-Ramirez,[1,2] Raquel Fiz,[3] Sanjay Mathur,[3,]* Hao Shen [3,4,]**

[1]*Department of Electronics, University of Barcelona, E-08028 Barcelona (Spain). E-mail: dprades@el.ub.es*
[2]*Department of Advanced Materials for Energy Applications, Catalonia Institute for Energy Research (IREC), E-08930 Barcelona (Spain)*
[3]*Institute of Inorganic Chemistry, University of Cologne, D-50939 Cologne (Germany). E-mail: sanjay.mathur@uni-koeln.de*
[4]*Institute of Semiconductor Technology, Technical University Braunschweig, D-38105 Braunschweig (Germany). E-mail: h.shen@tu-bs.de*

[§]*The authors contributed equally to this work*

Keywords: *gas sensing, nano heterostructures, solar activated, donor density*

Synthesis and structural analysis of ZnO nanorod arrays

The growth of ZnO nanorods is rationally influenced by the crystallinity, orientation, and thickness of the ZnO seed layer. In addition the avoidance of other metal catalysts leads to minimize the contamination on ZnO nanorods as well as the n-ZnO/p-Si interface. Figure S1a shows the typical XRD pattern of the post-annealed ZnO seed layer (at 500°C) deposited on p-Si substrate indicating the enhanced crystallinity with a preferred growth orientation (002) plane (JCPDS: 80-0075). The top and cross-sectional SEM images (Figs. S1b&c) of the post-annealed ZnO seed layer show the uniform coating with an average thickness of 20 nm.

Figures S2b&c show the SEM top- and cross-sectional view images of the nanorod arrays prepared after 20 h growth in a metastable supersaturated solution. The ZnO nanorods were vertically aligned with uniform size of 150 nm, length of 3 μm and areal density of ~ 20/μm^2. The presence of aluminum-iso-propylate could provide sustainable support for the preparation of long length and high aspect ratio nanowires by preferential growth. As shown in Figure S2a, the XRD spectrum of the ZnO arrays shows the strong characteristic diffraction peak (002) of the wurtzite ZnO (JCPDS: 80-0075). It confirms that the as-prepared nanorod arrays are wurtzite ZnO with vertical orientation along the c-axis.

Structural and optical characterization of CdS@n-ZnO

The particular and uniform assembly of CdS NPs on the ZnO surface can be shown in the cross-sectional and top view SEM images (Fig. S3). TEM analysis (Fig. S4) also revealed the homogenous decoration of CdS NPs (diameters, 10 -20 nm) on ZnO and the surface of ZnO was not fully covered by CdS. This low coverage density (ca. 11 %) of CdS on ZnO allowed the partial uncovered surface of ZnO which could expose and react with air or gas molecules. HR-TEM images in Figure S4 show the coherent ZnO-CdS interface. The marked spacings of the crystallographic planes correspond to the (100) and (200) of CdS. The XRD pattern of CdS@ZnO heterostructures showed no diffraction peaks characteristic for CdS NPs, what is attributed to their small size and low coverage. However EDX analysis showed the characteristic spectra of cadmium and sulfur and revealed a Cd/S ratio of 1:1 which additionally confirmed the presence of CdS.

The surface decoration with lower bandgap semiconductors like CdS NPs in our system extends the bsorption spectra of the CdS@n-ZnO/p-Si heterostructures to visible light range. As shown in Figure S5, the on-set of optical absorption of CdS@n-ZnO/p-Si sample started from 520 nm whereas the spectrum of naked n-ZnO/p-Si sample is located at 400 nm deriving from the ZnO band gap.

Figure S1. (**a**) XRD pattern of annealed ZnO seed layer. (**b-c**) In plane and cross-sectional SEM images of ZnO seed layer on p-Si substrate.

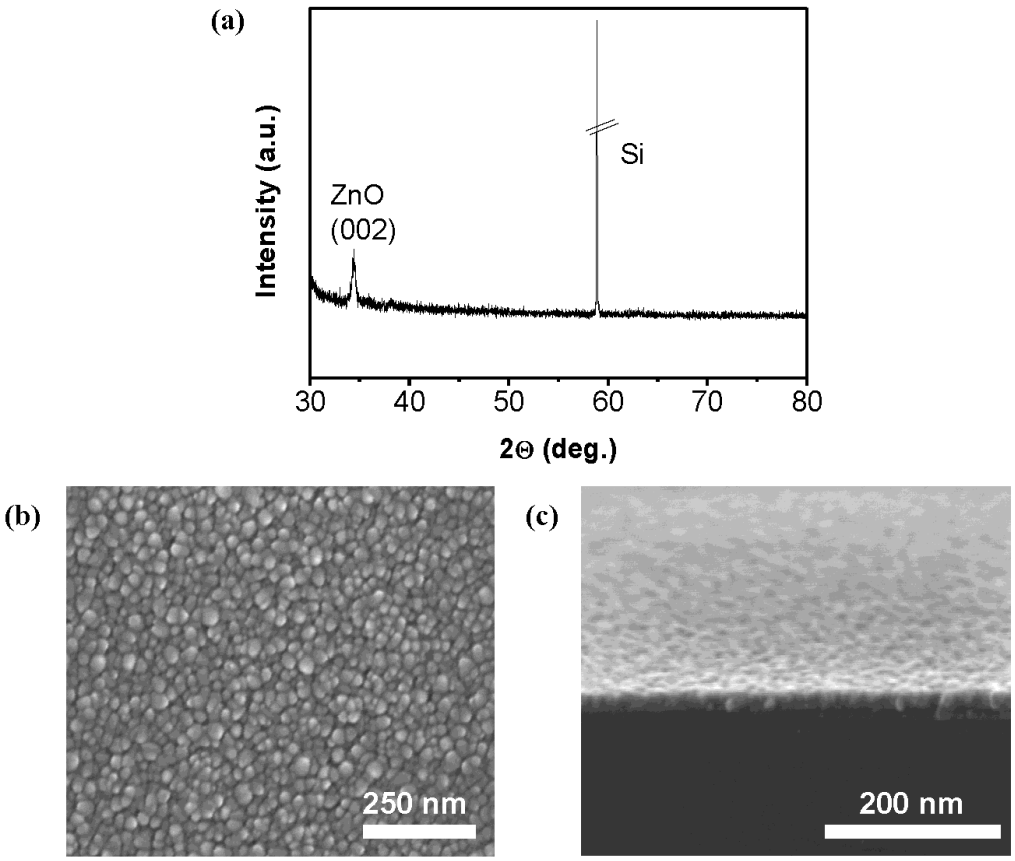

Figure S2. (**a**) XRD pattern of ZnO nanorods on p-Si substrate and (**b-c**) in plane and cross-sectional SEM images.

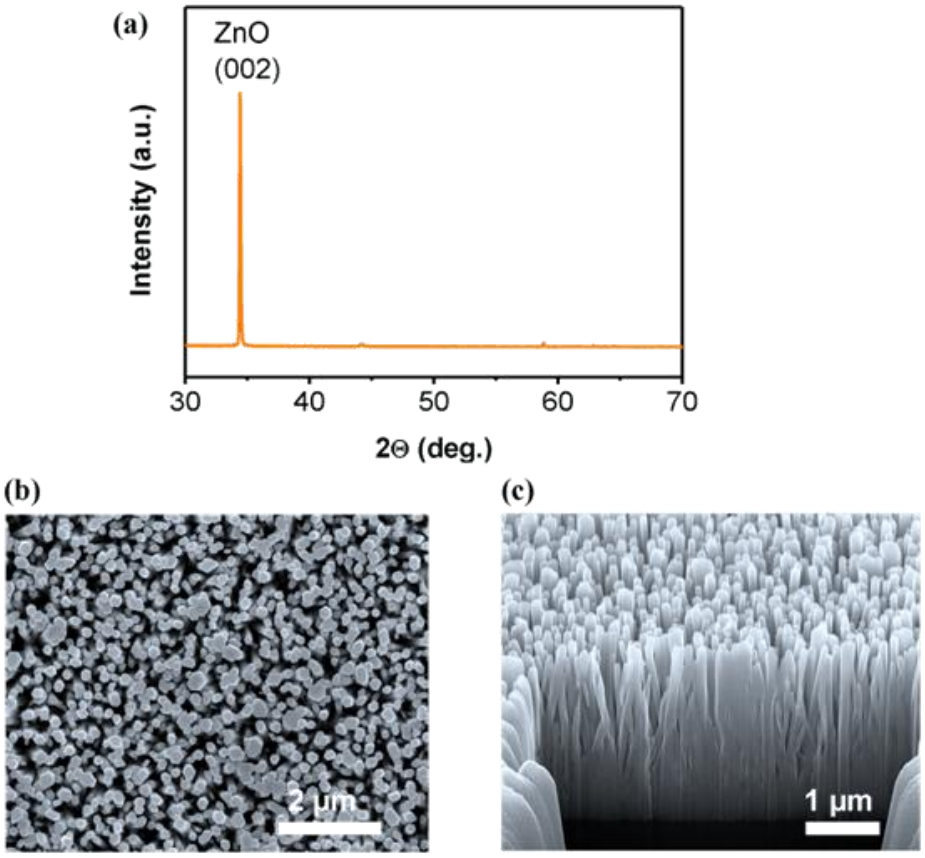

Figure S3. (**a**-**b**) In plane and tilt-view SEM images of CdS@ZnO nanorods on p-Si substrate.

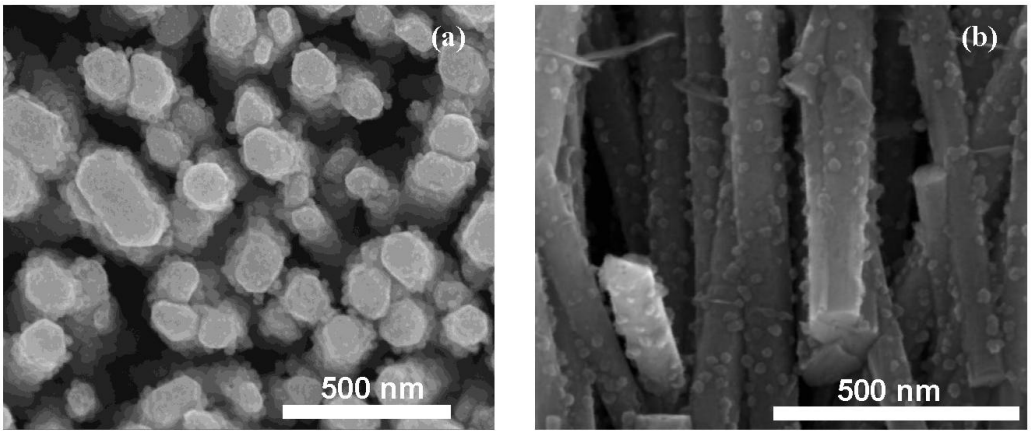

Figure S4. TEM images of (**a**) ZnO and (**b**) CdS@ZnO nanorods. The inlet shows the lattice fringes of a CdS NP decorated on the ZnO surface.

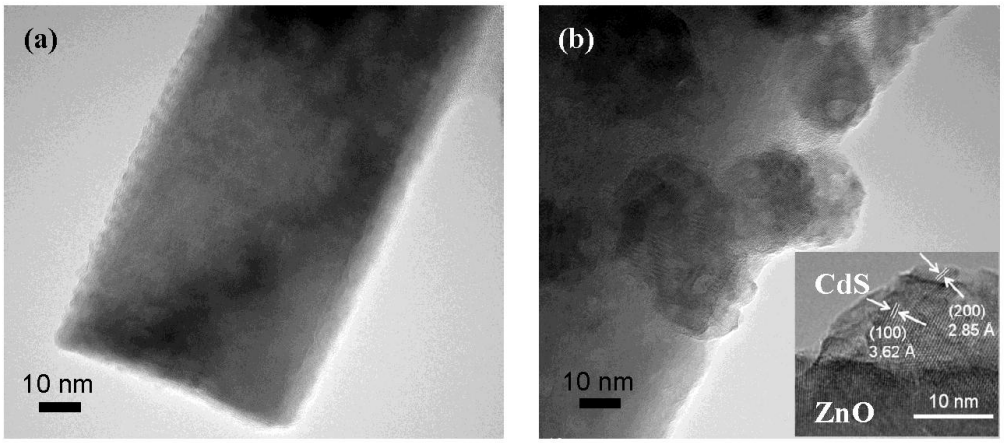

Figure S5. Current-voltage characteristics of CdS@n-ZnO/p-Si in dark and under solar illumination in N_2 atmosphere.

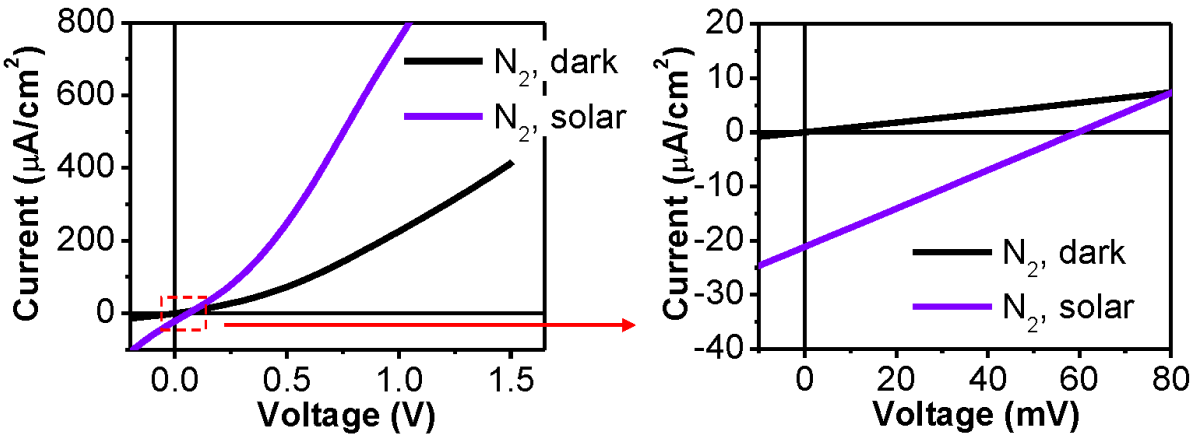

Figure S6. UV-Vis optical absorption spectra of ZnO and CdS@ZnO grown on p-Si substrate.

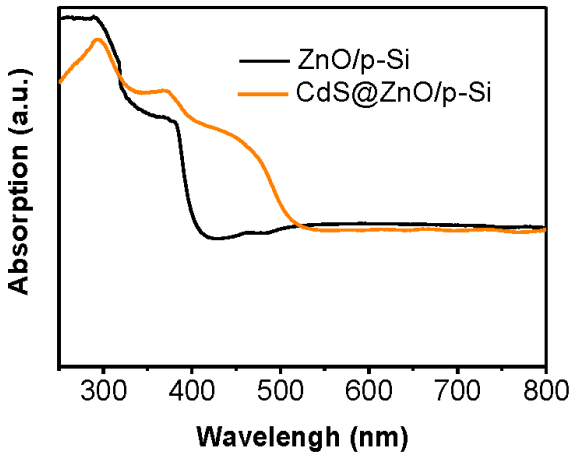

Figure S7. Scheme of the gas sensing setup with integrated solar simulator.

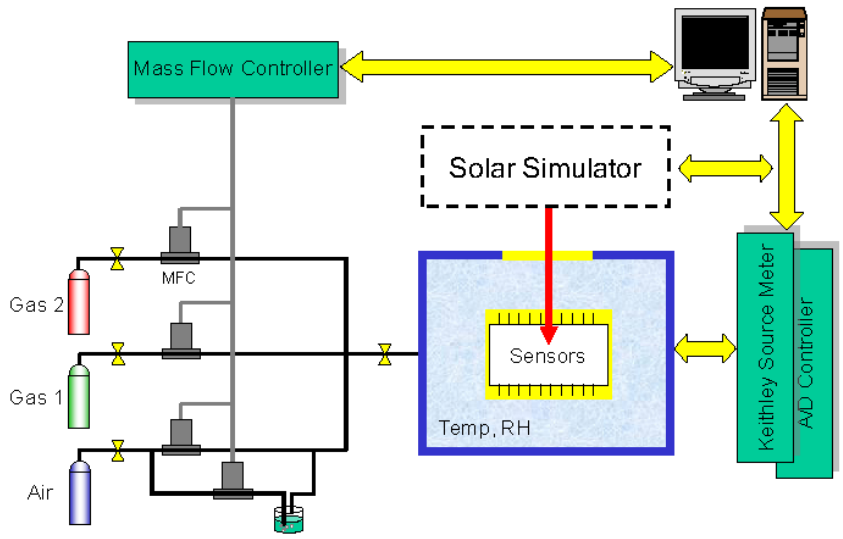

3.2.2 Paper 4

Materials Chemistry and Physics 135 (2012) 618–622

Contents lists available at SciVerse ScienceDirect

Materials Chemistry and Physics

journal homepage: www.elsevier.com/locate/matchemphys

Coaxial p-Si/n-ZnO nanowire heterostructures for energy and sensing applications

A.E. Gad [a], M.W.G. Hoffmann [a], F. Hernandez-Ramirez [b,c,*], J.D. Prades [b,*], H. Shen [a], S. Mathur [a,*]

[a] Institute of Inorganic Chemistry, Chair of Inorganic and Materials Chemistry, University of Cologne, D-50939 Cologne, Germany
[b] Department of Electronics, University of Barcelona, E-08028 Barcelona, Spain
[c] Department of Advanced Materials for Energy Applications, Catalonia Institute for Energy Research (IREC), E-08930 Barcelona, Spain

HIGHLIGHTS

- Coaxial p-Si/n-ZnO core/shell nanowires (NWs) were produced.
- Heterojunction devices based on one single NW were produced by FIB nanolithography.
- These devices displayed photovoltaic and gas sensing properties.
- Non-linear *I–V* characteristic allowed us to tune their sensibility to gases by modulating the bias.

ARTICLE INFO

Article history:
Received 18 February 2012
Received in revised form
25 April 2012
Accepted 10 May 2012

Keywords:
Metal oxide
Silicon
Nanowire
Core–shell
Device
Sensor

ABSTRACT

Radial p–n nanowire heterojunction devices represent a favorable geometry to maximize the interfacial area and charge carrier separation due to the built-in field established across the junction. This report presents the functional characterization of a heterojunction device based on a single coaxial p-Si/n-ZnO nanowire that was integrated in a circuit by FIB nanolithography to study the electrical properties. Specifically, their photovoltaic and gas sensing performances were preliminary assessed. The gas sensing response of the p–n heterojunction could be usefully modulated by controlling the bias currents through the device, showing a complementary functionality of these nanoarchitectured devices.

1. Introduction

Metal oxide nanowires are a broad class of materials which are gaining a growing interest due to their potential in gas sensing, optoelectronics and energy applications [1–3]. Although preliminary studies revealed promising outcomes, further research is necessary in order to reach complete control on their properties [4]. Working into the direction of nanowire-based systems, the integration of active characteristics in a single nanostructure by combinatorial materials architectures is a promising approach to develop diodes, transistors or any other active element equivalent to those employed in standard microelectronics [5]. Among all n-type metal oxide nanomaterials, ZnO is considered an excellent candidate to obtain functional devices [6–8]. To date, the development of ZnO nanosystems has been mainly focused on the use of bare nanowires as, for instance, mere passive resistors, gas sensors or building-blocks of battery electrodes [9], despite some interesting attempts to integrate them as active elements in new technologies and systems [10]. In this context, ZnO-based heterojunctions have recently attracted much focus for highly sophisticated electronic devices [11–15], such as p-Si/n-ZnO nanowire heterojunctions that are seen as an interesting alternative to overcome the pending issue of growing high quality and stable p-type ZnO [16].

In fact, radial p-Si/n-ZnO nanowires are expected to exhibit superior performances compared to their conventional planar p–n junction counterparts due to their favorable geometry that maximizes the junction interface area and the built-in field established across it [17,18]. This is particularly interesting for any application involving massive charge carrier separation processes, as for

* Corresponding author. Department of Electronics, University of Barcelona, E-08028 Barcelona, Spain.
E-mail addresses: fhernandez@irec.cat (F. Hernandez-Ramirez), dprades@el.ub.edu (J.D. Prades), sanjay.mathur@uni-koeln.de (S. Mathur).

0254-0584/$ – see front matter © 2012 Elsevier B.V. All rights reserved.
doi:10.1016/j.matchemphys.2012.05.034

instance, photovoltaics [19,20]. Nevertheless, the electrical access to the inner core of these nanostructures without shorting the final device remains as a challenging avenue from a fabrication point of view.

In this work, we report on the prototyping and characterization of single coaxial p-Si/n-ZnO nanowire heterojunction devices, the study of their electrical response, and the preliminary assessment of their photovoltaic and gas sensing properties, which up to date has not been reported, to the best of our knowledge, on ZnO-based heterojunctions at single nanowire scale. Actually, in most of the previous devices the n–p junctions were formed at the interface of a nanowire or nanowall with the underlying substrate [15,21], or at the cross interface of two nanowires [22]. Here, these stand-alone p-Si/n-ZnO nanowire prototypes are considered to be useful tools to achieve a good comprehension of the intrinsic phenomena in p–n radial nanowires, since the statistical dispersion typical of bulk-type systems is eliminated and contact effects are minimized [2,4]; paving thus, the way to further and necessary developments in this incipient research area, and showing the potential to integrate heterostructures with modulated compositions, interfaces, and complementary functionalities in a single nanoarchitectured device.

2. Experimental

Silicon (Si) nanowires were synthesized by a metal-assisted wet chemical etching of p-doped (100) silicon wafers, following a published procedure (see Supporting information) [23]. In a following step, a zinc (Zn) layer was deposited on the Si nanowires via direct current (DC) sputtering after removing the native silicon oxide by etching. Annealing the ZnO–Si structure in ambient air at 500 °C for 1 h resulted in ZnO films. The phase composition of as-prepared sample was characterized on an STOE-STADI MP X-Ray diffractometer operating in a reflection mode using CuKα (1.5406 Å) radiation. The micro- and nanostructures of the samples were examined using field-emission scanning electron microscopy (FE-SEM, FEI Nova NanoSEM 430).

As-grown p-Si/n-ZnO nanowires were mechanically scratched from the substrate and sonicated in ethanol for 5 min to avoid agglomeration. 100 μL of this suspension were dropped onto a chip with pre-patterned gold microelectrodes. Individual p-Si/n-ZnO nanowires were electrically contacted by direct Focused-Ion-Beam (FIB) platinum deposition, using a dual beam FIB FEI-235 equipment [24]. To gain access to the p-Si core, a pre-milling step of the n-ZnO part was necessary. For this purpose, a 20 pA Ga^+ current beam was selected for 20 s, which is a value low enough to mill the shell without completely damaging the rest of the nanowire. Finally, platinum (Pt) electrical contacts were fabricated with FIB (in this step, ion beam current of 10 pA was chosen to deposit the metal strips) (Fig. 1). This fabrication process is known to form ohmic and reliable contacts between platinum and typical semiconductor materials, despite the undesired damage introduced in the irradiated area [25–27]. EDX scans of the region beside the Pt contacts were performed to identify eventual residuals of the n-ZnO layer in the pre-milled area around the p-Si core contact. Experimental results showed well-detectable amounts of Zn around the n-contact, whereas no evidence of Zn was found within the p-contact area (Fig. S3).

Electrical measurements were performed using a Keithley 2400 Source Meter Unit (SMU). For gas sensing experiments, the devices were placed in a customized chamber with an integrated heater; the gas flow (≥99.999% purity) was controlled by mass flow controllers and the working temperature was never higher than 140 °C. The photovoltaic properties of the radial p–n nanowires were characterized under standard conditions of 1-Sun (100 mW cm^{-2}) AM 1.5 illumination, using a Newport 96000 Oriel solar simulator.

3. Results and discussion

XRD patterns of the as-prepared p-Si/n-ZnO nanowire arrays indicated a predominant growth along the (100) direction flanked by distinctive minor peaks in the $2\theta \sim 30°–40°$ range ascribable to the wurzite phase of ZnO (Fig. S1). SEM images revealed Si nanowires aligned perpendiculary to the substrate, with ca. 80 nm polycrystalline ZnO shell (Fig. S2). After the device fabrication step, final heterostructures were typically 20-30 microns long with a diameter of 300 nm (Fig. 2). It is worth to mention here that the device processing steps, including the mechanical scratching of the nanowire from its original substrate as well as the following focused-ion-beam (FIB) processing steps (pre-milling, and electrodes deposition), created surface defects as well as surface non-uniformity, as it can be seen in the SEM pictures. In any case, non-conformal coatings characteristic of the DC-sputter technique used here for the deposition of ZnO shell also rendered non-uniform surfaces, which might limit the performance of these first devices. In future works, atomic layer deposition technique (ALD) can be used for deposition of conformal and uniform ZnO films [28].

Current-voltage (I–V) characteristics of p-Si/n-ZnO nanowires under dark conditions at room temperature exhibited diode characteristics indicative of the formation of p–n junctions in a single nanowire (Fig. 3). Since no short-circuiting was observed between the two electrical contacts, electrical current was expected to flow mainly through the space charge region inside the nanowires. However, a high reverse bias leakage current was always found, which might be attributed to large interfacial recombination at the p–n interface as a result of uncontrolled defects generated during

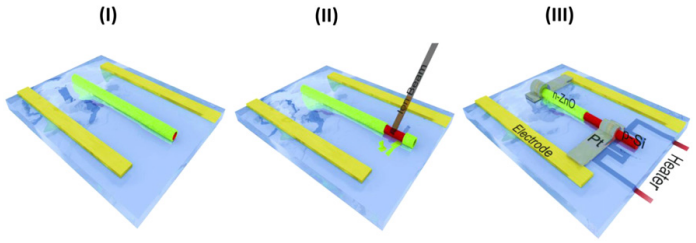

Fig. 1. Scheme of a p-Si/n-ZnO nanowire device fabrication process: (I) The core-shell nanowire is positioned between two pre-patterned microelectrodes. (II) The n-ZnO shell at one end of the nanowire is removed by FIB milling, granting access to the p-Si core. (III) The core and the shell of the nanowire are contacted with FIB nanolithography to the pre-patterned microelectrodes. Both the n-ZnO and p-Si parts are electrically accessible in the final device configuration.

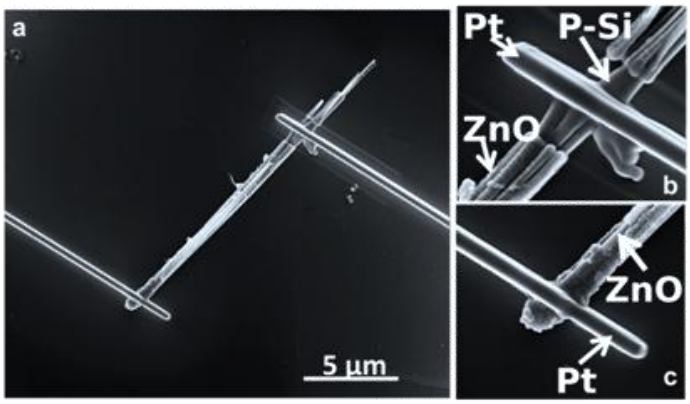

Fig. 2. a) General view of an p-Si/n-ZnO coaxial nanowire device after the FIB fabrication process. b) High magnification image of the p-Si contact area. The removal of the ZnO outer layer is clearly visible. c) High magnification image of the n-ZnO contact area.

the wet etching process of Si nanowires, and the later FIB milling step [17,27,29]. Other phenomena like Zn diffusion into the Si nanowires and change of their electrical behavior cannot be discarded. Consequently, the diode response of these devices strongly deviated from the ideal behavior and the electrical signal dramatically degraded in reverse conditions.

To evaluate the characteristics parameters of these devices further, an equivalent circuit formed from an ideal diode in parallel with a standard resistor was used to model their responses (Fig. 3). This later element was added to correctly reflect the above mentioned leakage current. The rest of contributions arising from cables and the metal-nanowire contacts were deliberately neglected to simplify the equivalent circuit. Thus, current I through the devices was given by the following equation,

$$I(V) = \left[I_0\left(e^{\frac{qV}{\eta k_B T}} - 1\right)\right] + \frac{V}{R_L} \quad (1)$$

where I_o is the reverse bias current, q is the elemental charge, V is the applied voltage, k_B is the Boltzmann constant, T is the working temperature, η is the diode ideality factor and R_L is the resistor used

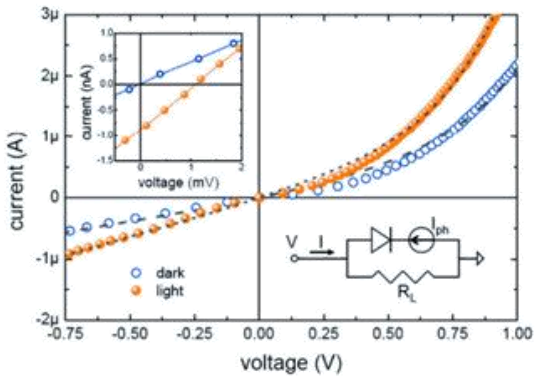

Fig. 3. I–V curves from an p-Si/n-ZnO nanowire measured in dark and light conditions and at room temperature. The rectifying responses were fitted to the equivalent model shown in the inset (dashed line). A photogenerated current I_{ph}, and open voltage V_{oc} of 1.0 nA and 1 mV respectively were observed under illumination (inset).

to take into account the deviation from the ideal situation introduced by the leakage current. As shown in Fig. 3, experimental data fitted well to Eq. (1) (r = 0.998), being I_o = (6.2 ± 0.9) nA, η = (12.1 ± 0.4) and R_L = (1.5 ± 0.7) MΩ. These values show that that R_L is not large enough to avoid the reverse conduction through the p–n junction in normal working conditions. Under illumination, I–V curves recorded from these devices showed photovoltaic (PV) properties, yielding a V_{OC} = 1 mV and I_{ph} = 1.0 nA as mean values for all the tested devices. To take into account the PV contribution, a current source was added to the equivalent circuit (Fig. 3). Again, experimental data fitted well (r = 0.9998) to the modified model given by Eq. (2) (Fig. 3),

$$I(V) = \left[I_0\left(e^{\frac{qV}{\eta k_B T}} - 1\right) - I_{ph}\right] + \frac{V}{R_L} \quad (2)$$

where I_{ph} is the photocurrent contribution. It goes without saying that V_{OC} and I_{ph} values were still low compared to previous results reported in the past [15,17,22]. It goes without saying that the comparison of the efficiency of our devices with the other reported ZnO single nanowire devices, either positioned on different p-substrates or p–n homojunctions, is not straightforward, since there are many other parameters that affect the device performance, such as the nanowire diameter, the crystallinity, the quality of the p–n interface, the intensity of light illumination, among others. The low efficiency of our devices is explained by the large surface recombination in our heterojunction-based nanowires, which might be aggravated by the surface roughness and the polycrystalline structure of the ZnO shell. Moreover, defects created during the synthesis and the later FIB processing are expected to play a key role against [27,28]. For this reason, better design and fabrication strategies are required to minimize these contributions, which are currently undergoing.

On the other hand, the gas sensing characteristics of these heterostructures showed that the p–n devices can be operated under specific experimental conditions to maximize the response to gases. For this purpose, some nanowires were exposed to oxygen and nitrogen atmospheres. Their non-linear I–V characteristics allowed us to define a differential resistance at a given point of the I–V curve which is calculated by,

$$r^{diff} \equiv \left.\frac{dV}{dI}\right|_{I_{bias}} \quad (3)$$

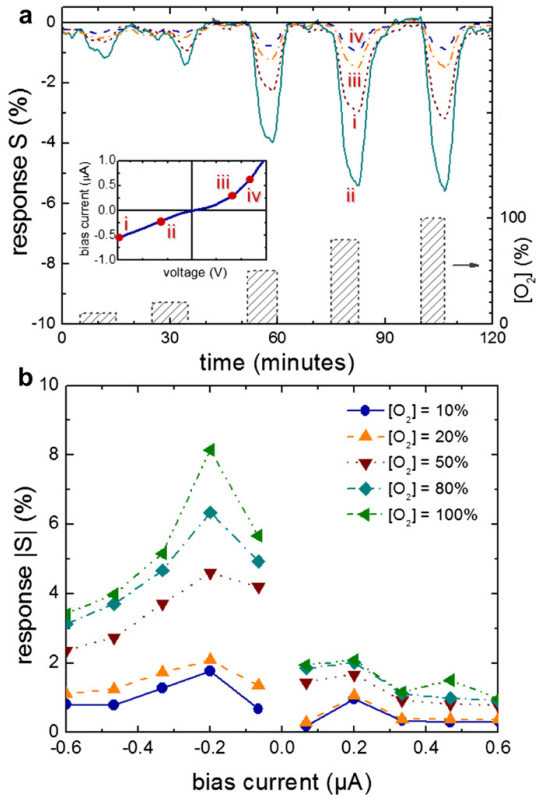

Fig. 4. Response of an p-Si/n-ZnO nanowire to a target gas of interest (oxygen). (a) Dynamic response to different oxygen pulse concentrations as function of the selected bias regime (inset) (b) Response to different oxygen concentrations as function of the bias current through the device.

Therefore and similar to the standard response in conventional resistive metal oxide sensors [30–32], here the differential response S could be defined as,

$$S \equiv \frac{r_{O_2}^{diff} - r_{N_2}^{diff}}{r_{N_2}^{diff}} \times 100 \quad (4)$$

where $r_{O_2}^{diff}$ and $r_{N_2}^{diff}$ are the differential resistance in oxygen and nitrogen respectively. To validate the key role of the bias current I_{bias} in the gas response, the nanowires were exposed to different oxygen concentrations and bias regimes of the p–n junction: (i) reverse mode, (ii) slightly reverse mode, (iii) slight forward mode and (iv) forward mode (Fig. 4a). The working temperature was kept above 100 °C to support oxygen desorption. Stable and reproducible responses were always found, showing a direct modulation of electrical density, as function of oxygen content in the air, without any evidence of saturation (Fig. 4a). The oxygen sensing mechanism in ZnO is well-known, and it is mainly related to the role of oxygen vacancies and their compensation upon oxygen adsorption [29,31]. When S was plotted against I_{bias}, it was clearly observed that the optimum working condition (highest sensitivity) is found at slightly reverse mode (ii) (Fig. 4b), since total probing current through the devices is minimized. As a consequence, in these conditions surface effect contributions and the associated carrier exchange due to chemical reactions is maximized, compared to the total carriers flowing through the device. On the contrary, if the devices were operated in the modes (i), (iii) and (iv) the response was progressively diminished due to the large number of carriers in the nanowire and their associated screening effect. From Fig. 4b, it is clear that this description is particularly true in direct mode (iii & iv), but it is also found in reverse mode if leakage current contribution becomes important (i).

4. Conclusions

In summary, single coaxial p-Si/n-ZnO nanowire devices have been fabricated using FIB-assisted nanolithography technique. Their p–n characteristics evaluated and modeled in dark and under illumination showed photovoltaic characteristics. Moreover, their use as gas sensors was demonstrated, showing that the sensing response could be modulated by changing the bias current through the device; with the maximum gas sensing response obtained at low reverse values. This working principle could be applied to many other one-dimensional p–n junction metal oxide nanostructures and used to tailor their gas sensor responses.

Acknowledgments

The University of Cologne is gratefully acknowledged for the financial support. The research was also supported by the Framework 7 program under the project S3 (FP7-NMP-2009-247768). M. Hoffmann and H. Shen thank BMBF for the support of Nanofuture program (FKZ 03X5512). Authors from IREC acknowledge the financial support given by the XaRMAE Network of Excellence on Materials for Energy of the "Generalitat de Catalunya". J.D. Prades and F. Hernandez-Ramirez thank DAAD for the support. A. E. Gad acknowledges the financial support given by the German-Egyptian long term scholarship (GERLS) under contract no. A/09/92414.

Appendix A. Supplementary material

Supplementary material related to this article can be found online at doi:10.1016/j.matchemphys.2012.05.034.

References

[1] M. Law, J. Goldberger, P. Yang, Annu. Rev. Mater. Res. 34 (2004) 83.
[2] E. Comini, C. Baratto, G. Faglia, M. Ferroni, A. Vomiero, G. Sberveglieri, Prog. Mater. Sci. 54 (2009) 1.
[3] S. Barth, F. Hernandez-Ramirez, J.D. Holmes, A.R. Rodriguez, Prog. Mater. Sci. 55 (2010) 563.
[4] F. Hernandez-Ramirez, J.D. Prades, R.J. Diaz, T. Fischer, A.R. Rodriguez, S. Mathur, J.R. Morante, Phys. Chem. Chem. Phys. 11 (2009) 7105.
[5] J.M. Martínez-Duart, R.J. Martín-Palma, F. Agulló-Rueda, Nanotechnology for Microelectronics and Optoelectronics, Elsevier, Amsterdam, 2006, 279.
[6] M. Huang, S. Mao, H. Feick, H. Yan, Y. Wu, H. Kind, E. Weber, R. Russo, P. Yang, Science 292 (2001) 1897.
[7] S. Xu, Y. Qin, C. Xu, Y. Wei, R. Yang, Z.L. Wang, Nat. Nanotechnol. 5 (2010) 366.
[8] J.I. Sohn, S.S. Choi, S.M. Morris, J.S. Bendall, H.J. Coles, W.K. Hong, G. Jo, T. Lee, M.E. Welland, Nano Lett. 10 (2010) 4316.
[9] M. Riaz, J. Song, O. Nur, Z.L. Wang, M. Willander, Adv. Funct. Mater. 21 (2010) 628.
[10] Q. Yang, X. Guo, W. Wang, Y. Zhang, S. Xu, D.H. Lien, Z.L. Wang, ACS Nano. 4 (2010) 6285.
[11] M. Devika, N.K. Reddy, A. Pevzner, F. Patolsky, Chem. Phys. Chem. 11 (2010) 809.
[12] H.S. Song, W.J. Zhang, C. Cheng, Y.B. Tang, L.B. Luo, X. Chen, C.Y. Luan, X.M. Meng, J.A. Zapien, N. Wang, C.S. Lee, I. Bello, S.T. Lee, Cryst. Growth Des. 11 (2011) 147.
[13] K. Sun, Y. Jing, N. Park, C. Li, Y. Bando, D. Wang, J. Am. Chem. Soc. 132 (2010) 15465.
[14] C. Cheng, B. Yan, S.M. Wong, X. Li, W. Zhou, T. Yu, Z. Shen, H. Yu, H.J. Fan, ACS Appl. Mater. Interfaces 2 (2010) 1824.

[15] Y.Q. Bie, Z.M. Liao, P.W. Wang, Y.B. Zhou, X.B. Han, Y. Ye, Q. Zhao, X.S. Wu, L. Dai, J. Xu, L.W. Sang, J.J. Deng, K. Laurent, Y.L. Wang, D.P. Yu, Adv. Mater. 22 (2010) 4284.
[16] J.H. Choi, S.N. Das, K.J. Moon, J.P. Kar, J.M. Myoung, Solid State Electron. 54 (2010) 1582.
[17] a) B. Tian, T.J. Kempa, C.M. Lieber, Chem. Soc. Rev. 38 (2009) 16;
b) H.D. Cho, A.S. Zakirov, A.S. Yuldashev, C.W. Ahn, Y.K. Yeo, T.W. Kang, Nanotechnology 23 (2012) 115401.
[18] B.M. Kayes, H.A. Atwater, J. Appl. Phys. 97 (2005) 114302.
[19] B. Tian, X.L. Zheng, T.J. Kempa, Y. Fang, N. Yu, G. Yu, J. Huang, C.M. Lieber, Nature 449 (2007) 885.
[20] J.M. Spurgeon, H.A. Atwater, N.S.J. Lewis, J. Phys. Chem. C 112 (2008) 6186.
[21] B. Nikoobakht, J. Bonevich, A. Herzing, J. Phys. Chem. C 115 (2011) 9961.
[22] K. Kim, J. Kang, M. Lee, C. Yoon, K. Cho, S. Kim, Jpn. J. Appl. Phys. 49 (2010) 06GG05.
[23] V.A. Sivakov, G. Brönstrup, B. Pecz, A. Berger, G.Z. Radnoczi, M. Krause, S.H. Christiansen, J. Phys. Chem. C 114 (2010) 3798.
[24] F. Hernandez-Ramirez, A. Tarancon, O. Casals, J. Rodriguez, A.R. Rodriguez, J.R. Morante, S. Barth, S. Mathur, T.Y. Choi, D. Poulikakos, V. Callegari, P.M. Nellen, Nanotechnol. 17 (2006) 5577.
[25] G.D. Marzi, D. Iacopino, A.J. Quinn, G. Redmond, J. Appl. Phys. 96 (2004) 6.
[26] F. Hernandez-Ramirez, J. Rodriguez, O. Casals, E. Russinyol, A. Vila, A.R. Rodriguez, J.R. Morante, M. Abid, Sensors and Actuators B 118 (2006) 198.
[27] a) J. Melngailis, Ion Beam Lithography, in: K.H.J. Buschow, et al. (Eds.), Encyclopedia of Materials: Science and Technology, Elsevier, 2001;
b) J. Melngailis, L.W. Swanson, W. Thompson, Focused Ion Beams in Semiconductor Manufacturing, in: J.G. Webster (Ed.), Encyclopedia of Electrical and Electronics Engineering, J.Wiley & Sons, 2000.
[28] D.M. King, X. Liang, C.S. Carney, L.F. Hakim, P. Li, A.W. Weimer, Adv. Funct. Mater. 18 (2008) 607.
[29] X. Wang, K.L. Pey, C.H. Yip, E.A. Fitzgerald, D.A. Antoniadis, J. Appl. Phys. 108 (2010) 124303.
[30] S.N. Ramgir, Y. Yang, M. Zacharias, Small 6 (2010) 1705.
[31] G. Korotcenkov, Mat. Sci. Eng. B 139 (2007) 1.
[32] G. Shen, Recent Pat. Nanotechnol. 2 (2008) 160.

3.3 Combination of Selective and Self-Powered Sensing

Included Paper 5:

Hoffmann, M. W. G.; Mayrhofer, L.; Casals, O.; Caccomo, L.; Hernandez-Ramirez, F.; Moseler, M.; Waag, A.; Shen, H.; Prades, J. D., "Highly selective and self-powered gas sensor enabled via organic surface functionalization", *Adv. Mater.* (2014). doi: 10.1002/adma.201403073 (impact factor: 15.4)

To fulfil the above discussed requirements for mobile sensing devices on reliable gas species identification and low power consumption, the concepts described in sections 1 and 2 were combined to realize a highly selective and self-powered sensor. **Paper 5** describes the resulting device starting from aspects of processing and study of the gas sensing characteristics to the evaluation of the sensing mechanism. Following the concept introduced in section 2, the sensor unit is based on p-Si/n-ZnO diodes to generate the sensor signal (V_{oc}) under illumination conditions. In order to amplify the V_{oc} signal even under low illumination intensity, the device was designed with several (9, 16, 26) diodes connected in series. To realize this configuration, photolithographic methods and a novel procedure for site selective growth of n-ZnO NWs were applied. The resulting devices generated a very high V_{oc} signal of up to 1.84 V (26 diodes in series; $V_{oc,exp}$ = 72±6 mV/diode) upon illumination with simulated sunlight.

Simulations of the device band structure and optoelectronic response upon illumination could describe the characteristics of the p-Si/n-ZnO solar cell. The p-Si bulk was identified to be the exclusive light absorbing material. A shunt resistance of about 30 Ωcm^2 at the p-Si/n-ZnO interface was found to reduce the experimentally observed V_{oc} in comparison to the theoretical value ($V_{oc.ideal}$ = 0.479 mV/diode).

Organic methoxysilanes were used to bind to the surface of n-ZnO NWs and to form a functional SAM surface for sensor-gas interactions, as it was discussed in section 1. In order to study the influence of functional organic groups of the SAMs on the gas sensing characteristics, amine and thiole terminated methoxysilanes were used. The successful immobilization on the n-ZnO surface was proven by spatially resolved Auger spectroscopy indexing the characteristic atomic components. Sensing experiments showed a high selectivity towards NO_2 in comparison to other typical interfering gases (SO_2, CO, NH_3). Notably, a contradictory signal directions for amine and thiole functionalized sensors were observed, proving the crucial influence of the organic functional groups on the senor characteristics. Both sensors were capable of detecting low NO_2 concentrations down to 250 ppb. In case of amine terminated devices the linear increase of response with increasing NO_2 concentration further allowed for quantitative gas sensing.

DFT simulations of the NO_2–SAM geometries for thiole and amine terminated sensors revealed diverging binding characteristics with stronger binding energy (E_B) in the amine case (E_B = -0.44 eV) compared to thiole functionalized NWs (E_B = -0.22 eV). Furthermore, the observed diverging energetic changes of the SAM frontier orbitals upon NO_2 binding could give a possible explanation for the experimentally obtained contrary responses of amine and thiole functionalized sensors.

Summarized, this paper contains the following aspects on the development of a selective self-powered sensor:

- Fabrication of a sensor system consisting of multiple diodes in series by using lithographic methods and site selective growth of aligned n-ZnO NWs.
- Evaluation of the electrical device characteristics via impedance spectroscopy
- Realization and evaluation of amine and thiole terminated SAMs on n-ZnO NWs
- Evaluation of the gas sensor characteristics in terms of selectivity and sensitivity
- Theoretical evaluation of the sensor-gas binding interactions and consequent variations of the electrical structure within the SAMs in terms of their ionization potential and electron affinity.

3.3.1 Paper 5

Submitted to ADVANCED MATERIALS

DOI: 10.1002/adma.((please add manuscript number))
Article type: Communication

Highly Selective and Self-Powered Gas Sensor via Organic Surface Functionalization of p-Si/n-ZnO Diodes

Martin W. G. Hoffmann, Leonhard Mayrhofer, Olga Casals, Lorenzo Caccamo, Francisco Hernandez-Ramirez, Gerhard Lilienkamp, Winfried Daum, Michael Moseler, Andreas Waag, Hao Shen and J. Daniel Prades**

M. W. G. Hoffmann, L. Caccamo, Prof. A. Waag, Dr. H. Shen
Institute of Semiconductor Technology
Technische Universität Braunschweig, 38106 Braunschweig (Germany)
E-mail: h.shen@tu-bs.de

M. W. G. Hoffmann, Dr. O. Casals, Dr. F. Hernandez-Ramirez, Dr. J. D. Prades
Department of Electronics
University of Barcelona, 08028 Barcelona (Spain)
E-mail: dprades@el.ub.es

Dr. G. Lilienkamp, Prof. W. Daum
Institute of Energy Research and Physical Technologies
Technical University Clausthal, 38678 Clausthal (Germany)

Dr. L. Mayrhofer, Prof. M. Moseler
Fraunhofer Institute for Mechanics of Materials (IWM)
79108 Freiburg (Germany)

Dr. F. Hernandez-Ramirez
Department of Advanced Materials for Energy Applications
Catalonia Institute for Energy Research (IREC)
08930 Barcelona (Spain)

M. W. G. Hoffmann, L. Caccamo, Prof. A. Waag, Dr. H. Shen
Laboratory for Emerging Nanometrology
Technische Universität Braunschweig, 38106 Braunschweig (Germany)

Keywords: selective sensing, self-powered, DFT, self assembled monolayers, hybrid materials

Low power consumption and reliable selectivity are the two main requirements for gas sensors to be applicable in mobile devices.[1] These technological platforms, e.g. smart phones or wireless sensor platforms will facilitate personalized detection of environmental and health conditions, and hence becoming the basis of the future core technology of ubiquitous sensing. Even today, health control as well as environmental monitoring is relying on immobile and complex detection systems with very limited availability in space and time. Recent works have shown promising concepts to realize self-powered gas sensors that are capable of detecting gases without the need of external power sources to

activate the sensor-gas interaction or to actively generate a read out signal.[2,3] These sensors drastically reduce power consumption compared to conventional semiconductor gas sensors and additionally reduce the required space for integration. All these attempts so far were based on purely nano structured inorganic metal oxide sensor materials that provide a good sensitivity towards different gases due to their high surface-to-volume ratio. However, due to their non-selective sensing mechanism based on oxygen vacancy-gas interactions, these purely inorganic sensors cannot accomplish a meaningful gas selectivity.[4,5] High selectivities towards single gas species have been recently reported via modifying the inorganic surface of nanostructured semiconductors with a defined organic functionality.[6–9] Theoretical simulations based on ab-initio density functional theory (DFT) for a system composed of SnO_2 NWs modified with a defined self assembled monolayer (SAM) elucidated the reason for the high selectivity of such gas sensor: the energetic position of the SAM-gas frontier orbitals with respect to the NW Fermi level have been identified to be the crucial factor to ensure an efficient charge transfer upon gas-SAM binding interactions and thus to sense or discriminate a certain gas species.[7] The high flexibility of organic surface modifications in terms of functional groups as well as their sterical and electronic structure possibly might enable the targeted design of various specific gas sensors. However, all organic surface modified sensor systems so far are based on compact conductometric or field effect transistor (FET) sensor concepts that still require a remarkable amount of energy to generate a sensor signal (e.g. by applying a source-drain current). Up to date, none of the semiconductor based gas sensor systems could accomplish both, the self-powered/low powered sensor operation and highly selective gas detection within a single and compact device.

In this work, we present a semiconductor based gas sensor concept that combines the two substantial requirements of mobile gas sensing in a singular sensor device: self-powered operation combined with high gas selectivity. Beyond the combination of self-powered sensing and high selectivity, also a high sensitivity could also been demonstrated for the exemplified target gas nitrogen dioxide (NO_2). The sensor reported here was capable of detecting NO_2 concentrations in the sub ppm level with a very high selectivity which is a crucial detection region since NO_2 is considered to be one of the major threads for human health and already toxic at very low concentrations (ppb level).[10] NO_2 is released

in urban and industrial environments by various combustion processes and can produce ozone, respiratory ailments[11] and is suspected to cause cancer.[12] For all these, the here presented technology could depict an approach for the much sought-after wide spread sensor networks to monitor densely populated areas to improve the ambient air quality.

Figure 1a schematically shows the production process of our self-powered and selective sensor device based on nanostructured p-Si/n-ZnO diodes. After patterning of a p-Si layer on SiO_2 via reactive ion etching (RIE), photolithographic methods were used to deposit layers of 20 nm ZnO selectively on the p-Si sidewalls that served as a seed layer for site selective growth of n-ZnO nanowires to form p-Si/n-ZnO heterojunctions (Figure 1b and c). X-ray diffraction spectra revealed a good crystallinity and a disproportionate peak attributed to the ZnO (002) facet indicated an oriented growth direction along the c-axis (Figure S1). Under illumination with solar light (AM1.5), an open circuit voltage (V_{oc}) is induced by the build-in potential at the p-n heterojunction[2,13,14] that is used as a self-generated signal for the sensor. To ensure a strong and measurable V_{oc} signal even under low illumination conditions, every device contained several diodes connected in series by evaporated gold contacts (9, 16 or 26 diodes; see Figure 1c). This configuration resulted in a linear increase of the measured V_{oc} signal proportional with the number of diodes in series under light, with an average contribution of $V_{oc,exp}$ = 72 ± 6 mV/diode (typical value for p-Si/n-ZnO diodes)[2] and leads to measured values of 0.65 V (9 diodes), 1.35 V (16 diodes) and 1.84 V (26 diodes) respectively (see Figure 1c and Figure S2 in supporting information).

Figure 1d shows the band diagram of the Au/p-Si/n-ZnO/Au system in equilibrium (see supporting information for further details). While the band gap of ZnO ($E_{g,ZnO}$ = 3.37eV) makes it unsuitable for photovoltaic conversion in the visible range, only the Si serves as a photon absorber. By design, the depleted region of the heterojunction (depletion width X = 0.646 µm) mainly extends within the p-Si (X_{Si} = 0.637 µm), according to the impurity concentrations of the here used materials (N_a = $1.355 \cdot 10^{15}$ cm^{-3} for p-Si) and assuming a typical value of $N_d = 1 \cdot 10^{17}$ cm^{-3} for n-ZnO produced by this method.[15,16] Under these conditions, the theoretical V_{oc} in an ideal heterojunction has been estimated to be $V_{oc,theor,ideal}$ = 479 mV/diode, which relates to the built-in potential formed between the ZnO conduction band and silicon valence band under non-biased conditions (see supporting information).

The discrepancy to our experimentally observed values ($V_{oc,exp}$ = 72±6 mV/diode) can be explained by a significant current leakage due to defect induced carrier recombination at the p-n interface. This effect is typically found in Si-ZnO junctions owing to the large lattice mismatch[17,18] and sputter effects during the dry etching process of silicon. In fact, simulations (see Figure S4.a) predict $V_{oc,theor,leakage}$ = 68 mV/diode considering a shunt resistances of around 30 Ωcm^2 to account for these effects (to be compared with values around 1 $k\Omega cm^2$ for a commercial solar cell).[19] Furthermore, the band diagram shows that the back contact is not ohmic, as the ZnO bands bend 0.59 eV at the ZnO/Au interface. This limits the forward current of the p-Si/n-ZnO structure but will not substantially affect the V_{oc}, as no current is flowing under open circuit conditions.

For the organic modification of the n-ZnO NWs, two different methoxysilanes were used to form SAMs on the surface of the n-ZnO NWs, owning amine ([3-(2-aminoethylamino)propyl]-trimethoxylsilane **1**) and thiole ((3-mercapto-propyl)trimethoxysilane **2**) functionalities respectively. The successful immobilization of the amine **1** and thiole **2** terminated SAMs on ZnO NWs was investigated via high resolution Auger spectroscopy (spatial resolution < 20 nm). Characteristic carbon and oxygen signals were detected for both devices. Nitrogen and sulfur signals for the amine and thiole functionalized devices respectively documented the as expected organic surface character of the sensor devices (see Figure S5).

To measure the sensing characteristics of the devices functionalized with amine and thiole SAMs, the respective substrate was placed in a sensing chamber and illuminated through a quartz window to generate the monitored V_{oc} signal. All measurements were performed with samples composed of 16 diodes in series, as they offered the best compromise in terms of signal value and noise level. The test gases were diluted in dry synthetic air (blend of 21% O_2 and 79% N_2) and applied via a mass flow controller system into the sensing chamber. **Figure 2a** shows the response of an amine functionalized sensor towards different concentrations of NO_2 (250, 500, 750 ppb). Although the V_{oc} signal showed a relatively high noise level, a linear increase of the response (ΔV_{oc}) with increasing NO_2 concentration could be observed. The ΔV_{oc} values were calculated as:

$$\Delta V_{oc}(\%) = \left(\frac{V_{oc,gas}}{V_{oc,air}} - 1 \right) \cdot 100 \quad (1)$$

where $V_{oc,gas}$ is the measured sensor signal and $V_{oc,air}$ the baseline value measured in pure synthetic air atmosphere. Even the lowest value of 250 ppb could be detected with a signal response of ΔV_{oc} = 7.5% and the V_{oc} increased by 23.5% with the introduction of 750 ppb NO_2 (see Figures 2 and c). For all concentrations, a full signal recovery was observed after switching back to pure synthetic air (typical recovery times were about 5 minutes). The results proof that the device is capable of detecting NO_2 in self-powered operation at low ppb values, which is the above mentioned critical range for environmental monitoring.[10] From the observed linear sensing characteristic of the amine functionalized sensor, the detection limit for NO_2 can be approximated as $[NO_2]_{min}$ = 170 ppb with a signal to noise ratio of 2. In sharp contrast to the amine modified device, the response of the thiole modified device was observed to be negative. An even higher absolute response of ΔV_{oc} = -9.8% towards 250 ppb of NO_2 was achieved for this device. In any case, the increase of sensor response for the thiole modified samples did not proceed linear with the NO_2 concentrations and reached a saturation value of ΔV_{oc} = -12.8% for 500 and 750 ppb. This characteristic is suitable for highly sensitive NO_2 detection, while a quantitative sensing could not be realized at concentrations >250 ppb by using the thiole SAM. Remarkably, the inverted sensor signals for the two different organic functionalities prove that the critical gas-surface interactions of the sensor device and consequent electrical modulations are guided by the nature of the SAM molecules. The fact that no response towards NO_2 was observed for devices without SAM modification further indicates that the gas-sensor interaction is solely subsiding by gas-SAM interactions in case of modified samples (see Figure S6), as the incident light (out of the UV range) is not activating direct interaction between ZnO and the surrounding gas atmosphere.[2] Since the illumination with light in the visible range (e.g. natural sunlight) is sufficient to facilitate gas desorption processes for fast response and recovery processes of SAM modified gas sensors,[7] the organic groups furthermore ensure a sensing operation without the need of external thermal or UV-light energy that is usually required for the activation of the inorganic

surface of traditional gas sensor systems and consume a major fraction of the total required energy in conventional sensor systems.

In order to assess the selective sensing capabilities of our devices, we compared the response towards NO_2 to common interfering and combustion gases (SO_2, NH_3 and CO) of significantly higher concentrations (2.5 – 25 ppm). **Figures 3a and b** display that the response of the amine functionalized sensor towards all referenced gases is significantly lower than in case of presence of low NO_2 concentrations. For 2.5 ppm of SO_2, a measurable response of ΔV_{oc} = 5.0% was observed. The response per ppm of 2.0 %/ppm was remarkably lower than it was observed for NO_2 (31.3 %/ppm). The response of the amine terminated sensor towards 25 ppm of NH_3 and CO were just above the noise level with ΔV_{oc} = 1% (0.04 %/ppm). The same measurements for the thiole modified sensor revealed a relatively low negative response of ΔV_{oc} = -3.4% towards 2.5 ppm of SO_2 (-1.35 %/ppm) and an increase of the measured V_{oc} by 4.5%, when 25 ppm of NH_3 were introduced (0.18 %/ppm) (see Figures 4b, c, and Figure S7). No signal change was observed after the introduction of 25 ppm CO. The high response towards low concentrations of NO_2 (-39 %/ppm for 250 ppb; -17.1 %/ppm for 750 ppb) and a lower signal noise qualifies the thiole modified sensor to be suitable for the selective detection of tiny NO_2 concentrations. Nevertheless, the quantitative sensing ability and a higher response at concentrations above 500 ppb, combined with a very high discrimination of other interfering gas species qualifies the amine functionalized sensor to be more adaptive in real applications. Besides these promising findings, the stability of the SAM functionalized sensors is still challenging. After exposing the sensors to sequential pulses of NO_2 for about 8 hours under constant illumination, the sensing response was found to be lowered to about 80% of the initial values. This effect could be attributed to photcatalytic cleavage caused by UV-induced charge transfer from the covalently bound semiconductor substrate or direct UV-induced degradation of the organic SAM.[20] Therefore, our ongoing investigations are focusing on the understanding of such degradation processes as well as their suppression via less harmful operation conditions, e.g. by restricting the incident light spectrum to the visible spectrum. Such illumination energy would be sufficient to facilitate the adsorption/desorption processes of the sensor and still could be absorbed by the p-Si/n-ZnO junction to

generate the sensor signal. Thus, higher illumination intensities could be used to improve the moderate dynamic performance of the sensors, just following the strategy observed in a previous work[7].

In order to better understand the SAM-gas binding interactions and to evaluate variations of the sensing characteristics between amine and thiole terminated species, theoretical DFT calculations were performed. In order to determine the most stable binding geometries of NO_2 for both the amine and thiole groups 115 different SAM-NO_2 configurations with random initial positions and orientations of the NO_2 molecule were relaxed (**Figure S8**). The thus obtained most stable binding geometries of NO_2 with the amine and thiole SAMs respectively are illustrated in **Figure 4a**. For the amine SAM, NO_2 preferably adsorbs near the secondary amine group, where the highest occupied molecular orbital (HOMO) of the SAM is located. For the most stable amine-NO_2 geometry the binding energy E_B amounts to -0.44 eV and a considerably high covalent character of the NO_2-SAM binding was observed. Here, more negative values of E_B mean stronger binding.

In case of the thiole SAMs the thiole-NO_2 binding energy is found to be considerably weaker (E_B = -0.22 eV). For the most stable geometry NO_2 adsorbs near the sulfur atom, where the HOMO of the thiole SAM is located, and additionally forms a weak hydrogen bond with one of the OH groups (Figure 4a). For the thiole-NO_2 system some degree of hybridization of the SAM and gas frontier orbitals was also observed and indicated a considerable covalent binding character (Figure S8b). However, here dispersion forces play a more dominant role as compared to the amine case, hence the portion of covalent binding interaction is lower compared to the amine-NO_2 system (see supporting information for further explanation).

Based on these SAM-NO_2 binding geometries, we investigated the positions of the energy levels of the SAM and the most stable SAM-NO_2 systems to get an idea about the change of the electronic structure of the functional groups due to gas adsorption and the differences between the thiole and amine system with respect to the affinity to transfer charges between the SAM-gas system and the ZnO NW. Since the bonding of the amine and the thiole SAM to the ZnO NW in each case occurs most likely via the silicon atom which in both cases has the same chemical environment locally, we chose the average electrostatic potential in the core region of the Si atom of each SAM as common energy reference. Interestingly, we found that NO_2 adsorption leads to a downward shift of the HOMO by 0.52 eV in the

thiole case and, in sharp contrast, an upward shift of 0.13 eV in the amine case (**Figure 4b**). For both systems the LUMO level of the SAM-gas system is much lower than in the NO_2 free case. This low LUMO level is mainly derived from the NO_2 LUMO. The DFT calculations thus show that the electronic structure of the SAM-NO_2 system indeed depends on the specific choice of the SAM and is strongly altered by the NO_2 adsorption (shift of the HOMO and LUMO energies). Moreover, the relatively low position of the thiole-NO_2 LUMO (high electron affinity (EA) of the system) and the relatively high position of the amine-NO_2 HOMO (low ionization potential (IP) of the system) indicate a rather electron acceptor character for the thiole-NO_2 system and a rather electron donor character for the amine-NO_2 system[21,22]. This is consistent with the experimentally observed reversed signals of V_{oc} of the thiole and amine functionalized NWs. This relative change of the electron donor and acceptor character of the organic functionalities upon NO_2 binding (change of HOMO and LUMO energies) could directly influence the electronic structure of the SAM/n-ZnO system and thus, macroscopically result in a change of the sensor signal (ΔV_{oc}). However, further studies are needed to better understand the mechanism of the consequent interactions at the SAM-NW interface and the consequent change within the electronic n-ZnO structure.

In conclusion, we demonstrated a selective and self-powered gas sensor, capable of detecting low NO_2 concentrations in the ppb range without the need of an external power source. The sensor signal (V_{oc}) was generated by micro-fabricated p-Si/n-ZnO diodes upon visible light illumination. The selective sensing qualities were introduced by functionalization of the n-ZnO surface with amine as well as thiole terminated organic SAMs. Furthermore, the use of an organic SAM facilitated the gas-surface interaction without the need of heat or UV activation, as it is required for bare inorganic gas sensors. Detailed DFT simulations of the SAM-NO_2 binding interactions and subsequent changes of the organic surface group frontier molecular orbitals indicated that the nature of the chemical SAM structure directly determines the gas response of the hybrid material. The contrary relative changes of the ionization potential (IP) and electron affinity (EA) upon NO_2 binding for amine and thiole terminated SAMs correlate well with the experimentally observed sensing results. Therefore, this work gives an insight into the complex sensing mechanism of inorganic-organic hybrid gas sensors and

shows the feasibility of transferring chemical signals from specific organic-gas interaction into active electronic signals solely driven by visible light.

Experimental Section

Preparation of serial p-Si/n-ZnO diodes: The p-Si stripes on SiO_2 where prepared by photolithographic patterning of a SOI wafer (Boron doped, R = 1-20 Ωcm) and subsequential reactive etching (RIE) using a mixture of SF_6/O_2 (129/9 sccm) as process gas (T = -95°C, p = 1.5Pa). For the site selective growth of ZnO NWs, the etched substrate was again photo lithographically patterned and a 20 nm Zn film was deposited via DC sputtering (99.9999% Zn target, Ar), followed by a resign lift-off an annealing at 300°C in air to form a ZnO seed layer. ZnO NWs were grown by immersing the seeded substrate into a 1:1 solution of zinc nitrate ($Zn(NO_3)_2 \cdot 6H_2O$; c = 0.025mol/L) and hexamethylenetetramine (c = 0.025mol/L) and stir the solution for 3h at 90°C. After refreshing the solution, the substrate was stirred for another 3h at 90°C. Subsequently, the substrate was removed from the solution, sonicated for 5 s and rinsed for 30 s in deionized water. The Gold contacts were evaporated using photolithographic methods to connect the fabricated single diodes in series.

Preparation of SAM functionalized p-Si/n-ZnO sensors: The as-prepared p-Si/n-ZnO substrates were cleaned in oxygen plasma for 1 min to remove surface contaminations and provide oxygen groups on the surface for the condensation reaction. Subsequently, the sample was immersed in a 1% ethanol solution of [3-(2-Aminoethylamino)propyl]trimethoxylsilane **1**(ABCR GmbH) or (3-Mercaptopropyl)trimethoxysilane **2** (Sigma Aldrich), and was stirred for 3 h. After removal, the sample was subsequently rinsed with ethanol and dried in a vacuum oven for 1 h at 60°C.

Gas sensing experiments: The SAM functionalized p-Si/n-ZnO sensors were electrically contacted via wire bonding and placed in a gas chamber with gas in-, outlet and a quartz window for external illumination. The gas flow was controlled by a flow control system (Gometrics MGP-2) and the V_{oc} sensor signal was monitored by a SMU (Keithley 2400 SourceMeter) that was controlled by self-programmed LabVIEW software (National Instruments Inc.). A Newport Oriel Sol1A 94021A solar simulator (150 W Xenon arc lamp; AM1.5 spectrum) was used for the illumination of sensor devices through a quartz window of the sensing chamber. Light intensities were measured with a calibrated reference cell (Newport). I/V characteristics of the sensor were performed with illumination intensities of 100 $mWcm^{-2}$ and gas sensing experiments with an intensity of 30 $mWcm^{-2}$. All gas sensing experiments were performed at room temperature.

DFT simulations: All calculations were performed within the PBE framework with the Vienna ab-initio Simulation Package (VASP).[23] Here, we used the PAW method and pseudopotentials [24,25] an energy cutoff of 400 eV and Gaussian smearing with a width of 0.1 eV. For relaxations a force cutoff of 0.01 eV/Å was used. Dispersion forces were taken into account by using the semi-empirical DFT-D2 method of Grimme[26] as implemented in VASP. The geometries of the amine and thiole functionalities have been relaxed in simulation boxes of the size 13x13x20 $Å^3$. For the evaluation of the electronic structure properties such as the energy level positions static calculations in simulation boxes with the dimensions 30x30x30 $Å^3$ were used in order to suppress spurious interactions between neighbouring images. The projection of the HOMO of the SAM-NO_2 system onto the molecular subsystems was performed by a preceding projection onto spherical harmonics centered around the corresponding atoms of the subsystems and the subsequent summation of all contributions.

Supporting Information
Supporting Information is available online from the Wiley Online Library or from the author.

Acknowledgements

The authors wish to express their sincere gratitude to J. Samà, P. García-Lebière, J. Arens and A. Schmidt for their experimental support. The research leading to these results has received funding from the European Research Council under the European Union's Seventh Framework Programme (FP/2007-2013) / ERC Grant Agreement n. 336917.

Received: ((will be filled in by the editorial staff))
Revised: ((will be filled in by the editorial staff))
Published online: ((will be filled in by the editorial staff))

[1] Z. L. Wang, *Adv. Mater.* **2012**, *24*, 280–285.

[2] M. W. G. Hoffmann, A. E. Gad, J. D. Prades, F. Hernandez-Ramirez, R. Fiz, H. Shen, S. Mathur, *Nano Energy* **2013**, *2*, 514–522.

[3] X. Xue, Y. Nie, B. He, L. Xing, Y. Zhang, Z. L. Wang, *Nanotechnology* **2013**, *24*, 225501.

[4] F. Hernandez-Ramirez, J. D. Prades, A. Tarancon, S. Barth, O. Casals, R. Jimenez-Diaz, E. Pellicer, J. Rodriguez, J. R. Morante, M. A. Juli, et al., *Adv. Funct. Mater.* **2008**, *18*, 2990–2994.

[5] R. M. Penner, *Annu. Rev. Anal. Chem.* **2012**, *5*, 461–85.

[6] B. Esser, J. M. Schnorr, T. M. Swager, *Angew. Chem. Int. Ed.* **2012**, *51*, 5752–5756.

[7] M. W. G. Hoffmann, J. D. Prades, L. Mayrhofer, F. Hernandez-Ramirez, T. T. Järvi, M. Moseler, A. Waag, H. Shen, *Adv. Funct. Mater.* **2014**, *24*, 595–602.

[8] M. C. McAlpine, H. D. Agnew, R. D. Rohde, M. Blanco, H. Ahmad, A. D. Stuparu, W. A. Goddard, J. R. Heath, *J. Am. Chem. Soc.* **2008**, *130*, 9583–9.

[9] W. Yuan, A. Liu, L. Huang, C. Li, G. Shi, *Adv. Mater.* **2013**, *25*, 766–771.

[10] Directive of the European Parliament and of the Council, *2008/50/EG*, EU, **2008**.

[11] D. Zhang, Z. Liu, C. Li, T. Tang, X. Liu, S. Han, B. Lei, C. Zhou, *Nano Lett.* **2004**, *4*, 1919–1924.

[12] R. V. Cooney, P. D. Ross, G. L. Bartolini, J. Ramseyer, *Environ. Sci. Technol.* **1987**, *21*, 77–83.

[13] A. E. Gad, M. W. G. Hoffmann, F. Hernandez-Ramirez, J. D. Prades, H. Shen, S. Mathur, *Mater. Chem. Phys.* **2012**, *135*, 618–622.

[14] A. Kargar, K. Sun, Y. Jing, C. Choi, H. Jeong, Y. Zhou, K. Madsen, P. Naughton, S. Jin, G. Y. Jung, et al., *Nano Lett.* **2013**, *13*, 3017–22.

[15] L. E. Halliburton, N. C. Giles, N. Y. Garces, M. Luo, C. Xu, L. Bai, L. A. Boatner, *Appl. Phys. Lett.* **2005**, *87*, 172108.

[16] D. Look, G. Farlow, P. Reunchan, S. Limpijumnong, S. Zhang, K. Nordlund, *Physi.Rev.Lett.* **2005**, *95*, 225502.

[17] F. Xiu, Z. Yang, D. Zhao, J. Liu, K. a. Alim, A. a. Balandin, M. E. Itkis, R. C. Haddon, *J. Cryst. Growth* **2006**, *286*, 61–65.

[18] A. Janotti, C. G. Van de Walle, *Rep. Prog. Phys.* **2009**, *72*, 126501.

[19] A. Ebong, V. Upadhyaya, B. Rounsaville, D. s. Kim, V. Meemongkolkiat, A. Rohatgi, M. m. Al-Jassim, K. M. Jones, B. To, *IEEE 4th World Conf. Photovolt. Energy Conf.* **2006**, 1376–1379.

[20] B. J. Howgate, S. J. Schoell, M. Hoeb, W. Steins, B. Baur, S. Hertrich, B. Nickel, I. D. Sharp, M. Stutzmann, M. Eickhoff, *Adv. Mater.* **2010**, *22*, 2632–2636.

[21] T. Koopmans, *Physica* **1934**, *1*, 104–113.

[22] C.-G. Zhan, J. A. Nichols, D. A. Dixon, *J. Phys. Chem. A* **2003**, *107*, 4184–4195.

[23] G. Kresse, J. Furthmüller, *Phys. Rev. B* **1996**, *54*, 11169–11186.

[24] G. Kresse, *Phys.Rev. B* **1999**, *59*, 1758–1775.

[25] P. Blöchl, *Phys. Rev. B* **1994**, *50*, 17953–17979.

[26] S. Grimme, *J. Comp. Chem.* **2006**, *17*, 1787–1799.

Submitted to ADVANCED MATERIALS

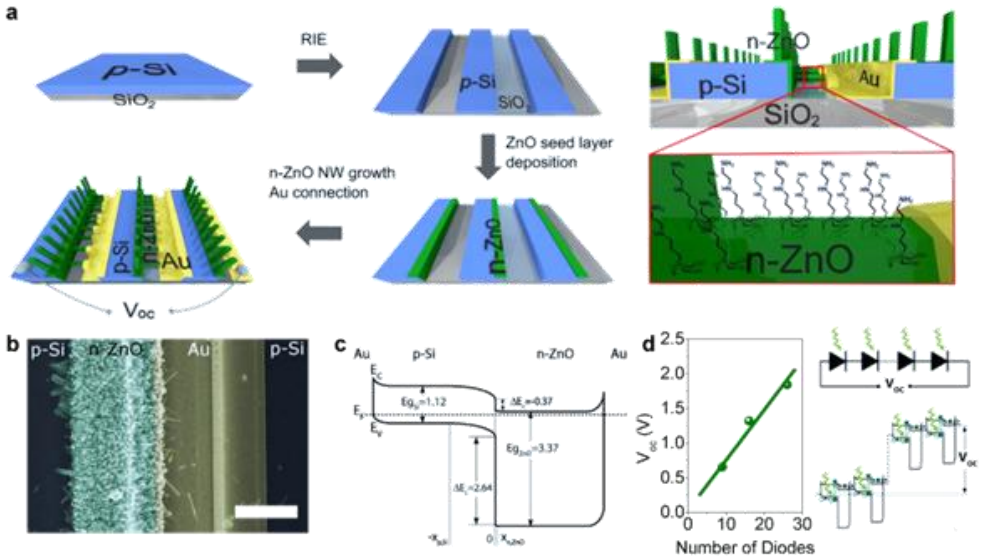

Figure 1. (a) Schematic description of the device fabrication. Higher magnification of a singular p-n unit composed of p-Si μ-trenches. In a subsequent step the n-ZnO nanowires surface was modified by adding a SAM of functional groups. (b) Scanning electron microscope (SEM) image of a singular p-Si/n-ZnO diode (scale bar: 10 μm). (c) Equilibrium band diagram of a single p-Si/n-ZnO diode including the Au contacts on both terminals (see Figure S3 for more details). d) Linear behaviour of the measured V_{oc} with increasing number of diodes under illuminated conditions (simulated sunlight; AM1.5). This is due to the series association of the photodiodes. Upon absorption of light in the depleted region of each one of them, electrons (solid green circles) drift to the n-ZnO part while holes are extracted though the p-Si (open green circles).

Submitted to ADVANCED MATERIALS

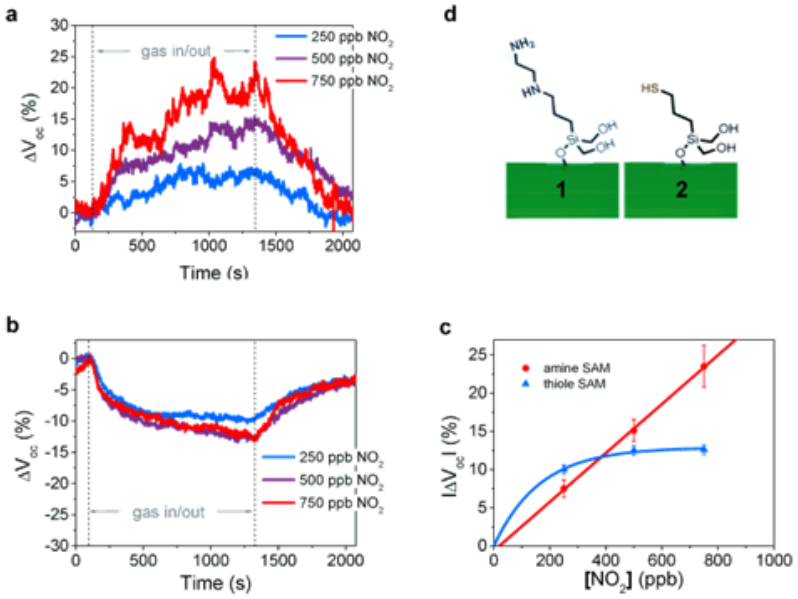

Figure 2. Response of the sensors in a self powered operation towards different concentrations of NO_2 with a) amine and b) thiole terminated SAM functionalizations. c) Diagram of the ΔV_{oc} response versus different NO_2 concentrations for amine and thiole functionalized devices. d) Molecular structure of the amine ([3-(2-aminoethylamino)- propyl]trimethoxylsilane **1**) and thiole ((3-mercapto-propyl)trimethoxysilane **2**) terminated SAMs.

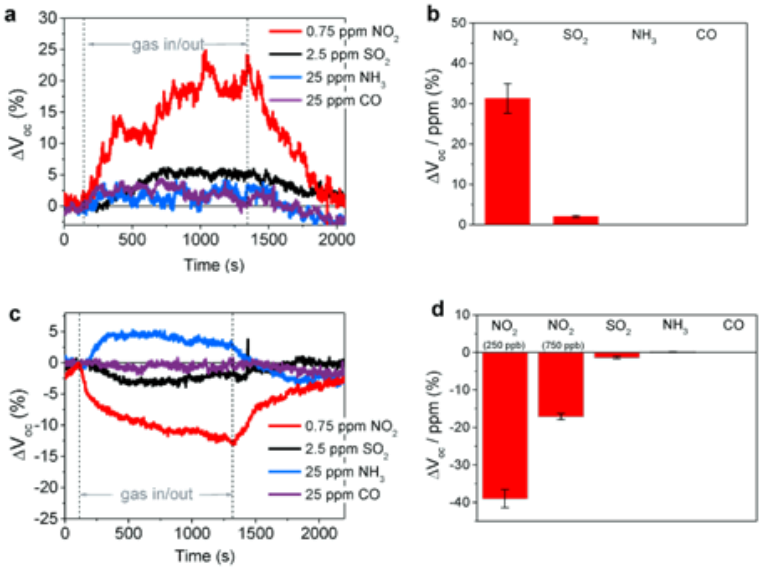

Figure 3. a) Responses of the amine functionalized sensor towards NO_2 in comparison to interfering species (SO_2, NH_3, CO) and b) summary of the sensitivity values. c) Comparative responses of the thiole functionalized sensor and d) summary of the sensitivity values.

Submitted to ADVANCED MATERIALS

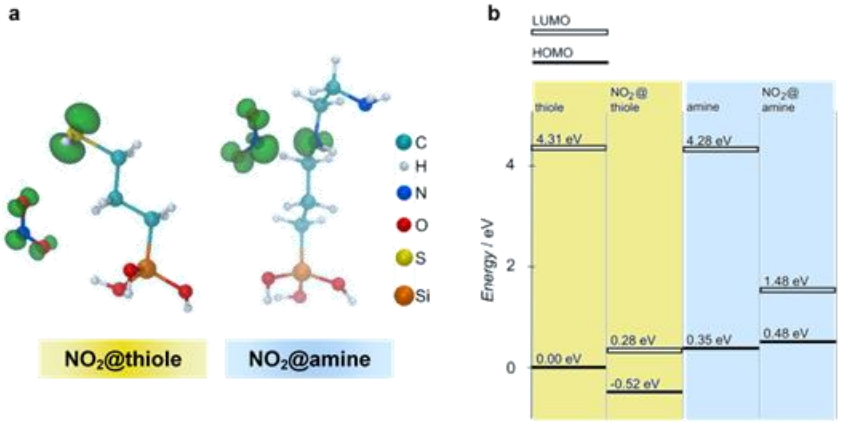

Figure 4. a) Most stable geometries of a NO_2 molecule adsorbed at the thiole and amine functionality respectively. The charge densities of the HOMO wave functions are shown as green isosurfaces. The isosurfaces are drawn at a value of 0.075 e/Å^3. In both cases the HOMOs are hybrids of the HOMO of the organic functionality and the NO_2 LUMO. In the amine case strong mixing between the amine HOMO and the NO_2 LUMO occurs whereas in the thiole case the HOMO of the combined system is dominated by the thiole HOMO. b) Energy levels of the HOMO and LUMO of the functionalities without adsorbed NO_2 and with adsorbed NO_2. The averaged electrostatic potential from the core region of the Si atom of each functionality was used as reference potential. The HOMO level of the isolated thiole functionality was set to 0 for convenience.

Supporting Information

for *Adv. Mater.*, DOI: 10.1002/adma.((please add manuscript number))

Highly Selective and Self Powered Gas Sensor Enabled via Organic Surface Functionalization of p-Si/n-ZnO Nanowire Diodes

Martin W. G. Hoffmann, Leonhard Mayrhofer, Lorenzo Caccamo, Olga Casals, Francisco Hernandez-Ramirez, Gerhard Lilienkamp, Winfried Daum, Michael Moseler, Andreas Waag, Hao Shen and J. Daniel Prades

A. Crystallographic analysis of n-ZnO NWs grown on p-Si substrate

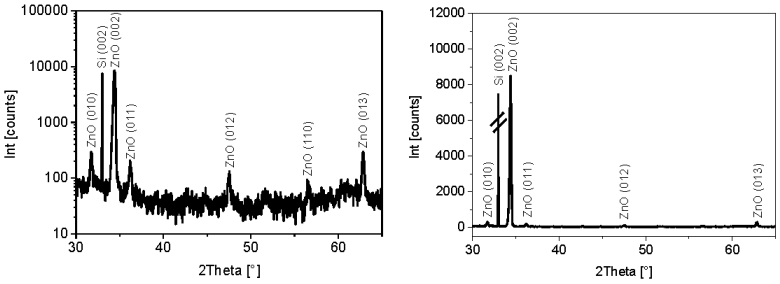

Figure S1. a) Logarithmic and b) linear plot of the XRD spectrum from ZnO NWs, showing the characteristic reflections of hexagonal ZnO, and of the prominent ZnO (002) reflectance that is indicating an aligned growth along the c-axis, respectively

Submitted to ADVANCED MATERIALS

Selectivity and low power consumption are major challenges in the development of sophisticated gas sensor devices. *In this work we present a sensor system that unifies selective gas-sensor interactions and energy harvesting properties, using defined organic-inorganic hybrid materials. Simulations of chemical binding interactions and the consequent electronic surface modulation give more insight into the complex sensing mechanism of selective gas detection.*

Sensors/Biosensors

M. W. G. Hoffmann, L. Mayrhofer, L. Caccamo, O. Casals, F. Hernandez-Ramirez, G. Lilienkamp, W. Daum, M. Moseler, A. Waag, H. Shen and J. D. Prades

Highly Selective and Self Powered Gas Sensor Enabled via Organic Surface Functionalization of p-Si/n-ZnO Diodes

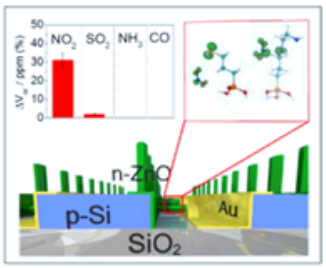

B. Electrical characterization of sensor devices

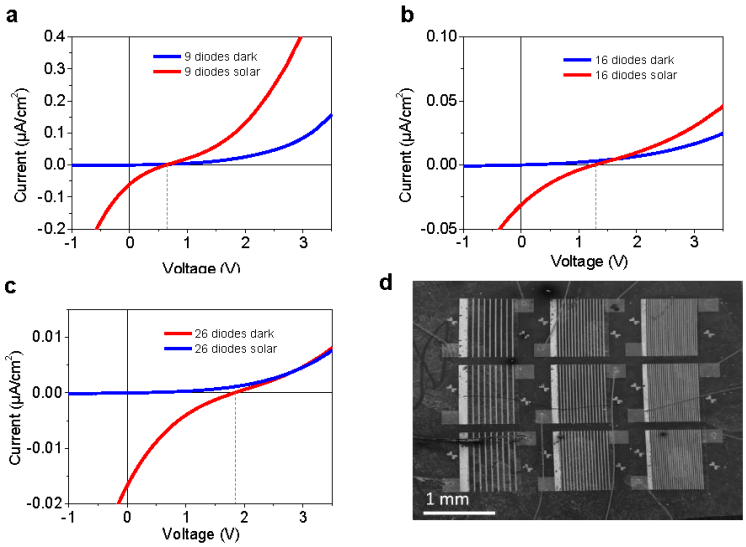

Figure S2. I-V diagrams of p-Si/n-ZnO devices with a) 9, b) 16 and c) 26 diodes in dark conditions (blue) and under solar illumination (AM1.5). The dotted line depicts the V_{oc} values at $I = 0\,A$. d) SEM image of a sensor chip with devices of 9, 16 and 26 diodes.

C. Equilibrium band diagram of the heterojunction structure

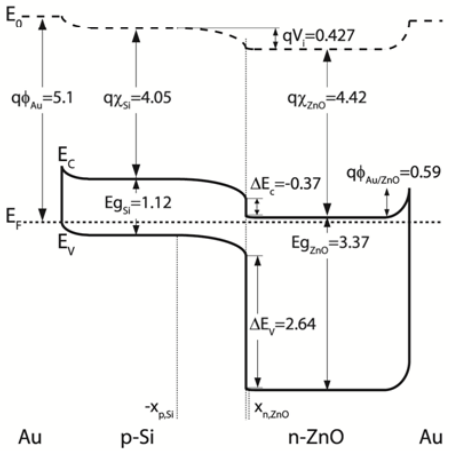

Figure S3. Detailed band diagram of one single p-Si/n-ZnO heterojunction including the two Au metal contacts.

The discontinuity of the conduction (ΔE_c) and valence (ΔE_v) equation (1) and (2)-, the build in potential (V_{bi}) -equation (2)-, the depletion width in the p- (X_{Si}) and n-region (X_{ZnO}) -equations (4) and (5)-, and the bending of the energy bands ($\Delta\phi_{Si}$ and $\Delta\phi_{ZnO}$) -equations (6) and (7)- [1], where calculated using the values shown in Table S1 for the impurity concentrations of the p- (N_a) and n-type (N_d) materials, the intrinsic carrier concentration (n_i), the work function (ϕ), the electron affinity (χ), the band gap (E_g), the equivalent density of states of the conduction band minimum (N_c) and valence band maximum (N_v), and the dielectric constant (ε) of each material.

$$\Delta E_c = q(\chi_{Si} - \chi_{ZnO}) = -0.37eV \quad (1)$$

$$\Delta E_v = (E_{g,ZnO} - E_{g,Si}) - q(\chi_{Si} - \chi_{ZnO}) = 2.64eV \quad (2)$$

$$qV_{bi} = q(\phi_{Si} - \phi_{Si}) = (q\chi_{Si} + (E_f - E_v)) - (q\chi_{ZnO} + (E_c - E_f) = 0.427eV \quad (3)$$

$$-X_{Si} = \sqrt{\frac{2\varepsilon_{Si}\varepsilon_{ZnO}V_{bi}}{q(N_d\varepsilon_{ZnO} + \varepsilon_{Si}N_a)}\frac{N_d}{N_a}} = -0.637\mu m \quad (4)$$

$$X_{ZnO} = \sqrt{\frac{2\varepsilon_{Si}\varepsilon_{ZnO}V_{bi}}{q(N_d\varepsilon_{ZnO} + \varepsilon_{Si}N_a)}\frac{N_a}{N_d}} = 0.009\mu m \quad (5)$$

$$q\Delta\phi_{Si} = q\left(\phi\big|_0 - \phi\big|_{-x_{Si}}\right) = \frac{qN_a}{2\varepsilon_{Si}} X_{Si}^2 = 0.419eV \quad (6)$$

$$q\Delta\phi_{ZnO} = q\left(\phi\big|_{x_{ZnO}} - \phi\big|_0\right) = \frac{qN_d}{2\varepsilon_{ZnO}} X_{ZnO}^2 = 0.008eV \quad (7)$$

Table S1. Electron structure properties of p-Si and n-ZnO.

	Si	**ZnO**
N_x (cm^{-3})	$1.35\cdot10^{15}$	$1.0\cdot10^{17}$[2]
n_i (cm^{-3})	$1.45\cdot10^{10}$ [1]	$4.00\cdot10^{-11}$ [1]
$q\phi$ (eV)	4.939 [1]	4.424 [2,3]
$q\chi$ (eV)	4.05 [1]	4.42 [3]
E_g (eV)	1.12 [1]	3.37 [4]
N_c(cm^{-3})	$2.8\cdot10^{19}$[1]	$3.7\cdot10^{18}$ [5]
N_v(cm^{-3})	$1.0\cdot10^{19}$[1]	$7.2\cdot10^{17}$[6]
ε	11.9 [1]	8.656 [7]

The band bending of ZnO at the ZnO/Au interface was calculated using equation (8), where $q\phi_{Au}$ = 5.1 eV [8] and $q\phi_{ZnO}$ = 4.424 eV (see Table S1) are the work function of gold and ZnO, respectively:

$$q\Delta\phi_{ZnO}\big|_{Au} = q\left(\phi_{Au} - \phi_{ZnO}\right) = 0.59eV \quad (8)$$

D. Simulation of the optoelectronic device response

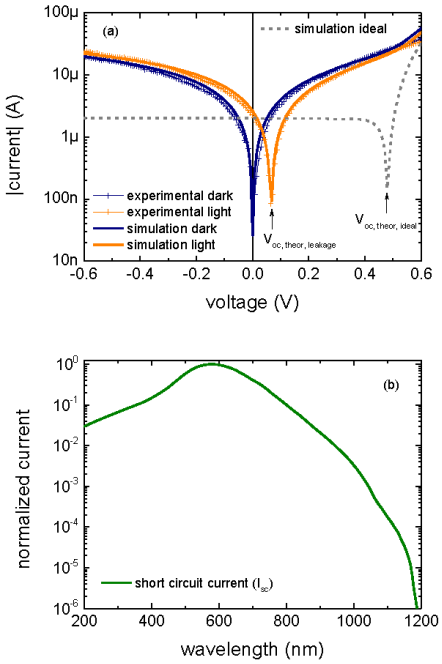

Figure S4. (a) Simulated and experimental I/V diagrams of a p-Si/n-ZnO heterojunction with and without illumination considering interface leakage. For reference, the predicted I/V curve for an ideal p-Si/n-ZnO heterojunction is also given. (b) Simulated spectral response of the p-Si/n-ZnO heterojunctions represented as the normalized short circuit current as a function of the incident photon wavelength.

The electrical behavior of one single p-Si/n-ZnO hereojunction was simulated with PC1D (v5.9), one of the most widely used semiconductor simulators for modeling crystalline solar cells [9].

Our devices were modelled as 1D structures of 10 µm and 2.2 µm in length for the Si and ZnO parts and a cross section of 7000 μm^2, in accordance with the real geometry. Each semiconductor was described by the values given in Table S1. As for the illumination, an AM1.5g source with 100 mW/cm^2 of intensity was selected.

The simulations of the band structure in equilibrium lead to results fully consistent with the band diagram shown in Figure S3.

First, the I-V characteristic of an ideal heterojunction was calculated, showing remarkable differences with the experimental data. Specifically, a theoretical open circuit voltage in ideal conditions of $V_{oc,theor,ideal}$ = 479 mV/diode was obtained, in big contrast with the experiments ($V_{oc,exp}$ = 72±6 mV/diode) (see Figure S4.a).

Then, non-ideal effects were included to obtain a more realistic picture of the device performance. In order to account for the leakage current at the p-n interface, attributed to a significant amount of defect induced carrier recombination [10,11], a shunt resistor in parallel with the structure was considered [12]. Such model successfully predicts the experimental data, with and without illumination, for shunt resistance values of 30 Ω/cm^2. In these conditions, the shape of the I-V curve at low voltages is more linear and the open circuit voltage is reduced down to $V_{oc,theor,\mathbf{leakage}}$ = 68 mV/diode, in accordance with the experimental estimations.

Finally, the spectral response of the device was also modelled, taking into account the light absorption properties of both materials [4]. Figure S4.b shows the spectral response of the device as the normalized short circuit current at wavelengths ranging from 200 to 1200 nm. This result proves that the structure is suitable for operating in the visible range. In fact, additional calculations of the photogeneration rates along the 1D device axis show that visible photons are collected to generate electron-hole pairs only in the Si region, as expected from its bandgap ($E_{g,Si}$ = 1.12 eV [1]).

E. Analysis of the organic surface functionalities

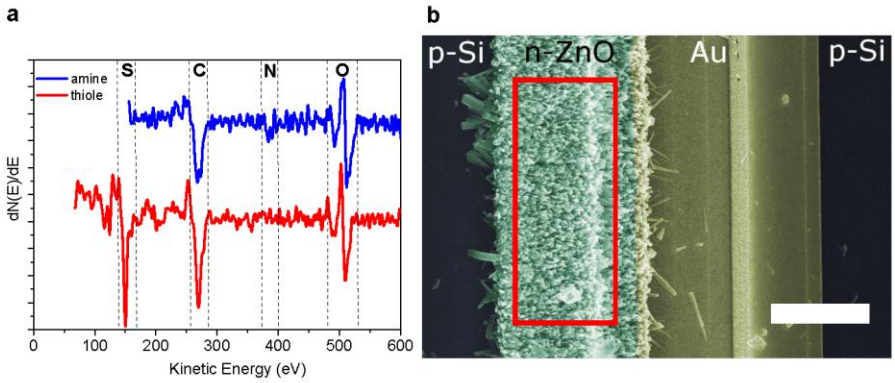

Figure S5. a) Auger spectra for amine and thiole modified ZnO NWs showing nitrogen and sulphur signals respectively as well as carbon and oxygen signals for both samples. b) SEM image of a p-Si/n-ZnO device with depicted measurement area on ZnO NWs. (scale bar: 5 µm)

F. Supplementary data on sensing experiments

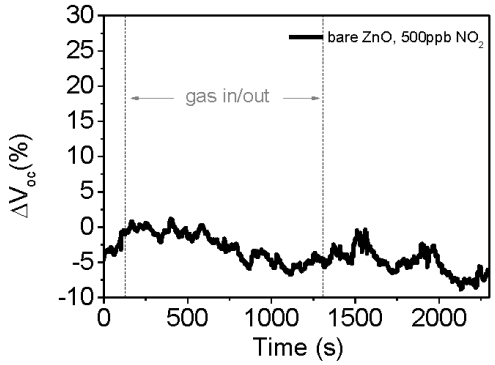

Figure S6. Monitored V_{oc} signal of an unmodified sensor device during a pulse of 500 ppb NO_2

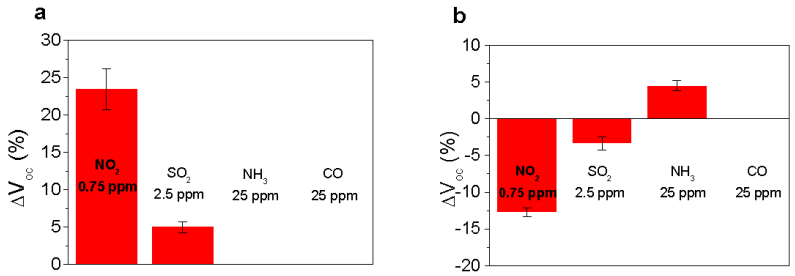

Figure S8. Absolute response values of a) amine and b) thiole functionalized sensors towards NO_2, SO_2, NH_3 and CO.

Table S1: Summary of sensitive and selective properties for different state of the art NO_2 sensors in comparison to the sensing device (amine terminated) of this work.

material	NO_2 conc. (ppb)	|S| (%)*	|S|/ppm (%)	selective	Self-powered	source
This work	250-750	7.5	**30**	yes	yes	
SAM-SnO_2 NWs**	250-750	850	**3400**	yes	no	[13]
mod. graphene	1,000-30,000	25	**25**	yes	no	[14]
PANI-PEO/PVP	125-1,000	<2	**<12**	moderate	no	[15]
mod. graphene	200,000	25	**<<1**	no	no	[16]
In_2O_3 NWs	5-1,000	2	**400**	no	no	[17]
SnO_2 NW	500	1	**<1**	no	no	[18]
WO_3/MWCNT	500	2.2	**<1**	no	no	[19]
Si NWs	20-20,000	10	**500**	no	no	[20]

* absolute sensitivity; related to the lowest given NO_2 concentration in the particular source

** recent work presented by our group

G. Simulation of SAM-gas binding energies and respective HOMO projections

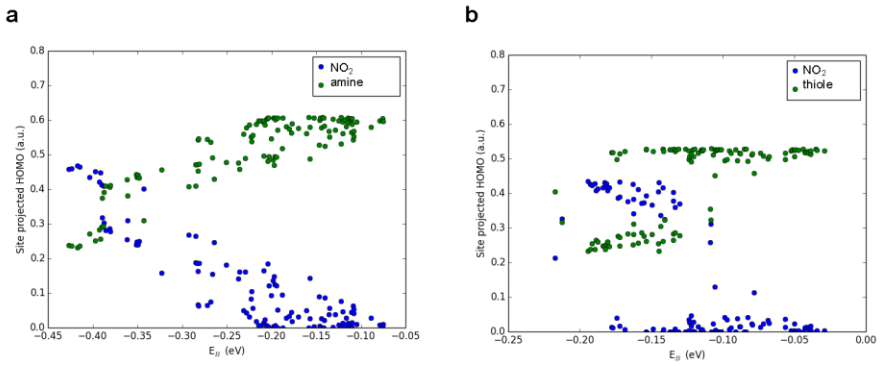

Figure S8. Projection of the HOMO of the SAM-NO_2 system onto the NO_2 molecule and the SAM molecules versus the binding energy for all 115 relaxed investigated SAM-NO_2 systems. a) The hybridization of the HOMO of the amine-NO_2 system strongly correlates with the binding energy. This means that for geometries with strong amine-NO_2 binding the HOMO extents over both subsystems. With decreasing binding strength the HOMO more and more completely localizes on the amine. b) Also for the thiole-NO_2 system we find that hybridization can occur, as the HOMO extents over the NO_2 and the thiole molecule for the strongest binding energies. However, also relatively stable configurations do not necessarily show strong hybridization and a localization of the HOMO is found to be majorly on the thiole (dispersive forces are predominant). The covalent character of the thiole-NO_2 binding interaction, thus, is less dominant than in the amine-NO_2 system.

For the most stable of the considered geometries of the NO_2-amine system the site projected HOMO indicates a considerable hybridization of the amine HOMO and the lowest occupied molecular orbital (LUMO) of the NO_2 when forming the HOMO and LUMO of the combined SAM-NO_2 system (Figure S8a). Figure 4a shows the charge density associated with the HOMO of the most stable amine-NO_2 system that extends over the LUMO of the NO_2 molecule and the HOMO of the amine functionality. From the strong correlation between this hybridization of amine and NO_2 frontier orbitals and the binding energy of the different relaxed amine-NO_2 geometries we conclude that the amine-NO_2 binding has a considerable covalent character. Yet, if dispersive interaction forces are neglected, $|E_B|$ is only reduced from 0.44 eV to 0.29 eV for the most stable configuration.

In case of the thiole SAMs the thiole-NO_2 binding energy is found to be considerably weaker (E_B = -0.22 eV). For the most stable geometry NO_2 adsorbs near the sulfur atom, where the HOMO of the thiole SAM is located, and additionally forms a weak hydrogen bond with one of the OH groups, **Figure 4a**. In the thiole case also some degree of hybridization of the SAM and gas frontier orbitals is observed (Figure S8b). However, here the correlation between binding energy and hybridization is less strict than in the amine case. Dispersion forces play a more dominant role here compared to the amine case. Disregarding dispersion forces $|E_B|$ is reduced from 0.22 eV to 0.12 eV for the most stable thiole-

NO_2 geometry, thus, the portion of covalent binding interaction is lower compared to the amine-NO_2 system.

In the thiole case also some degree of hybridization of the SAM and gas frontier orbitals is observed (Figure S8b). However, here the correlation between binding energy and hybridization is less strict than in the amine case. Dispersion forces play a more dominant role here compared to the amine case. Disregarding dispersion forces $|E_B|$ is reduced from 0.22 eV to 0.12 eV for the most stable thiole-NO_2 geometry, thus, the portion of covalent binding interaction is lower compared to the amine-NO_2 system.

H. References

[1] S. M. Sze, K. K. Ng, *Physics of Semiconductor Devices*, John Wiley & Sons, New Jersey, **2007**.

[2] a) L. E. Halliburton, N. C. Giles, N. Y. Garces, M. Luo, C. Xu, L. Bai, L. A. Boatner, "*Appl. Phys. Lett.* **2005**, 87, 172108.; b) D. Look, G. Farlow, P. Reunchan, S. Limpijumnong, S. Zhang, K. Nordlund, *Phys. Rev. Lett.* **2005**, *22*, 225502.

[3] Chiang, T. C., Himpsel, F. J.: *2.1.21 ZnO*. Goldmann, A., Koch, E.-E. (ed.). SpringerMaterials - The Landolt-Börnstein Database (http://www.springermaterials.com). DOI: 10.1007/10377019_25

[4] S. Adachi, Properties *of Group-IV, III-V and II-VI Semiconductors*, John Wiley & Sons, New Jersey, **2005**.

[5] K. Ellmer, A. Klein, B. Rech, Transparent Conductive Zinc Oxide: Basics and Applications in Thin Film Solar Cells, Springer, Berlin, **2007**.

[6] Calculated from $m_h=0.59m_0$. Ref [3]

[7] S. J. Pearton, D. P. Norton, K. Ip, Y. W. Heo, T. Steiner, Superlattices Microstruct. **2003**, 1–2, 3–32.

[8] D. E. Eastman, *Phys. Rev. B* **1970**, *1*, 1–2.

[9] D. A. Clugston, P. A. Basore, Conference Record of the 26th IEEE Photovoltaic Specialists Conference **1997**, 207-210.

[10] F. Xiu, Z. Yang, D. Zhao, J. Liu, K. a. Alim, A. a. Balandin, M. E. Itkis, R. C. Haddon, *J. Cryst. Growth* **2006**, *286*, 61–65.

[11] A. Janotti, C. G. Van de Walle, *Rep. Prog. Phys.* **2009**, *72*, 126501.

[12] A. Luque, S. Hegedus, *Handbook of photovoltaic science and engineering*, John Wiley & Sons, New Jersey, **2011**.

[13] M.W.G. Hoffmann *et al.*, *Adv. Funct. Mater.* **2014**, 24, 595–602.

[14] W. Yuan, A. Liu, L. Huang, C. Li, G. Shi, G. *Adv. Mater.* **2013** 25, 766–771.

[15] E. Zampetti, *et al. Biosens. Bioelectron.* **2011**, 26, 2460–5.

[16] M. G. Chung, *et al. Sens. Actuat. B* 2012, 166-167, 172–176

[17] D. Zhang *et al.*, *Nano Lett.* **2004**, 4, 1919–1924.

[18] J. D. Prades, *et al.*, *Appl. Phys. Lett.* **2008**, 93, 123110 (2008).

[19] C. Bittencourt *et al.*, *Sens. Actuat.B* **2006**, 115, 33–41.

[20] M. C. McAlpine, H. Ahmad, D. Wang, J. R. Heath, *Nature Mater.* **2007**, 6, 379–384.

Asunto: Acceptance of your submission to Advanced Materials (adma.201403073R2) - [EMID:e930f58f5bcec036]
Fecha: Fri, 12 Sep 2014 02:53:41 -0400
De: Advanced Materials <em@editorialmanager.com>
Responder a: Advanced Materials <advmat@wiley-vch.de>
Para: J. Daniel Prades <dprades@el.ub.edu>

Dear Dr. Prades,

Thank you for submitting your manuscript "Highly Selective and Self-Powered Gas Sensor via Organic Surface Functionalization of p-Si/n-ZnO Diodes" to Advanced Materials. The reviewer report and comments are included at the end of this email.

I'm pleased to inform you that your manuscript has been accepted for publication without change.

You do not need to send additional files at this time.

We will copyedit the accepted version of your manuscript and if we require any further information at this stage we will contact you. After copyediting we will let you know when you can expect to receive the proofs. Instructions for returning your proof corrections will be provided when the proofs are sent to you.

Open access publication of this work is possible via Wiley OnlineOpen, enabling you to meet institutional and funder open access mandates. Wiley OnlineOpen allows you to post the final, published PDF of your OnlineOpen article on your website, your institutional repository, or any other free public server straight away. The fee for OnlineOpen is US$3000. More information about Wiley OnlineOpen can be found at http://olabout.wiley.com/WileyCDA/Section/id-406241.html.

Congratulations on your results, and thank you for choosing Advanced Materials for publishing your work. I hope you will consider us for the publication of your future manuscripts.

Yours sincerely,

Anne Pfisterer

--
Dr. Anne Pfisterer, Editor

Advanced Materials
E-mail: advmat@wiley-vch.de
Tel: +49(0)6201-606-235/432

http://advmat.de/

*****

4

Conclusion

Within the here presented thesis, a device novel concept for selective sensing of NO_2 without the need of external energy input was developed. The realization of the thesis outline required an interdisciplinary approach involving fields of chemistry, physics and electrical engineering. It was demonstrated that the specific unification of functional inorganic (hetero) materials with defined organic functionalities can lead to powerful hybrid devices with performances far beyond their singular units. It was described, that the understanding of the observed sensing characterizations of these hybrid devices cannot be described by a consideration of isolated inorganic and organic stakes. Moreover, an understanding of the complex aggregated system from SAM-gas binding and electronic modulations within the inorganic as well as organic structures are needed to understand the sensor-gas interaction mechanisms that can lead to selective gas sensing properties.

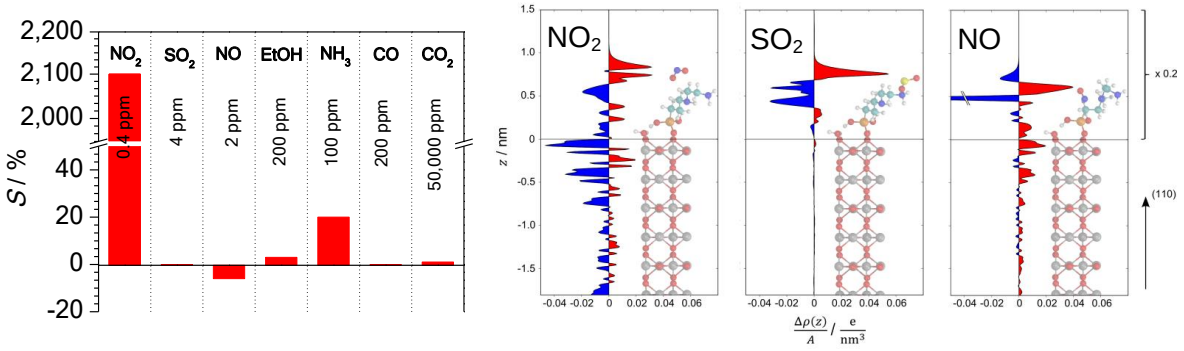

Fig. 4.1: (left) Summary of sensing responses observed for the SAM-NW hybrid sensor and (right) DFT simulations of the charge transfer dynamics upon NO_2-SAM binding.

Section 1 described the concept of a selective sensor based on SAM modified inorganic NWs. An extraordinary sensing performance in terms of selectivity and sensitivity towards NO_2 could be achieved when compared to known semiconductor based systems. For the first time, the underlying mechanism of sensor-gas binding interactions and consequent charge transfer sequences between the organic and inorganic components were analysed via DFT methods and revealed a consistence of experimental and theoretical evaluations. The

finding that the energetic positions of SAM-gas frontier orbitals with respect to the NW-SAM Fermi Energy (E_F) is the crucial factor to enable selective sensing could lead to a new rout of sensor development.

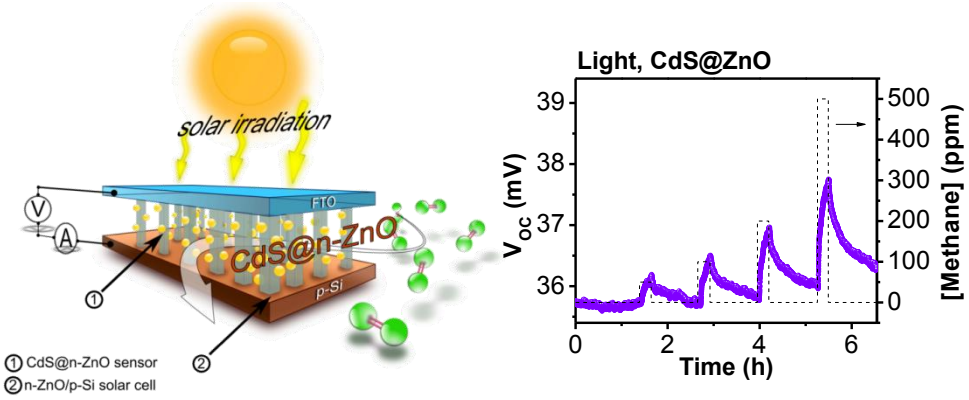

Fig. 4.2: (left) Schematic illustration of the self-powered sensor deice based on an CdS@n-ZnO/p-Si heterostructure and (right) sensing response towards different concentrations of methane under self-powered sensing conditions.

The self-powered sensor concept described in section 2 was realized by a photovoltaic CdS@n-ZnO/p-Si heterostructure with a functional overlap of n-ZnO NWs as n-type material of the p-n junction and active sensing component. Furthermore, the use of CdS nano particles (NPs) on the ZnO surface enabled the activation of the sensor upon visible light illumination. The sensor showed quantitative sensing responses towards oxidizing and reducing gas species without the need of an external energy source. Other than conventional gas sensor concepts, the signal generation of the sensor and surface activation of the sensitive material was solely driven by the absorbed visible photons within the p/n junction (signal generation) and CdS NPs (surface activation). Mechanistic studies revealed the change of the charge carrier density (N_D) within n-ZnO, induced gas-surface interactions, to be responsible for the observed change of the self-generated sensor signal (ΔV_{oc}).

Based on the concepts and findings described above, a new sensor device was designed unifying the capabilities of selective gas sensing and self-powered operation in a compact micro structured setup. Moreover, the new self-powered device platform was used to study the influence of the chemical nature of the SAM termination (amine and thiole functionalities). Both sensor types showed very high selectivity and sensitivity towards NO_2 down to concentrations required for human health safety. As it could already be expected from the findings of section 1, the experimental results proved that the organic functionality

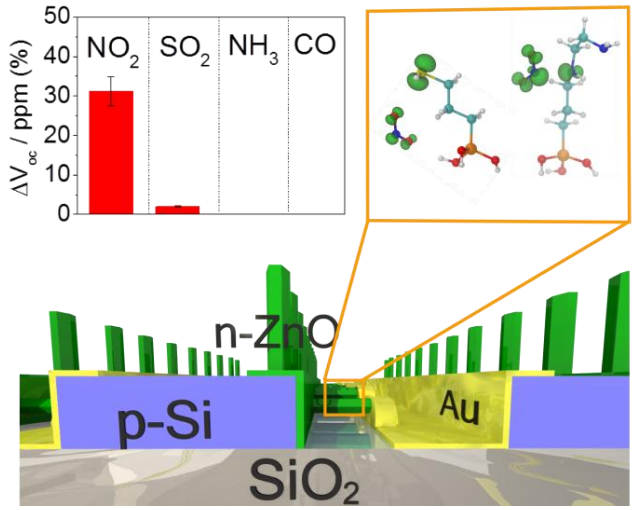

Fig. 4.3: Schematic illustration of the selective and self-powered gas sensor with graphical presentation of gas responses, as well as of the SAM-gas binding geometries for thiole (left) and amine (right) terminated sensors.

determines the sensor characteristics. The contrary response was further reflected by DFT analysis of the SAM-gas binding interactions and consequent modulation of the energetic positions of the frontier molecular orbitals.

The finding and developments presented within the here presented thesis describe a new approach of sensor development. The introduction of active hybrid materials with organic SAMs as well defined and flexible receptor components opens new possibilities for the design of selective sensor units. Crucial parameters for selective gas interactions are not only specific binding interactions, but also the electric modulation of the organic and inorganic components. These complex interconnections facilitate the discrimination of interfering gas species, but also complicate the precise forecast of the actual sensor characteristics. It could be evaluated that theoretical DFT methods are a powerful tool to predict or understand experimentally observed sensor-gas interactions. Thus, the experimental development of hybrid gas sensors should go along with the support of theoretical methods to achieve an efficient development of selective gas sensors.

5

Outlook

Two major requirements on gas sensors could be achieved by the sensor concepts developed within this thesis:

- High selectivity and
- Low power consumption

These properties are of basic importance for the application in widespread sensor networks and mobile devices and the here presented realization could give an outlook on prospective developments within sensor technologies. However, the non-finite diversity of organic molecules that could be bound to inorganic surfaces opens a wide field of studies and improvements about the chemical and electrical influence of the organic surface groups on sensor-gas interactions. The here presented studies (see section 1 and 3) could describe that terminal functional groups of the SAM have crucial influences on the binding geometries and bond strength to the respective gas species. Furthermore, these parameters as well as the probability of an efficient NW-SAM charge transfer are determined by the electronic structure of the organic molecule, described by the energetic position and geometries of its frontier orbitals.

Therefore, further studies and developments should analyse the influence of functional terminal SAM groups as well as modulations of the organic backbone of the singular molecules. Here, the influence of electron density and polar groups (e.g. carbonyl, hydroxyl or imine groups) will be a major focus of following investigations. Another promising approach would be the mixture of gas receptor SAMs with strongly electron withdrawing SAMs, as perflourinated methoxysilenes. Hereby, a direct electronic modulation of the inorganic material could be achieved via surface transfer doping (modulation of E_F), and thus, allows for the setting of the selective sensor properties. All these examinations will require detailed and reliable DFT systems.

Furthermore, environmental operation in a commercial sense will additionally makes high demands on sensors in the fields of

- Sensor lifetime
- Signal quality and
- Device design

Critical parameters for ensuring higher sensor lifetime are the illumination conditions during sensing operations. On one hand, the introduced energy ensures fast response and recovery characteristics during sensing operations (see section 1). On the other hand, continuous illumination in particular within the UV-range, is promoting the decomposition of the organic SAM as well as irreversible SAM-gas reactions and thus, can lead to a reduced sensor lifetime. Taking into account these considerations, light sources and illumination routines have to be adapted in a way that high energy photons can be excluded and pulsed on/off light sequences reduce the duration of incident light.

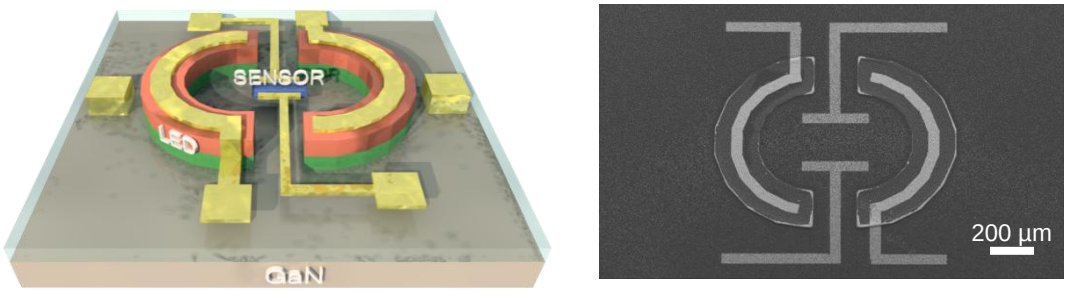

Fig. 5.1: (left) Schematic illustration and (right) SEM image of the gas sensor platform with integrated GaN based µLED.

At the same time, the sensor system must keep a compact design to allow the integration into electronic platforms. A current work is engaged with the integration of gallium nitride (GaN) based µLED structures ($\lambda > 420$ nm) with resistive hybrid sensor units. This platform will allow the full control of the illumination source and enables minor power consumption (µW range) due to the direct proximity to the sensor (µm distance). The integration of a self-powered sensor unit into the µLED platform would additionally reduce the power demand of the system, as the µLED illumination would allow for fast sensor response and recovery processes, as well as the sensor signal generation (V_{oc}).

6

References

1. United Nations. *World Urbanization Prospects - The 2011 Revision*. (2012).

2. World Health Organization. *WHO Air quality guidelines for particulate matter, ozone, nitrogen dioxide and sulfur dioxide*. (2006).

3. Penner, R. M. Chemical sensing with nanowires. *Annu. Rev. Anal. Chem.* **5,** 461–85 (2012).

4. Chen, X., Wong, C. K. Y., Yuan, C. a. & Zhang, G. Nanowire-based gas sensors. *Sens. Actuat. B* **177,** 178–195 (2013).

5. Prades, J. D. *et al.* Harnessing self-heating in nanowires for energy efficient, fully autonomous and ultra-fast gas sensors. *Sens. Actuat. B* **144,** 1–5 (2010).

6. Prades, J. D., Cirera, A. & Morante, J. R. Ab initio calculations of NO_2 and SO_2 chemisorption onto non-polar ZnO surfaces. *Sens. Actuat. B* **142,** 179–184 (2009).

7. Prades, J., Cirera, A., Morante, J., Pruneda, J. & Ordejon, P. Ab initio study of NOx compounds adsorption on SnO2 surface. *Sens. Actuat. B* **126,** 62–67 (2007).

8. Yamazoe, N. New approaches for improving semiconductor gas sensors. *Sens. Actuat. B* **5,** 7–19 (1991).

9. Huang, J. & Wan, Q. Gas sensors based on semiconducting metal oxide one-dimensional nanostructures. *Sensors* **9,** 9903–24 (2009).

10. Barth, S., Hernandez-Ramirez, F., Holmes, J. D. & Romano-Rodriguez, A. Synthesis and applications of one-dimensional semiconductors. *Prog. Mater. Sci.* **55,** 563–627 (2010).

11. Zou, X. *et al.* Rational design of sub-parts per million specific gas sensors array based on metal nanoparticles decorated nanowire enhancement-mode transistors. *Nano Lett.* **13,** 3287–92 (2013).

12. Shao, F. *et al.* Heterostructured p-CuO (nanoparticle)/n-SnO_2 (nanowire) devices for selective H_2S detection. *Sens. Actuat. B* **181,** 130–135 (2013).

13. Sysoev, V. V, Goschnick, J., Schneider, T., Strelcov, E. & Kolmakov, A. A gradient microarray electronic nose based on percolating SnO_2 nanowire sensing elements. *Nano Lett.* **7,** 3182–8 (2007).

14. Sysoev, V. V, Button, B. K., Wepsiec, K., Dmitriev, S. & Kolmakov, A. Toward the Nanoscopic " Electronic Nose ": Hydrogen vs carbon monoxide discrimination with an array of individual metal oxide nano- and mesowire sensors. *Nano Lett.* (2006).

15. Paska, Y., Stelzner, T., Christiansen, S. & Haick, H. Enhanced sensing of nonpolar volatile organic compounds by silicon nanowire field effect transistors. *ACS Nano* **5,** 5620–6 (2011).

16. Bushdid, C., Magnasco, M. O., Vosshall, L. B. & Keller, A. Humans can discriminate more than 1 trillion olfactory stimuli. *Science* **343,** 1370–1372 (2014).

17. The Nobel Assembly at Karolinska Institutet. *The Nobel Prize in Physiology or Medicine 2004 to Richard Axel and Linda B. Buck - Press release*. (2004).

18. Goldsmith, B. R. *et al.* Biomimetic chemical sensors using nanoelectronic readout of olfactory receptor proteins. *ACS Nano* **5,** 5408–16 (2011).

19. Zheng, G., Patolsky, F., Cui, Y., Wang, W. U. & Lieber, C. M. Multiplexed electrical detection of cancer markers with nanowire sensor arrays. *Nat. Biotechn.* **23,** 1294–301 (2005).

20. Glatz, R. & Bailey-Hill, K. Mimicking nature's noses: from receptor deorphaning to olfactory biosensing. *Progr. Neurobiol.* **93,** 270–96 (2011).

21. McAlpine, M. C. *et al.* Peptide-nanowire hybrid materials for selective sensing of small molecules. *J. Am. Chem. Soc.* **130,** 9583–9589 (2008).

22. Cid, C. C. *et al.* Selective detection of SO_2 at room temperature based on organoplatinum functionalized single-walled carbon nanotube field effect transistors. *Sens. Actuat. B* **141,** 97–103 (2009).

23. Esser, B., Schnorr, J. M. & Swager, T. M. Selective detection of ethylene gas using carbon nanotube-based devices: utility in determination of fruit ripeness. *Angew. Chem. Int. Ed.* **51,** 5752–6 (2012).

24. Cui, Y., Kim, S. N., Naik, R. R. & McAlpine, M. C. Biomimetic peptide nanosensors. *Acc. Chem. Res.* **45,** 696–704 (2012).

25. Qi, D. *et al.* Surface transfer doping of diamond (100) by tetrafluoro-tetracyanoquinodimethane. *J. Am. Chem. Soc.* **129,** 8084–8085 (2007).

26. Love, J. C., Estroff, L. A., Kriebel, J. K., Nuzzo, R. G. & Whitesides, G. M. Self-assembled monolayers of thiolates on metals as a form of nanotechnology. *Chem. Rev.* **105,** 1103–69 (2005).

27. Ulman, A. Formation and structure of self-assembled monolayers. *Chem. Rev.* **96,** 1533–1554 (1996).

28. Chen, R. J., Zhang, Y., Wang, D. & Dai, H. Noncovalent sidewall functionalization of single-walled carbon nanotubes for protein immobilization. *J. Am. Chem. Soc.* **123,** 3838–3839 (2001).

29. Maier, F., Riedel, M., Mantel, B., Ristein, J. & Ley, L. Origin of surface conductivity in diamond. *Phys. Rev. B* **85,** 3472–3475 (2000).

30. Kong, J. & Dai, H. Full and Modulated chemical gating of individual carbon nanotubes by organic amine compounds. *J. Phys. Chem. B* **105,** 2890–2893 (2001).

31. Gao, X. P., Zheng, G. & Lieber, C. M. Subthreshold regime has the optimal sensitivity for nanowire FET biosensors. *Nano Lett.* **10,** 547–52 (2010).

32. Chen, W., Qi, D., Gao, X. & Wee, A. T. S. Surface transfer doping of semiconductors. *Progr. Surf. Sci.* **84,** 279–321 (2009).

33. Calhoun, M. F., Sanchez, J., Olaya, D., Gershenson, M. E. & Podzorov, V. Electronic functionalization of the surface of organic semiconductors with self-assembled monolayers. *Nat. Mater.* **7,** 84–89 (2008).

34. Kim, T. H. *et al.* Selective and sensitive TNT sensors using biomimetic polydiacetylene-coated CNT-FETs. *ACS Nano* **5,** 2824–30 (2011).

35. Sorgenfrei, S. *et al.* Label-free single-molecule detection of DNA-hybridization kinetics with a carbon nanotube field-effect transistor. *Nat. Nanotechn.* **6,** 126–32 (2011).

36. Kontermann, R. & Dübel, S. *Antibody Engineering*. (Springer Berlin Heidelberg, 2010). doi:10.1007/978-3-642-01144-3

37. Hoare, S. R. J. Mechanisms of peptide and nonpeptide ligand binding to Class B G-protein-coupled receptors. *Drug Discov. Today* **10,** 417–427 (2005).

38. Petsalaki, E., Stark, A., García-Urdiales, E. & Russell, R. B. Accurate prediction of peptide binding sites on protein surfaces. *PLoS Comput. Biol.* **5,** e1000335 (2009).

39. Pal, K., Melcher, K. & Xu, H. E. Structure and mechanism for recognition of peptide hormones by Class B G-protein-coupled receptors. *Acta Pharmacol .Sin.* **33,** 300–11 (2012).

40. Cui, Y., Wei, Q., Park, H. & Lieber, C. M. Nanowire nanosensors for highly sensitive and selective detection of biological and chemical species. *Science* **293,** 1289–1292 (2001).

41. Li, Z. *et al.* Sequence-specific label-free DNA sensors based on silicon nanowires. *Nano Lett.* **2**, 10–12 (2004).

42. Bunimovich, Y. L. *et al.* Quantitative real-time measurements of DNA hybridization with alkylated nonoxidized silicon nanowires in electrolyte solution. *J. Am. Chem. Soc.* **128**, 16323–16331 (2006).

43. Sorgenfrei, S., Chiu, C.-Y., Johnston, M., Nuckolls, C. & Shepard, K. L. Debye screening in single-molecule carbon nanotube field-effect sensors. *Nano Lett.* **11,** 3739–43 (2011).

44. McAlpine, M. C. *et al.* Peptide-nanowire hybrid materials for selective sensing of small molecules. *J. Am. Chem. Soc.* **130,** 9583–9 (2008).

45. Schnorr, J. M., van der Zwaag, D., Walish, J. J., Weizmann, Y. & Swager, T. M. Sensory Arrays of Covalently Functionalized Single-Walled Carbon Nanotubes for Explosive Detection. *Adv. Funct. Mater.* (2013). doi:10.1002/adfm.201300131

46. Bergin, E. Asymmetric catalysis. *Annu. Rep. Prog. Chem., Sect. B* **108,** 353 (2012).

47. Kolb, H. C., Vannieuwenhze, M. S. & Sharpless, K. B. Catalytic Asymmetric Di hydroxylation. *Chem. Rev.* **94,** 2483–2547 (1994).

48. Mukherjee, S., Yang, J. W., Hoffmann, S. & List, B. Asymmetric enamine catalysis. *Chem. Rev.* **107,** 5471–569 (2007).

49. Seayad, J. & List, B. Asymmetric organocatalysis. *Org. Biomol. Chem.* **3,** 719–24 (2005).

50. Taylor, M. S. & Jacobsen, E. N. Asymmetric Catalysis by Chiral Hydrogen-Bond Donors. *Angew. Chem. Int. Ed.* **45,** 1520–1543 (2006).

51. Wang, B. & Haick, H. Effect of functional groups on the sensing properties of silicon nanowires toward volatile compounds. *ACS Appl. Mater. Interfaces* **5,** 2289–99 (2013).

52. Wang, B., Cancilla, J. C., Terocella, J. S. & Haick, H. Artificial sensing intelligence with silicon nanowires for ultra-selective detection in the gas phase. *Nano Lett.* (2014). doi:10.1021/nl404335p

53. Engel, Y. *et al.* Supersensitive detection of explosives by silicon nanowire arrays. *Angew. Chem. Int. Ed.* **49,** 6830–6835 (2010).

54. Hughes, E. D. & Ingold, C. K. 55. Mechanism of substitution at a saturated carbon atom. Part IV. A discussion of constitutional and solvent effects on the mechanism, kinetics, velocity, and orientation of substitution. *J. Chem. Soc.* (1935). doi:10.1039/jr9350000244

55. Wang, Z. L. Self-powered nanosensors and nanosystems. *Adv. Mater.* **24,** 280–285 (2012).

56. Richards, M., Ghanem, M., Osmond, M., Guo, Y. & Hassard, J. Grid-based analysis of air pollution data. *Ecol. Model.* **194,** 274–286 (2006).

57. Silva, D., Ghanem, M. & Guo, Y. WikiSensing: an online collaborative approach for sensor data management. *Sensors* **12,** 13295–332 (2012).

58. Prades, J. D. *et al.* Ultralow power consumption gas sensors based on self-heated individual nanowires. *Appl. Phys. Lett.* **93,** 123110 (2008).

59. Lin, Z.-H. *et al.* A self-powered triboelectric nanosensor for mercury ion detection. *Angew. Chem. Int. Ed.* **52,** 5065–9 (2013).

60. Xu, S. *et al.* Self-powered nanowire devices. *Nat. Nanotech.* **5,** 366–73 (2010).

61. Yang, Y. *et al.* Simultaneously harvesting mechanical and chemical energies by a hybrid cell for self-powered biosensors and personal electronics. *Energy Environ. Sci.* **6,** 1744 (2013).

62. Xue, X. *et al.* Surface free-carrier screening effect on the output of a ZnO nanowire nanogenerator and its potential as a self-powered active gas sensor. *Nanotechnology* **24,** 225501 (2013).

63. Xue, X. *et al.* Surface free-carrier screening effect on the output of a ZnO nanowire nanogenerator and its potential as a self-powered active gas sensor. *Nanotechnology* **24,** 225501 (2013).

64. Wang, X., Song, J., Liu, J. & Wang, Z. L. Direct-current nanogenerator driven by ultrasonic waves. *Science* **316,** 102–5 (2007).

65. Zhu, G., Yang, R., Wang, S. & Wang, Z. L. Flexible high-output nanogenerator based on lateral ZnO nanowire array. *Nano Lett.* **10,** 3151–5 (2010).

66. Peng, L., Hu, L. & Fang, X. Energy Harvesting for Nanostructured Self-Powered Photodetectors. *Adv. Funct. Mater.*(2014). doi:10.1002/adfm.201303367

67. Pan, C. *et al.* Generating electricity from biofluid with a nanowire-based biofuel cell for self-powered nanodevices. *Adv. Mater.* **22,** 5388–92 (2010).

68. Hansen, B. J., Liu, Y., Yang, R. & Wang, Z. L. Hybrid nanogenerator for concurrently harvesting biomechanical and biochemical energy. *ACS Nano* **4,** 3647–52 (2010).

69. Xu, C., Wang, X. & Wang, Z. L. Nanowire structured hybrid cell for concurrently scavenging solar and mechanical energies. *J. Am. Chem. Soc.* **131,** 5866–72 (2009).

70. Korotcenkov, G. Metal oxides for solid-state gas sensors: What determines our choice? *Mater. Sci. Eng. B* **139,** 1–23 (2007).

71. Directive of the European Parliament and of the Council. *2008/50/EG*. (2008).

Appendix

A: Scientific Vita

Martin W. G. Hoffmann
Born in April 7th of 1984 in Bornheim (Germany)

Current positions:

- PhD student in the Department of Electronics of the University of Barcelona.
- Managing director of the research center *Laboratory for Emerging Nanometrology* at the Braunschweig University of Technology (Germany)

A.1 Academic Degrees

DIPLOMA in Chemistry (Dipl. Chem.); Cologne, 12/2009
Diploma thesis: "Synthesis and self-assembly of iron oxide nanoparticles"
Qualification: 1.0; with honors
Department of Chemistry, University of Cologne (Germany)

PREDIPLOMA in Chemistry; Cologne, 11/2007
Qualification: 1.2
Department of Chemistry, University of Cologne (Germany)

ABITUR; Bonn, 6/2003
Qualification 1.7
Beethoven-Gymnasium Bonn (Germany)

A.2 Publications

1) Hoffmann, M. W. G.; Mayrhofer, L.; Casals, O.; Caccamo, L.; Hernandez-Ramirez, F.; Moseler, M.; Waag, A.; Shen, H.; Prades, J. D., "Highly selective and self-powered gas sensor enabled via organic surface functionalization", *Adv. Mater.*(2014) doi: 10.1002/adma.201403073.
2) Hoffmann, M. W. G.; Prades, J. D; Mayrhofer, L.; Hernandez-Ramirez, F.: Moseler, M.; Waag, A. and Shen, H. "Highly selective SAM-nanowire hybrid NO_2 sensor: insight into charge transfer dynamics and alignment of frontier molecular orbitals", *Adv. Funct. Mater.* 24, 595–602 (2014). (inside Cover 5/2014)

3) Hoffmann, M. W. G.; Gad, A.; Prades, J. D.; Hernandez-Ramirez, F.; Fiz, R.; Shen, H.; Mathur, S., "Solar diode sensor: Sensing mechanism and applications", *Nano Energy* 2, 514–522 (2013).

4) Hoffmann, M. W. G.; J.D. Prades, A.E. Gad, F. Hernandez-Ramirez, H. Shen, S. Mathur, European Patent Application EP 2565645A1, „Fluid detector and method for detecting fluids", publication: 06.03.2013. (nominated for the *Nicolaus August Otto Prize* 2011)

5) Li, J; Hoffmann, M.W.G.; Shen, H.; Fabrega, C.; Prades, J. D.; Andreu, T.; Hernandez-Ramirez, F.; Mathur, S., " Enhanced photoelectrochemical activity of an excitonic staircase in CdS@TiO_2 and CdS@anatase@rutile TiO_2 heterostructures", *J. Mater. Chem.* 22, 20472 (2012).

6) Gad, A. E.; Hoffmann, M. W. G.; Hernandez-Ramirez, F.; Prades, J. D.; Shen, H.; Mathur, S., "Coaxial p-Si/n-ZnO nanowire heterostructures for energy and sensing applications", *Mater. Chem. Phys.* 135, 618–622 (2012).

7) Shao, F.; Hoffmann, M.W.G.; Prades, J.D.; Morante, J.R.; Lopez, N.; Hernandez-Ramirez, F., "Interaction mechanisms of ammonia and tin oxide: A combined analysis using single nanowire devices and DFT calculations" *J. Phys. Chem. C* 117, 3520-3526 (2013).

8) Shao, F.; Hoffmann, M. W. G; Prades, J.; D; Zamani, R; Arbiol, J.; Morante, J. R.; Varechkina, E.; Rumantseva, M.; Gaskov, A.; Giebelhaus, I.; Fischer, T.; Mathur, S.; Hernandez-Ramirez, F., "Heterostructured p-CuO (nanoparticle)/n-SnO_2 (nanowire) devices for selective H_2S detection", *Sens. Actuat. B* 181, 130-135 (2013).

9) Hoffmann, M.; von Hagen, R.; Shen, H.; Mathur, S., "Synthesis and self-assembly of iron oxide nanoparticles", *Ceram. Eng. Sci. Proc.* 2010, 31, 21-27.

10) Caccamo, L.; Hartmann, J.; Fàbrega, C.; Estradé, S.; Lilienkamp, G.; Prades, J. D.; Hoffmann, M. W. G.; Ledig, J.; Wagner, A.; Wang, X.; Lopez-Conesa, L.; Peiró, F.; Rebled, J. M.; Wehmann, H.; Daum, W.; Shen, H.; Waag, A. "Band engineered epitaxial 3D GaN-InGaN core-shell rod arrays as an advanced photoanode for visible-light-driven water splitting" *ACS Appl. Mater. Interfaces 6*, 2235–40 (2014).

A.3 Awards and Fellowships

Förderpreis des Department für Chemie, University of Cologne, 6/2010

Poster price (2nd place), 34th International Conference and Exposition on Advanced Ceramics and Composites (ICACC), Daytona, FA, 1/2010

DAAD PhD grant at the University of Barcelona and the Catalonia Institute for Energy Research (IREC), 02/2012-08/2012

A.4 Participation in Projects

1) Title of the project: *Design und Modifikation von einzelnen und angeordneten Metall-Oxid Nanodrähten für optische und gas-sensitive Anwendungen (MONOGAS)*
Project number: 03X5512
Founded by: German Ministry of Education and Science
Period: January 2010 – Dezember 2011
Coordinator: Dr. Hao Shen (University of Cologne)

2) Title of the project: 3D GaN for high efficiency solid state lighting *(GECCO)*
Founded by: European Commission
Period: September 2012 – May 2013
Coordinator: Prof. Dr. Andreas Waag (TU Braunschweig)

B: Resum en català

El control efectiu dels impactes ambientals a l'entorn de les zones urbanitzades és un desafiament clau per garantir la salut humana i la preservació dels sistemes biològics. [1,2] Es preveu que les xarxes de sensors d'àmplia distribució amb alta resolució local han de jugar un paper important cara aquests problemes creixents. Pel que fa a la monitorització de gasos en aquest context, s'exigeixen sensors amb alta especificitat de detecció i baix consum d'energia. Fins al moment, no es disposa d'una tecnologia de sensor de gas que unifiqui ambdós requisits i, per tant, són necessaris noves aproximacions dins d'aquest camp de la tecnologia. [3] Per tant, l'objectiu de la present tesi és explorar i desenvolupar un nou concepte de sensor de gas que unifiqui aquests dos requeriments: **alta especificitat** i **baixa demanda d'energia**.

Els materials inorgànics nano estructurats han mostrat un gran potencial per a aplicacions de detecció de gasos, tots ells amb altes sensibilitats. A més, la mida compacta dels dispositius disponibles, la robustesa i els seus baixos costos de producció els fan molt adequats per a la integració en plataformes electròniques. Tot i aquests aspectes positius, la seva aplicació en xarxes de sensors està sent obstaculitzada per la seva detecció no selectiva de gasos i l'alta demanda d'energia que requereixen per poder funcionar. La superfície del material inorgànic , com pot ser un òxid metàl·lic, experimenta interaccions d'oxidació/reducció inespecífiques amb les molècules de gas perquè cal activar amb fonts d'energia externes (per exemple escalfant-los). [6–8]

En els últims 10 anys s'han desenvolupat biosensors altament selectius, sempre en mitjans aquosos, mitjançant la modificació de la superfície dels materials semiconductors inorgànics amb grups de receptors orgànics, com per exemple anticosos[19] o ADN de cadena senzilla (ssDNA). [41,42] Les parelles corresponents antigen-anticòs són conegudes des de fa temps amb aplicacions en el camp de la biotecnologia. El seu ús ha permès l'obtenció de deteccions específiques a través d'interaccions selectives d'unió entre les dues parts. En paral·lel s'han pogut desenvolupar demostradors de sistemes de sensors basats en aquest principi: materials híbrids inorgànics-orgànics detecten molècules específiques en fase gas.[21,23,45] En part, aquests sistemes han mostrat resultats prometedors en termes de selectivitat, però l'enfocament de disseny del receptor orgànic encara seguia sent bàsicament empíric.

Les monocapes orgàniques auto-acoblades (SAMs) tenen potencialment un efecte modulador de les propietats elèctriques dels materials semiconductors, quan aquestes s'uneixen a la seva superfície. [30] Resultats recents mostren que la posició energètica dels orbitals de frontera SAMs respecte del nivell de Fermi del semiconductor extens (E_F) és un dels factors determinants per garantir la transferència de càrrega eficient a través de la interfície orgànica-inorgànica. [25,32] Tot i això, el coneixement dels mecanisme d'interacció elèctrica a les interfícies orgàniques-inorgàniques i per extensió el processos de detecció associats en sensors híbrids ha estat limitat. La seva comprensió en termes d'interaccions d'unió entre gas i sensor i la dinàmica de transferència de càrrega conseqüents són per tant un requisit pendent i necessari per assolir un complet control de la detecció selectiva de gasos amb aquests sistemes.

Per altra banda, la recerca en sistemes de sensors autònoms es concentrava fins ara en la juxtaposició d'unitats independents que recol·lectaven energia i d'altres de detecció [55,60,62,63]. Ja que els sensors de gas convencionals basats en semiconductors requereixen d'una font d'energia externa (en el rang dels mW) per a l'activació de la seva superfície i la generació de senyal, els components de recollida d'energia ambiental miniaturitzats no són suficient per poder alimentar aquest tipus de dispositius. Cal doncs, unificar l'aprofitament de l'energia i la unitat de detecció activa amb l'objectiu de reduir la mida dels sistemes sensors autònoms, fentviable la seva integració en plataformes mòbils.

Resultats i Discussió

La Secció 1 de la tesi descriu el concepte d'un sensor selectiu basat en nanofils inorgànics modificats amb SAM. Es demostra com s'aconsegueix una extraordinària millora en termes de selectivitat i sensibilitat cap al NO_2 si es compara amb els sistemes basats en semiconductors coneguts. Per primera vegada, s'ha analitzat a través de mètodes DFT el mecanisme subjacent en les interaccions d'unió del sensor de gasos i les seqüències de transferència de càrrega entre els components orgànics i inorgànics, revelant una gran consistència entre les avaluacions experimentals i teòriques. La principal troballa d'aquest treball és que les posicions energètiques dels orbitals de frontera SAM-gas respecte a l'energia de Fermi del semiconductor són el factor determinant per permetre la detecció selectiva de gasos. Aquest concepte pot conduir a una nova tendència en el desenvolupament de sensors.

Els sensors autònoms descrits en la Secció 2 es van realitzar mitjançant una heteroestructura CdS@n-ZnONW/p-Si. En aquest cas, els nanofils actuaven simultàniament com a element constitutiu de la unió PN i com a component de detecció de gasos. A més, l'ús de nanopartícules de CdS en la superfície de ZnO va permetre l'activació del sensor mitjançant llum visible. Aquests sensors van mostrar respostes quantitatives cap a la presència de gasos oxidants i reductors, en absència de cap font d'alimentació externa. El principal avantatge en el funcionament d'aquest dispositiu es que la generació del senyal del sensor i l'activació de la superfície del material es deguda únicament als fotons visibles absorbits en la unió p/n (generació del senyal) i en les nanopartícules de CdS (CdS NPs) (activació de la superfície). Estudis addicional han identificat els canvi de la densitat de portadors de càrrega (N_D) dins del n-ZnO i les interaccions de gas-superfície induïdes, com a principals responsables de la variació observada del senyal del sensor (ΔV_{oc}).

En base a tots els resultats anteriors, s'ha dissenyat un nou dispositiu microelectrònic per tal d'unificar les capacitats de detecció selectiva de gasos i l'operació d'autoalimentació energètica. Els resultats es presenten i discuteixen a la Secció 3. A més a més, s'ha utilitzat la nova plataforma de dispositiu autònom per estudiar la influència de la naturalesa química de la terminació SAM utilitzada (amina i funcionalitats tiol). Tots dos tipus de sensors han demostrat tenir una selectivitat i sensibilitat molt alta cap a NO_2, a les concentracions necessàries per a la seguretat de la salut humana. Com ja es podia esperar dels resultats presentats a la Secció 1, els experiments han demostrat que la funcionalitat orgànica determina les característiques últimes del sensor. Anàlisis DFT de les interaccions d'unió SAM-gas expliquen teòricament aquest comportament.

En resum, els desenvolupaments presentats a aquesta tesi descriuen un nou enfocament de cara al desenvolupament de sensors de gasos. La introducció de materials actius híbrids amb SAMs orgànics i components flexibles del receptor obren noves possibilitats per al disseny d'unitats de dispositius altament selectius. Els paràmetres crucials per a les interaccions selectives de gas no són únicament especifiques de les interaccions d'unió, sinó també de la modulació elèctrica dels components orgànics i inorgànics. Aquestes interconnexions complexes faciliten la discriminació de les espècies de gas que interfereixen entre elles, però també compliquen el pronòstic precís de les característiques reals del sensor. S'ha pogut mostrar com els mètodes teòrics DFT són una poderosa eina per entendre les interaccions observades experimentalment en els sensors de gas.

Conclusions

Aquesta tesi ha desenvolupat un concepte nou de dispositiu per a la detecció selectiva de NO_2 sense la necessitat d'aportació d'energia externa. La seva realització ha fet necessari un enfocament interdisciplinari que involucra camps de la química, la física i l'enginyeria electrònica. S'ha demostrat que la unificació d'(hetero) materials funcionals inorgànics amb funcionalitats orgàniques ben definides permet obtenir dispositius híbrids interessants. S'ha descrit com el funcionament d'aquest tipus de sistemes requereixen de la interacció conjunta de els diferents elements.

Resumen

Las tecnologías de sensores de gas basadas en la utilización de semiconductores presentan limitaciones importantes tales como pobre selectividad y alto consumo de energía. Por tanto, se hace necesaria la exploración de nuevos dispositivos capaces de satisfacer estos dos requerimientos para que puedan ser integrados en plataformas móviles. En esta tesis se presenta una tecnología de sensores altamente selectivos y autónomos desde un punto de vista energético, incluyendo su evaluación experimental y el análisis de los mecanismos físico-químicos subyacentes. Se han fabricado materiales nanohíbridos basados en nanohilos (NW) inorgánicos, funcionalizados con monocapas autoensambladas (SAMs). En la disertación se presenta la extraordinaria selectividad y sensibilidad de estos materiales: los estudios teóricos son consistentes con los experimentos y permiten identificar la estructura electrónica de los orbitales moleculares de frontera SAM, que es el parámetro determinante para poder garantizar una interacción eficaz entre el sensor y los gases. Además, se presenta un nuevo concepto de sensor autónomo sobre la base de una heteroestructura p-Si/n-ZnONW que responde exclusivamente a la luz solar eliminando la necesidad de fuentes energéticas adicionales. Los cambios de tensión en circuito abierto (ΔV_{oc}) que se utilizan para controlar la presencia de gases siguen una correlación directa con la densidad de portadores de cárga (N_d) en el nanohilo de n-ZnO. Finalmente, se presenta el uso de técnicas de microfabricación en el diseño de un dispositivo que integra los conceptos de selectividad y autonomía energética, capaz por tanto de detectar concentraciones de NO2 habituales en aplicaciones de seguridad (ppb) sin utilizar fuentes de energía externa. Su

tamaño reducido, la demanda reducida de energía y su robustez convierten esta tecnología en altamente prometedora para ser integrada en futuras plataformas móviles.